

Hyperbolic metamaterials: production, properties, applications, and prospects

M V Davidovich

DOI: <https://doi.org/10.3367/UFNe.2019.08.038643>

Contents

1. Introduction. Electromagnetic (photonic) crystals and metamaterials	1173
2. Fresnel equation and media with indefinite metrics. Ideal hyperbolic metamaterials	1175
3. Fabrication and properties of ideal hyperbolic metamaterials	1181
3.1 Super-Planck radiation, channeling and stimulation of radiation, and image processing; 3.2 Absorbers, screens, lenses, and metasurfaces; 3.3 Sensors, nanoantennas, waveguides, and control of fluorescence and Raman spectroscopy	
4. Methods of analyzing hyperbolic metamaterials	1186
4.1 Electrodynamic dispersion equations; 4.2 Homogenization, methods of averaging, and isofrequency surfaces; 4.3 Correspondence between rigorous and model approaches	
5. Possible effects, applications, and prospects	1200
6. Conclusion	1203
References	1204

Abstract. Manmade media (MMMs) consisting of uniaxial photonic crystals with inserts of layers (films) or cylinders embedded in a periodic way into a dielectric substrate with dielectric permeability (DP) are considered. Approximate model-based and accurate electrodynamic methods for describing such MMMs, which are referred to in the case of metal (conductive) or ferrite (metaatom) inserts as a ‘hyperbolic metamaterial’ (HMM), are analyzed. Homogenization methods, the role of dissipation, spatial dispersion (SD), and slow plasmon-polaritons are reviewed. The feasibility of obtaining the hyperbolic dispersion law in a macroscopic description of DP of inserts using the Drude–Lorentz model is studied. In the general case with dissipation and SD, the surface of the Fresnel-equation isofrequencies is shown to differ from a rotation hyperboloid and to be bounded. The ambiguity of a description based on effective material parameters, the effect of dissipation and SD on hyperbolicity, currently observable and possible physical phenomena, and HMM applications are discussed.

Keywords: hyperbolic metamaterial, photonic crystal, plasmon, permittivity, dispersion, band structure, homogenization, volume integral equations

M V Davidovich

N G Chernyshevskii Saratov State University,
ul. Astrakhanskaya 83, 410012 Saratov, Russian Federation
E-mail: DavidovichMV@info.sgu.ru

Received 19 April 2018, revised 20 December 2018
Uspekhi Fizicheskikh Nauk **189** (12) 1249–1284 (2019)
DOI: <https://doi.org/10.3367/UFNr.2019.08.038643>
Translated by V L Derbov; edited by B A Klumov

1. Introduction. Electromagnetic (photonic) crystals and metamaterials

The wide theoretical study and fabrication of artificial media (AMs) in the form of electromagnetic crystals or photonic crystals (PCs) began on the eve of the 21st century and was largely initiated and stimulated by the idea of obtaining negative (left-handed) metamaterials — artificial media with both permittivity $\varepsilon(\omega) < 0$ and permeability $\mu(\omega) < 0$ negative at a given frequency. This coincided with new technological possibilities of creating AMs, due to which considerable progress in this field has been achieved. However, multiple publications on metamaterials are based on simplified model approaches. In the present review, we make an attempt to overcome a number of model simplifications. Everywhere below, we consider spectral fields and quantities with the dependence $\exp(i\omega t)$; real parts of complex quantities are labeled with a prime and imaginary parts with double prime. The negative permittivity is characteristic for metals in the dissipation-free approximation with the spatial dispersion $\varepsilon(\omega) = \varepsilon_L - \omega_p^2/\omega^2$. In this case, the condition $\omega < \omega_p/\sqrt{\varepsilon_L}$ must hold, where the term ε_L describes the Lorentz dispersion of the crystal lattice and the contribution to permittivity from interband transition, and ω_p is the plasma frequency. From the middle of the 20th century, plasmons in metal-dielectric structures became a subject of extensive study, and from the beginning of the current century a boom began in the study of metallic, metal-dielectric PCs, and metamaterials with carbon (in particular, graphene) and semiconductor structures [1–53]. To consider the dissipation, it is necessary to introduce the collision rate by the replacement $\omega^2 \rightarrow \omega^2 - i\omega\omega_c$. Then, $\varepsilon'(\omega) < 0$, if $\omega < (\omega_p^2/\varepsilon_L - \omega_c^2)^{1/2}$.

It should be noted that the issue has a long history that developed over the entire 20th century (see, e.g., reviews [50,

55]. Practical demands initiated the study and fabrication of AMs — artificial dielectrics that could also possess magnetic properties (wave-induced magnetism) [1–4]. The first such papers appeared in the late 1940s–early 1950s [56–65]. Worth mentioning is the pioneering work by L Levin [56] (see also [59]), in which the homogenization of a PC with spherical inclusions forming a cubic lattice was carried out. We would also like to mention the work by S M Rytov, who performed homogenization of a uniaxial PC in the form of a periodic planar layered AM. Rayleigh (1887) and Brillouin (1943) had already considered the propagation of waves in periodic structures. M L Levin [65] investigated the case of wave propagation normal to the layers. Nonlocal properties of such metamaterials with the spatial dispersion (SD) taken into account were demonstrated, e.g., in [66–69]. Such metal-dielectric planar layered AMs, demonstrating specific dispersion properties at not too high frequencies [16, 25–48], as well as wire media [1–9, 13, 15, 17–21, 24–28, 49], were called ‘hyperbolic metamaterials’ (HMMs). In ideal HMMs (in which the components of permittivity or the permeability tensor have different signs and do not depend on the wave vectors), the isofrequency surface of the Fresnel equation is a hyperboloid of revolution [27, 40]. This means the absence of spatial dispersion and dissipation, while frequency dispersion is possible. Wire media and planar layered AMs were called HMMs of the first and the second type, respectively.

The theoretical and experimental promotion of the left-handed material idea was mainly based on proposals concerning their multiple configurations, which were studied using the universal packages of electrodynamic modeling that have appeared in recent decades, or experimentally within a number of simplified models. Less frequently, approximate analytical and numerical-analytical mathematical models were used. The difficulty of constructing an exact model lies in the high complexity of the structures and configurations to be investigated. Attention was focused on the study of backward waves and obtaining negative refraction. However, negative refraction and backward waves are different phenomena [50–53]. Thus, there can be negative refraction without a backward wave and vice versa, a backward wave without negative refraction.

Examples of positive refraction for a backward wave and negative refraction without a backward wave are presented in [50], where the essential dependence of the refraction type on the angle of incidence and the environment (its optical density and structure), as well as the boundary orientation relative to the dispersion (isofrequency) surface, are also shown. Commonly left-handed metamaterials are associated with negative group velocity (GV) [70–75]. However, such AMs are characterized, at least, by strong frequency dispersion (the structures are resonant), spatial dispersion, and high losses, just in the spectral region considered.

The negative GV can be associated with the velocity of the energy motion in model nondissipative problems (Leontovich–Lighthill–Rytov theorem [73]) or, approximately, far from the frequency regions of dissipation and resonances, like bandgaps in PCs, plasmon resonance frequencies, etc., with strong dispersion and losses. From the Kramers–Kronig relations [76], the appearance of a narrow band (or bands) with huge losses follows, if beyond this band dispersion without dissipation takes place. In a number of papers, the values $\varepsilon < 0$, $\mu < 0$ were merely postulated, and the waves in structures with such parameters were considered, commonly even without the dissipation allowed for (see, e.g., [76–78]). In

some papers, e.g., [79, 80], weak dissipation was then taken into account. In an overwhelming majority of such publications, metamaterials are considered isotropic and homogeneous media having scalar permittivity and permeability together with a negative refractive index. However, the permittivity and permeability cannot be negative simultaneously due to the presence of dissipation. It is necessary to take this into account, since left-handed metamaterials imply strong frequency dispersion.

In the considered AM or PC structures, strong spatial dispersion is also present, and they cannot be described by scalar ε and μ [6–13, 81–90]. Moreover, AMs (in particular, PCs) can be described without using permeability at all, i.e., only by permittivity, generally tensorial and having spatial dispersion [83–90]. This is because there are several forms of Maxwell equations for continuous media, in particular, the Landau–Lifshitz and Casimir forms [89, 90], and the material parameters are defined ambiguously [75, 83–95]. This statement is valid for homogenization of an infinite AM. At the interfaces, generally, surface closed currents can be present, described by a jump of the magnetization or the normal component of \mathbf{B} , which requires the introduction of μ .

The homogenization operation itself is also ambiguous. For media with polarization coupling, constitutive equations in the Boys–Post, Condon–Tellegen, Drude–Born–Fedorov, or Casimir forms are known [89–95]. In the general case of a bianisotropic AM, their equivalence is not proven. If the polarizations are independent, it is possible to use the symmetric Casimir form, introducing $\hat{\varepsilon}$ and $\hat{\mu}$, or only $\hat{\varepsilon}$, into the equations in the Landau–Lifshitz form [89]. The refraction in a PC depends on the wave vector, its orientation relative to the boundary, and the orientation of the boundary relative to the isofrequency surface [50–54]. Therefore, it is impossible to introduce only a refractive index, especially a scalar one, and even more so a negative one [81, 82]. In PCs, the problem of unambiguous definition of wave impedances also exists.

A metamaterial in the general (wide) sense is an AM that can be either periodic or a heterogeneous mixture of particles consisting of different sorts of substances. In chaotic mixtures, solid particles can touch each other (statistical heterosystems) or be chaotically embedded in a certain matrix medium [96]. Below, we consider only periodic linear metamaterials. Frequently, metamaterials are understood as PCs in a low-frequency limit far from Bragg resonances [51–53]. We will use the general meaning including the resonance region, too. In a periodic PC, Floquet–Bloch electromagnetic waves exist, which differ from electron Bloch waves in that in a solid the number of particles is conserved (without considering the creation and annihilation of electrons and holes) and in a PC it is not conserved. Photons are absorbed by matter. Even in the case of weak absorption, photons escape through the boundaries of the PC (radiative damping). This damping can be ignored if the PC has many periods in each of the directions.

J C Maxwell can be considered a founder of the effective media theory (mix formulas) [96]. At present, the effective parameters can be found based on the percolation theory, the statistical theory of multiple scattering, the method of compact groups in the permittivity theory, and a number of other approaches [95–97]. PC homogenization based on mix formulas is possible in the low-frequency limit using depolarization coefficients, which allows deriving the tensorial effective permittivities [97]. A metamaterial in a narrow

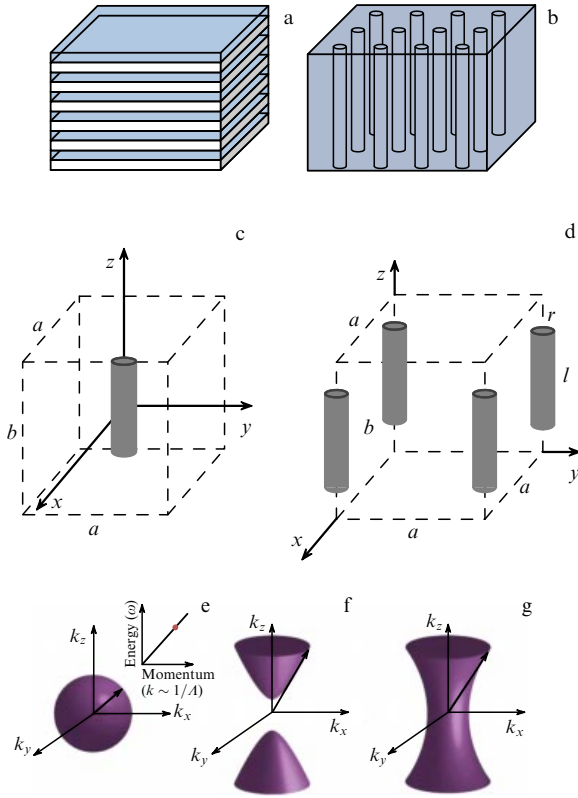


Figure 1. (Color online.) Structures of planar layered (a) and wire HMM formed by long ($l \gg \lambda$) wires (b), a unit cell (c), structure of a PC formed by metallic cylinders with radius r and length l (d), isofrequency surfaces for an isotropic dielectric (e), and HMM of the first (f) and second (g) type.

sense is treated as a homogeneous AM [52] which implies a small lattice constant and size of meta-atoms (and all characteristic sizes) compared to the wavelength. In optics, this ratio is of the order of 10^{-4} . For the PC lattice constant $a = 100$ nm, the minimal wavelength in the metamaterial turns out to be of the order of 1 mm (millimeter range). At low frequencies, such a periodic AM behaves like a homogeneous anisotropic mixture with spatial dispersion, possessing no resonance properties. This is one of the reasons why isotropic left-handed metamaterials are still not produced, either in the optical range or in the microwave range. A simplified approach to HMMs implies postulating real-valued and different-sign diagonal components of the permittivity tensor in a uniaxial PC.

If we consider a metamaterial isotropic and nondissipative, the Fresnel equation for it has the form $\mathbf{k}^2 = k_0^2 \epsilon \mu > 0$ [76, 98]. This is a medium with definite (positive) metrics in the \mathbf{k} -space. In a model nondissipative medium, for a wave with a real-valued wave vector, the quantity $(\mathbf{k}, i k_0 \sqrt{\epsilon \mu})$ is a wave 4-vector that transforms similarly into $(\mathbf{r}, i v t)$, $v = c / \sqrt{\epsilon \mu}$ [98]. Here, it is important that the condition $\sqrt{\epsilon \mu} > 0$ must hold. The group velocity vector $\mathbf{v}_g = c \nabla_{\mathbf{k}} k_0$ transforms similarly into the velocity of a material particle and is bounded: $|\mathbf{v}_g| \leq c$. However, such media cannot exist in nature; the dissipative \mathbf{k} -space becomes six-dimensional and the quantity $\sqrt{\epsilon \mu}$ becomes complex-valued. The group velocity defined via the real part of vector \mathbf{k} loses the boundedness property and the property of a polar vector.

Note that the hypothetical Veselago's medium with $\epsilon = \mu = -1$ (antivacuum) is described by the same metrics as the

vacuum: $\mathbf{k}^2 = k_0^2 > 0$. An isotropic medium with indefinite metrics arises, e.g., at $\mu = 1$, $\epsilon < 0$ (cold collisionless plasma), which corresponds to the presence of imaginary components and damping waves. Anisotropic magnetized plasma is already an example of an anisotropic medium with indefinite metrics, where large-magnitude components of wave vectors are possible. An HMM is commonly understood just as a uniaxial PC (Fig. 1) with unlimited values of wave vector components and the isofrequency surface in the form of a hyperboloid of revolution:

$$\frac{k_{\perp}^2}{\epsilon_{\perp}} + \frac{k_{\parallel}^2}{\epsilon_{\parallel}} = k_0^2 > 0. \quad (1)$$

It is assumed that ϵ_{\parallel} and ϵ_{\perp} are real-valued constants having opposite signs: $\epsilon_{\parallel} \epsilon_{\perp} < 0$. At $\epsilon_{\parallel} < 0$, only HMMs of the first type exist whose isofrequency surface is doubly connected, and at $\epsilon_{\perp} < 0$ HMMs of the second type with a single-connected surface [38–40] (see Fig. 1). Note that in real AMs, ϵ_{\parallel} and ϵ_{\perp} cannot be real-valued and constant as well, because of spatial dispersion. The frequency also enters the left-hand side of Eqn (1), and such frequency dispersion changes the asymptotes of the hyperboloid. Taking the spatial dispersion into account leads to the fact that the above components depend on the complex wave vector $\mathbf{k} = \mathbf{k}' - i \mathbf{k}''$. Therefore, the question arises as to when the properties of the PC (1) are close to the properties of an ideal HMM. This question is considered below.

2. Fresnel equation and media with indefinite metrics. Ideal hyperbolic metamaterials

We define the indefinite metrics in the \mathbf{k} -space as usual, via the scalar product $(\mathbf{x}, \mathbf{y}) = g_{kl} x^k y^l$ using the Hermitian metric tensor \hat{g} [99–101] (assuming summation over the repeated indexes, the asterisk denoting the complex conjugate). Assume that $\mathbf{x} = \mathbf{k}$, $k_0^2 = (\mathbf{k}, \mathbf{k})$, and $k_{\parallel} = k_z$, i.e., the PC axis is directed along the z -axis, and the indices of \mathbf{k} are lowered. For Eqn (1), the metric tensor is diagonal: $g_{11} = g_{22} = 1/\epsilon_{\perp}$, $g_{33} = 1/\epsilon_{\parallel}$. For isotropic plasma, $g_{kk} = 1/\epsilon < 0$. The Fresnel equation is obtained considering the dispersion of the wave $\mathbf{E} = \mathbf{E}_0 \exp(i\omega t - i\mathbf{k}\mathbf{r})$ with amplitude \mathbf{E}_0 in a crystal described by some effective material parameters. The propagation of a plane wave instead of Floquet–Bloch waves already implies homogenization; therefore, the Fresnel equation (1) comprises homogenized material parameters. In the Landau–Lifshitz concept, a PC is described only by the tensor of effective permittivity $\hat{\epsilon}(\omega, \mathbf{k})$ [75, 84–88]. Writing down the wave equation for \mathbf{E} and substituting the above wave into it, we get the Fresnel equation in the form

$$\det(\hat{k}^2 - k_0^2 \hat{\epsilon}) = 0, \quad \det(\hat{k} \hat{\epsilon}^{-1} \hat{k} - \hat{I} k_0^2 \hat{\epsilon}) = 0. \quad (2)$$

Here, for convenience, we introduced the permittivity $\hat{\epsilon}$ of a certain base (matrix) in which meta-atoms (in our case conducting cylinders or layers) are embedded. Without loss of generality, we can assume $\hat{\epsilon} = 1$, including the above permittivity into $\hat{\epsilon}$. Equation (2) incorporates the matrices

$$\hat{k} = -i \begin{pmatrix} 0 & -k_z & k_y \\ k_z & 0 & -k_x \\ -k_y & k_x & 0 \end{pmatrix},$$

$$\hat{k}^2 = \begin{pmatrix} k_y^2 + k_z^2 & -k_x k_y & -k_x k_z \\ -k_x k_y & k_x^2 + k_z^2 & -k_y k_z \\ -k_x k_y & -k_x k_z & k_x^2 + k_y^2 \end{pmatrix}. \quad (3)$$

These matrices (3) are equivalent to the action of the curl operator $\nabla \times \mathbf{E} = \hat{k}\mathbf{E}$ and $\nabla \times \nabla \times \mathbf{E} = \hat{k}^2\mathbf{E}$ on the field of a plane wave. The first matrix is singular; therefore, the ‘curl’ operator is defective (has no inverse operator), and the matrix \hat{k}^{-2} exists. Two forms of the Fresnel equation (2) result from two wave equations for \mathbf{E} and \mathbf{H} . They are seen to be equivalent. In the symmetric Casimir approach [89] with the introduction of permittivity $\hat{\epsilon}$ and permeability $\hat{\mu}$ tensors, the Fresnel equations take the form

$$\det(\hat{\epsilon}^{-1}\hat{k}\hat{\mu}^{-1}\hat{k} - \hat{I}k_0^2\hat{\epsilon}) = 0, \quad \det(\hat{\mu}^{-1}\hat{k}\hat{\epsilon}^{-1}\hat{k} - \hat{I}k_0^2\hat{\mu}) = 0. \quad (4)$$

Finally, describing a PC as a linear medium with the response of the electric polarization \mathbf{P}^e and magnetic polarization $\mathbf{P}^m = \mu_0\mathbf{M}$ (\mathbf{M} being the magnetization) to the fields in the form

$$\mathbf{P}^e = \epsilon_0(\hat{\epsilon} - \hat{I})\mathbf{E} + c^{-1}\hat{\zeta}\mathbf{H}, \quad \mathbf{P}^m = \mu_0(\hat{\mu} - \hat{I})\mathbf{H} + c^{-1}\hat{\zeta}\mathbf{E}, \quad (5)$$

we arrive at the following Fresnel equations [102]:

$$\begin{aligned} \det[(k_0^{-1}\hat{k} + \hat{\zeta})\hat{\mu}^{-1}(k_0^{-1}\hat{k} - \hat{\zeta}) + \hat{\epsilon}] &= 0, \\ \det[(k_0^{-1}\hat{k} - \hat{\zeta})\hat{\epsilon}(k_0^{-1}\hat{k} + \hat{\zeta}) + \hat{\mu}] &= 0. \end{aligned} \quad (6)$$

Here, the effects of cross-polarization are taken into account, i.e., the effect of the magnetic field on the electric polarization and the effect of the electric field on the magnetic one, which required introducing two more tensor quantities. The bianisotropy property for HMMs having an inversion axis is not characteristic and will not be considered.

In contrast to hypothetical isotropic left-handed materials, HMMs are anisotropic and really implementable, which has led to great interest in their fabrication and application. A nonmagnetic ($\hat{\mu} = \hat{I}$) HMM (see Eqn (1)) is described by the permittivity tensor

$$\hat{\epsilon}(k_0, \mathbf{k}) = \begin{pmatrix} \epsilon_{xx} & 0 & 0 \\ 0 & \epsilon_{xx} & 0 \\ 0 & 0 & \epsilon_{zz} \end{pmatrix}. \quad (7)$$

Assume that the permittivity $\hat{\epsilon}$ is included in Eqn (7). In the literature on HMMs, Eqn (7) is commonly considered without spatial dispersion and dissipation, assuming $\epsilon_{xx}\epsilon_{zz} < 0$ [38–41]. On the one hand, this assumption corresponds to small $k = |\mathbf{k}|$; on the other hand, in this approximation the waves in an HMM possess an unlimited value of k .

First, let us consider anisotropic media and structures, in which the diagonal components of the permittivity and permeability tensors can have opposite signs in nondissipative models. Plasma presents an example of such a natural medium. From the first equation (2), we get Eqn (1) for an extraordinary wave and the equation $\epsilon_{\perp}^{-1}\mathbf{k}^2 = k_0^2$ for an ordinary wave [76, 98]. In our case, $\mathbf{k}_{\perp}^2 = k_x^2 + k_y^2$, $k_{\parallel} = k_z$, $\epsilon_{\perp} = \epsilon_{xx}$, and $\epsilon_{\parallel} = \epsilon_{zz}$. This follows from the fact that the Fresnel equation is a fourth-order equation with respect to the components of the wave vector. In crystal optics, the dissipation is considered weak or not considered at all. In this case, one can introduce the metric tensor $g_{kl} = g_{lk}^*$. As an example, let us also consider the permittivity tensor of cold

magnetized (magnetoactive) plasma, ignoring dissipation and thermal motion in a constant magnetic field H_{0z} [84–87, 98]:

$$\hat{\epsilon} = \begin{pmatrix} \epsilon_{xx} & -ib & 0 \\ ib & \epsilon_{xx} & 0 \\ 0 & 0 & \epsilon_{zz} \end{pmatrix}, \quad (8)$$

where $\epsilon_{xx} = 1 - \omega_p^2/(\omega^2 - \omega_0^2)$, $\epsilon_{zz} = 1 - \omega_p^2/\omega^2$, and $b = \omega_0\omega_p^2/[\omega(\omega^2 - \omega_0^2)]$. Here, ω_p is the Langmuir or plasma frequency (the plasma may be multicomponent) and the cyclotron frequency for single-component electron plasma is $\omega_0 = \mu_0(e/m)H_{0z}$. In this case, the condition $\epsilon_{xx}\epsilon_{zz} < 0$ can be fulfilled, similar to that in HMMs. The difference is that plasma is a gyrotropic medium, and the propagating waves are generally elliptically polarized.

Let us consider the longitudinal and the transverse waves. For longitudinal propagation, $k_z^2 = k_0^2(\epsilon_{xx} \pm b)$, where the signs \pm correspond to left-handed and right-handed rotation of the polarization plane. For the extraordinary wave transverse propagation, $k_{\perp}^2 = k_0^2(\epsilon_{xx}^2 - b^2)/\epsilon_{xx}$. If in the transversely propagating wave the magnetic field is not perpendicular to the z -axis, then the ordinary wave does not exist. Considering either one-dimensional or two-dimensional \mathbf{k} -space, it is possible to introduce metrics with diagonal tensors. In the first case, it is a scalar, $g^{\pm} = (\epsilon_{xx} \pm b)^{-1}$. In the case of propagation at an arbitrary angle, let us specify k_z and k_{\perp} . Let us rotate the coordinate system to make the equality $k_{\perp} = k_x$ valid. It is more convenient to use the first of Eqns (2) and the biquadratic equation

$$\begin{aligned} k_z^4 - 2k_z^2 \left[k_0^2 \epsilon_{xx} - \frac{k_x^2(\epsilon_{xx}/\epsilon_{zz} + 1)}{2} \right] \\ - [\epsilon_{xx}(k_x^2 - k_0^2 \epsilon_{xx}) + k_0^2 b^2] \left(k_0^2 - \frac{k_x^2}{\epsilon_{zz}} \right) = 0, \end{aligned}$$

which cannot be factorized, so that it is impossible to introduce a metric tensor in the \mathbf{k} -space that would define the scalar product as a quadratic form. When $k_0 \rightarrow 0$, we have $\epsilon_{zz}k_z^4 + k_x^2k_x^2(\epsilon_{xx} + \epsilon_{zz}) + k_x^4\epsilon_{xx} = 0$. If the coefficients in this equation have different signs, the squares of components are not bounded. Therefore, for waves in an ideal plasma, the unbounded values of the components k_l are also possible (if the dissipation is not taken into account).

Depending on the type of plasma and plasma waves, there are several models of linear response that lead to plasma permittivity [84–87], both with account for spatial dispersion and without it, as well as considering or not the effect of temperature and the magnetic field. The dependence of permittivity on the spatial dispersion, in particular, means that the form of tensor (8) depends on polarization. Considering only circularly polarized waves propagating along the z -axis, we can represent the tensor in the diagonal form: $\epsilon_{11} = \epsilon_{xx} + b$, $\epsilon_{22} = \epsilon_{xx} - b$, and $\epsilon_{33} = \epsilon_{zz}$. In many cases, it is possible to ignore the gyration vector and to consider the diagonal tensor (8) [84, 86].

If we consider the dissipation, in the simplest case, it is reduced to the replacement $\omega^2 \rightarrow \omega(\omega - i\omega_c)$ in all components of $\hat{\epsilon}$ (8). Here, ω_c is the rate of collisions (pulse relaxation). For HMMs (7), the introduction of dissipation means the replacements $\epsilon_{xx} \rightarrow \epsilon'_{xx} - i\epsilon''_{xx}$, $\epsilon_{zz} \rightarrow \epsilon'_{zz} - i\epsilon''_{zz}$, $k_z = k'_z - ik''_z$, $k_{\perp} = k'_{\perp} - ik''_{\perp}$, and from Eqn (1) it follows that $(\mathbf{k}, \mathbf{k}) = \delta_{ij}(g'_i + ig''_i)k_j/k_j$. Therefore, it is impossible to introduce a Hermitian metric tensor, and it is possible to introduce only a diagonal complex-valued tensor with the

components

$$g_1' = g_2' = \frac{\varepsilon_{zz}'}{\varepsilon_{zz}'^2 + \varepsilon_{zz}''^2}, \quad g_3' = \frac{\varepsilon_{xx}'}{\varepsilon_{xx}'^2 + \varepsilon_{xx}''^2},$$

$$g_1'' = g_2'' = \frac{\varepsilon_{zz}''}{\varepsilon_{zz}'^2 + \varepsilon_{zz}''^2}, \quad g_3'' = \frac{\varepsilon_{xx}''}{\varepsilon_{xx}'^2 + \varepsilon_{xx}''^2}.$$

However, to ensure the condition of positive definiteness $k_0^2 = (\mathbf{k}, \mathbf{k}) \geq 0$, such a tensor cannot be arbitrary, since it is related to the wave vector as

$$g_1''(k_1'^2 + k_2'^2 - k_1''^2 - k_2''^2) + g_3''(k_3'^2 - k_3''^2) = 2g_1'(k_1'k_1'' + k_2'k_2'') + 2g_3'k_3'k_3''. \quad (9)$$

Rigorous consideration of dissipation in plasma requires the solution of the kinetic integro-differential equation with the Landau collision integral [87] taken into account and the determination of anti-Hermitian part of the permittivity tensor. It is important that the permittivity tensor and the metric tensor become non-Hermitian. As shown in Sections 2 and 4, the dissipation and, especially, the spatial dispersion bound the components k_i , so that in nonideal HMMs the isofrequency surfaces are no more hyperboloids of revolution and become closed. In common uniaxial (elliptic) crystals, the components are always bounded: $|k_z| < k_0\sqrt{|\varepsilon_{\perp}|}$, $|k_{\perp}| < k_0\sqrt{|\varepsilon_{zz}|}$. Therefore, it is reasonable to consider HMMs in the generalized sense as AMs, in which the opposite inequalities for the real parts of the wave vector components are possible. In this sense, plasma and ferrite in a magnetic field can also be considered HMMs. Plasma is a particular case of gas of oscillators, not bound elastically, i.e., of free charged particles. It follows that all resonance frequencies in the Lorentz dispersion formula can be simply put equal to zero. For an isotropic nondissipative gas of oscillators with one resonance frequency ω_0 , the classical permittivity is given by the Lorentz formula $\varepsilon(\omega) = 1 + \omega_p^2/(\omega_0^2 - \omega^2)$, according to which the permittivity can be negative.

A rigorous approach requires considering all resonances and the internal field. Near a resonance frequency, it is usually assumed that $\varepsilon(\omega) = \varepsilon_{\infty} + \omega_p^2/(\omega_0^2 - \omega^2)$, where ε_{∞} is the permittivity at the frequencies $\omega \gg \omega_0$, but substantially lower than the next first resonance, so that $\varepsilon(0) = \varepsilon_{\infty} + \omega_p^2/\omega_0^2$. The quantum-mechanical approach is based on calculating matrix elements $\mathbf{d}_{kl} = e\langle\psi_k|\mathbf{r}|\psi_l\rangle$ of electric dipole-dipole transitions and oscillator strengths [75, 98, 103, 104]. In the first approximation of the perturbation theory for quantum transition probabilities, the quantum-mechanical approach yields the formulas of the same type as the classical Lorentz approach. It is important that there be a frequency region where $\varepsilon(\omega) < 0$. Quadrupole and higher multipole contributions, if there are any, are commonly disregarded under the condition that there is an electric dipole transition. The permittivity is obtained from a linear response of all transitions to the field. The dissipation and small oscillator strengths, proportional to the transition matrix elements, can lead to the violation of the condition $\varepsilon(\omega) < 0$. If $\mathbf{d}_{kl} = 0$ or when it is also desirable to take the magnetic properties into account, then for the probability of a magnetic dipole transition the first-order approximation of the perturbation theory is used:

$$p_{kl}^m(\tau) = \left(\frac{\tau}{\hbar}\right)^2 (\mathbf{m}_{kl}\mathbf{H})^2 \text{sinc}^2[(\omega - \omega_{kl})\tau],$$

where $\mathbf{m}_{kl} = \langle\psi_k|\mathbf{m}\mathbf{H}|\psi_l\rangle$, \mathbf{m} is the magnetic moment of the atom, and the function $\text{sinc } x = (\sin x)/x$ is introduced. For a meta-atom in an AM, \mathbf{m} is related to an induced closed current. Similar to rarified matter, for a rarified AM the formula for μ can be derived. However, it should be kept in mind that the magnetic moment is affected by the internal field, which in an isotropic magnetic medium is equal to $\mathbf{B}/(\mu_0\mu)$ [98]. Therefore, for a condensed medium or condensed metamaterial (with the mutual influence of meta-atoms taken into account), a Lorentz-type formula can be derived, generally, only for $\hat{\mu}^{-1}$. Reference [75] presents an example of a contribution to the tensor $\hat{\varepsilon}(\omega, \mathbf{k})$ from magnetic dipole and electric quadrupole transitions and shows the limited nature of introducing $\hat{\mu}$ at high frequencies, which is also mentioned in [105].

The negative effective permittivity can also be obtained by calculating the dipole moment of a periodicity cell near the resonance, where the current density phase changes sign relative to the field phase. Indeed, the density of the meta-atom polarization current in a PC is related to the field by the equality $\mathbf{J}_p = i\omega\varepsilon_0(\varepsilon(\omega) - \tilde{\varepsilon})\mathbf{E}$, where $\varepsilon(\omega)$ and $\tilde{\varepsilon}$ are the permittivity values for the inclusion and the dielectric base, respectively. The above current density gives rise to the charge density $\rho = i\nabla\mathbf{J}_p/\omega$, which determines the polarization $\mathbf{J}_p = i\omega\mathbf{P}$. In the frequency region, where $\varepsilon(\omega) > 0$, the quantities \mathbf{P} and \mathbf{E} are in phase. In the region where $\varepsilon(\omega) < 0$, a negative component of the effective permittivity is possible, which can be obtained based on the mix formulas of the effective medium model [94, 95] as proposed by D K M Garnett, D A G Bruggeman, and many others. To determine the permittivity tensor, depolarization coefficients are introduced in these formulas to allow for the shape and orientation of the particles [90, 97]. A greater wavelength than the characteristic dimensions is a necessary condition of the effective medium theory. The condition $\varepsilon(\omega) < 0$ for the macroscopic meta-atom permittivity also relates to structures in the resonance region in it. The resonance frequency should be smaller than the frequencies of the Bragg resonances. The polarization \mathbf{P} should be defined as the average dipole moment per unit volume, $\langle\mathbf{P}\rangle = \langle\rho(\mathbf{r})\mathbf{r}\rangle$. The integration is performed over the cell of periodicity. For $\varepsilon(\omega) < 0$, it is necessary that \mathbf{P} and \mathbf{E} in a meta-atom be in antiphase, and for an HMM this should be so for the components $\langle P_i\rangle$ and $\langle E_i\rangle$ along one of the coordinate axes.

To obtain negative permittivity in an AM, metallic constructions supporting induced closed currents are considered [3, 4, 106–108]. The simplest of them is a loop current (a conducting ring) [108]. In this case, it is often assumed that a relation like $\mu(\omega) = 1 + \omega_m^2/(\omega_0^2 - \omega^2)$ is valid, if the current loop is affected by the field \mathbf{H} of an electromagnetic wave, considering the loop with current as a magnetic dipole in a vacuum. However, the electrons are affected by the Lorentz force, depending on the magnetic induction \mathbf{B} that determines the internal field in a rarefied AM. Therefore, the presented formula is valid for $\mu^{-1}(\omega)$. The magnetism induced by the field in such structures is diamagnetism: the induction current in the loop gives rise to a field that opposes the change of magnetic flux. It is easily shown that in the low-frequency (nonresonance) region it is always $0 < \mu(\omega) < 1$ [109]. In the high-frequency region, the general meaning of permeability, even an induced one, is lost [75, 76, 105]. The permeability cannot be isotropic, since the PC, on the one hand, should be cubic and rarefied, and, on the other hand, the metallic particle (meta-atom) should be a resonance one.

Cubic PCs consisting of resonance spirals are bianisotropic, and PCs consisting of split-ring meta-atoms are anisotropic. Losses restrict the possibility of obtaining negative real parts of the permittivity and permeability components. This is one of the main reasons for the impossibility of left-handed isotropic materials. For them, the resonances must cause electric and magnetic polarizations, cross-polarization being absent, the PC should be cubic and rarefied, and the meta-atoms should be resonant. Even hypothesizing that all these conditions are satisfied, a spatial dispersion takes place that leads to anisotropy [75]. In the optics of homogeneous media, it is possible to ignore the spatial dispersion, but in crystal optics, it is not possible. The condition $a \ll \lambda$ should hold, where a is the lattice constant. HMMs do not require fulfillment of the isotropy condition or the condition of ‘simultaneous negativity’ of the permittivity and permeability components, their technological implementation being easy; therefore, they are of great interest. In connection with the study of metamaterials, publications appeared that ‘disprove’ the conclusion of Ref. [76] on the impossibility of observing essential magnetic properties in the optical range. We do not present the appropriate references, because all the appropriate infinite AMs can be described without introducing magnetic properties.

Thus, a magnetic PC with the Fresnel equation

$$\frac{\mathbf{k}_\perp^2}{\mu_\parallel \varepsilon_\parallel} + \frac{k_\parallel^2}{\mu_\perp \varepsilon_\perp} = k_0^2 > 0 \quad (10)$$

will also be an HMM, for which the permittivity can be a scalar. In the presence of dissipation, we assume that $\varepsilon = \varepsilon' - i\varepsilon''$, $\varepsilon' > 0$, $\mu_\parallel = \mu'_\parallel - i\mu''_\parallel$, and $\mu_\perp = \mu'_\perp - i\mu''_\perp$, where all quantities with a double prime are positive, and for the HMM the condition $\mu'_\parallel \mu'_\perp < 0$ should be valid. Such an HMM is easily implementable in the microwave range in the form of a few ferrite layers, periodically arranged between layers of an insulator (see [110–113]). The case of scalar permittivity is realized when the insulator and ferrite permittivities coincide. The external magnetic field H_{0z} and the z -axis should be directed across the layers. In this case, slow magnetostatic waves (SMWs) can propagate in ferrite films [97, 110–113]. Using tangent magnetization makes such a PC biaxial, while still supporting waves at large k . For a ferrite without dissipation [98, 114],

$$\hat{\mu} = \begin{pmatrix} \mu_{xx} & -ia & 0 \\ ia & \mu_{xx} & 0 \\ 0 & 0 & \mu_{zz} \end{pmatrix}, \quad (11)$$

where $\mu_{xx} = 1 - \omega_M \omega_0 / (\omega^2 - \omega_M^2)$, $a = \omega \omega_0 / (\omega^2 - \omega_M^2)$, $\omega_0 = \mu_0 g M_0$, $\omega_M = \mu_0 g M_0 (\alpha k^2 + \beta + H_{0z} / M_0)$, M_0 is the saturation magnetization, α is the constant of inhomogeneous exchange interaction, and β is the constant of magnetic anisotropy for the spin magnetic moment $g = e/m$ [114]. The terms α and β are often disregarded [111]. The component μ_{xx} in Eqn (11) can be positive or negative. In the case of a planar layered PC with ferrite and metallic layers and the magnetic field perpendicular to them (see [115]), it is possible to implement an AM, described by both the permittivity tensor (8) of the metallic layer and the permeability tensor (11) of the ferrite films. In such an AM, hybrid forward and backward bulk plasmon-magnonic polaritons are possible. In this case, a backward wave is possible if $\mathbf{k} \cdot \langle \mathbf{S} \rangle < 0$, which is not directly related to simultaneously negative permittivity and perme-

ability (or their components). Here, $\langle \mathbf{S} \rangle$ is the Poynting vector averaged over the period.

At the HMM boundary, Dyakonov-type plasmon polaritons (PPs) are possible, which can also be forward or backward. For example, in Refs [110–112], surface backward magnetostatic waves (MSWs) along the ferrite films under tangent magnetization are considered. For a biaxial planar layered PC consisting of ferrite and metallic films with tangent magnetization, one should consider the general Fresnel equation (4) leading to fourth-order equations for the components of wave vectors. Waves with large k are possible in such a PC.

Thus, in the anisotropic case, it is easy to implement AMs in which the real parts of the tensor components can be independently changed. It is worth noting that frequently tensor (11) is obtained based on the solution of the linearized equation of Landau–Lifshitz magnetization precession in a weak (relative to H_{0z}) magnetic field \mathbf{H} of a monochromatic wave without the internal field taken into account [111]. In the case of a single thin ferrite film with a slow surface MSW, the field strongly decays in the film, making it possible to suppose that the internal field is the field \mathbf{H} of the wave in the structure. In the case of a bulk ferrite sample and magnetic HMM, the magnetic moments affect each other, and the internal field should be taken into account [115] (defined as a variational derivative of the free energy with respect to the magnetic moment) which changes the frequency ω_M . Damping is usually taken into account phenomenologically by adding a few relaxation terms [115], which leads to a non-Hermitian permeability tensor. The properties of the waves and the form of the tensors depend on \mathbf{k} , i.e., for such HMMs spatial dispersion is essential.

The properties of ideal HMMs can be considered regarding both the waves in an infinite sample and the diffraction of plane waves by a finite sample. In the latter case, the sample should contain many periods in every direction and be extended along the axis, so that the transmitted wave can acquire the properties of a Bloch wave, formed by multiple reflections. The main property of an extraordinary wave in an ideal HMM lies in the unboundedness of the wave vector components. For a wave in an isotropic dielectric, $g_{kl} = \tilde{\varepsilon}^{-1} \delta_{kl}$ and $\mathbf{k}^2 = \tilde{\varepsilon} k_0^2$. For a biaxial crystal reduced to principal axes, $g_{kl} = \varepsilon_{kk}^{-1} \delta_{kl}$ and $k_0^2 = \mathbf{k} \mathbf{k} = \varepsilon_{11}^{-1} k_1^2 + \varepsilon_{22}^{-1} k_2^2 + \varepsilon_{33}^{-1} k_3^2$. If all three components of the permittivity tensor are real-valued and positive, it is a triaxial ellipsoid in the real \mathbf{k} -space degenerating into a sphere in the isotropic case. The unboundedness arises when one of the components is negative. At $k_0 > 0$, this hyperboloid of one sheet ($\varepsilon_{33}^{-1} < 0$) degenerates at $k_0 \rightarrow 0$ into a second-order cone. The unclosed surface means unbounded \mathbf{k} . In the literature, just such a uniaxial PC is understood as an HMM.

In view of the foregoing, by HMMs in the generalized sense we will mean weakly dissipative uniaxial PCs, in which the condition $k^2 \gg k_0^2$ is fulfilled. Since the wave vector is related to the quasi-photon (polariton) momentum $\mathbf{p} = \hbar \mathbf{k}$, the hyperbolicity leads to its unlimited (actually large compared to $\hbar k_0$) magnitude and related possible effects, e.g., the Compton effect [116, 117] in the optical range.

In an HMM, slow plasmon polariton bulk waves [40–49, 118–121] are possible. In a dissipative wire HMM, a bulk plasmon polariton has both longitudinal and transverse components of the wave vector, i.e., it propagates obliquely and with damping [47, 49]. In planar layered HMMs, the same situation takes place [69, 118–121], in which case the



Figure 2. (Color online.) Radiators with a wire medium and the ray paths in the ENZ layer (with the permittivity close to zero) for a wire HMM.

bulk plasmon polariton is like a surface one, the only difference being that the dispersion equation of the latter is determined by the equality of the p-wave s-wave impedance in the vacuum and the corresponding input impedance of a semi-infinite periodic structure [69, 122, 123]. The dispersion equation will be different depending on whether the HMM is terminated by a metallic layer or a dielectric one. The dispersion equation for a bulk plasmon polariton is determined based on the Floquet–Bloch equation from the condition of the input impedance periodicity in the sections shifted by a period [69], or using other equations, e.g., describing the averaged Poynting vector and the wave vector, or in the form of coupling the averaged field components via averaged impedances. In this case, both E- and H-plasmon polaritons exist. The excitation of a surface E-plasmon polariton can be implemented by a plane wave with p-polarization or by an electron beam, while the H-plasmon polariton can be excited by an s-polarized wave.

One more effect observed in HMMs is related to the enhanced spontaneous emission of an atom or a dipole [14, 16, 22, 38–42, 124–160]. This effect, discovered by Purcell for the radiation of an atom in a cavity [124], consists of an increase in the spontaneous emission rate (Einstein’s coefficient) by $f_P = 3(4\pi^2)^{-1}Q\Lambda^3/V$ times, where f_P is the Purcell factor, Q is the Q -factor, V is the cavity volume, and Λ is the wavelength in the cavity. The expression for f_P shows that the Purcell effect should strongly manifest itself in high- Q nanostructures, such as HMMs. Since $Q \sim a/\delta$, where a is the characteristic size and δ is the penetration depth, to increase f_P it is important to increase the conductivity of metallic structures, i.e., reduce the collision rate. In plasmonics, where $\epsilon' < 0$, disregarding ω_c , we have $\delta = c/(\omega_p^2 - \epsilon_L\omega^2)^{1/2}$.

The Purcell effect is characteristic of general-type structures, including small metallic cavities [128, 129, 133], metal-dielectric metamaterials [137], extremely anisotropic elliptic metamaterials [138], photonic quasicrystals [140], nanodiamond crystallites doped with nitrogen [146, 160], quantum emitters near silicon nanoparticles [147], fully dielectric structures [148], metamaterials with epsilon-near-zero (ENZ) permittivity [152], PCs [126], and multiperiodic hyper-PCs [153, 155]. In the last case, the PC has two essentially different periods, i.e., there is a small-scale periodic structure within the large period. Both electric and magnetic dipoles are considered. The closeness of a component of the permittivity to zero (ENZ) manifests itself in different effects, e.g., in a change in the source directional pattern (Fig. 2). For waveguides made

of HMMs the effect manifests itself in a sharp change in the wave properties. The diffraction by an HMM layer also changes substantially in the ENZ region. Two ENZ regions are possible: $\epsilon_{xx} \approx 0$ and $\epsilon_{zz} \approx 0$. When the real part of the permittivity passes zero, losses play an essential role.

The maximal Purcell effect is achieved in AMs consisting of resonance nanoparticles, when $f_P \sim \Lambda^3/(a\delta^2)$. The probability p_{if} of a transition from the initial state $|i\rangle$ to the final state $|f\rangle$ of a quantum oscillator in the presence of structures in an ideal HMM (1) in the first-order perturbation theory, according to the Fermi Golden Rule, has the form

$$p_{if} = \frac{1}{\tau} = \frac{2\pi}{\hbar} \sum_{\mathbf{k}, \sigma} \left| \langle f | H'(\mathbf{k}, \sigma) | i \rangle \right|^2 \delta(\hbar\omega - \hbar\omega_{\mathbf{k}, \sigma}).$$

Here, $H'(\mathbf{k}, \sigma)$ is the Hamiltonian of interaction between the oscillator and the field, $\langle f | H'(\mathbf{k}, \sigma) | i \rangle$ is the transition matrix element, and the summation (integration) is performed over all wave vectors and polarizations σ of quasi-photons. In the case under consideration, the density of states (DOS) ρ_σ of quasi-photons as a sum over the quasi-momenta of delta functions $\delta(\hbar\omega - \hbar\omega_{\mathbf{k}, \sigma})$ diverges for a hyperboloid of revolution, since the delta function reduces the volume integral to the integral over an infinite surface. In the case of electric dipole, $H' = e\mathbf{d}\mathbf{E}$, and in the case of a magnetic one, $H' = -\mu_0\mathbf{m}\mathbf{H}$.

In real HMMs the isofrequency surface is always bounded. In review [40], four reasons for DOS ρ_σ boundedness are pointed out: the finiteness of the period a , which restricts k by a value of the order of $k \sim 1/a$ in the first Brillouin zone; the spatial dispersion of permittivity; the finite source size d that determines the overlap of the wave functions of the states; and the possibility of a finite distance h from the dipole to the HMM. In these cases, the maximal Purcell factor has the order of $f_P \sim (\lambda/a)^3$, $f_P \sim (c/v_F)^3$, $f_P \sim (\lambda/d)^3$, $f_P \sim (\lambda/h)^3$, respectively, where v_F is the Fermi velocity in the metal. In the second case, the magnitude of k was considered to be bounded by the Fermi momentum. However, the limitation for Hk-quasi-photons is also related to the appearance of k^2 in the components of the permittivity in (1). The dissipation also bounds the isofrequency surface and DOS and leads to dissipative damping alongside with the spontaneous radiative decay. The sum of the above probabilities of emission is determined using the tensor Green’s function (GF) as $f_P = (3/2)\mathbf{n}\hat{G}_{\sigma\sigma}(0)\mathbf{n}/k^3$. Note that this GF describes an individual point source in a medium with permittivity (7) [131]. Due to the singularity of the GF, the

Purcell factor of a point source diverges. In Ref. [131], the Purcell factor is obtained for a finite source described by a wave packet $\Phi(\mathbf{r})$ satisfying the unit normalization. For a Gaussian packet $\Phi(\mathbf{r}) = (\sqrt{2\pi}a)^{-3} \exp[-r^2/(2a^2)]$ and an HMM free of dissipation with $\varepsilon_{\perp} > 0$, $\varepsilon_{\parallel} < 0$ for the dipole orientation along the axis in the approximation of small source size $ka \ll 1$, it was found that

$$f_P = \sqrt{\varepsilon_{\perp}} - \frac{3\sqrt{\pi\varepsilon_{\perp}}(2\varepsilon_{\perp} + |\varepsilon_{\parallel}|)}{8ka(\varepsilon_{\perp} + |\varepsilon_{\parallel}|)^{3/2}} + \frac{3\sqrt{\pi\varepsilon_{\perp}}}{8(ka)^3(\varepsilon_{\perp} + |\varepsilon_{\parallel}|)^{3/2}}.$$

Here, the main contribution comes from the third term on the right-hand side. To determine the oscillator radiation character more precisely, it is necessary to solve the electrodynamic problem considering the real microstructure and real radiator. In the case of a quantum oscillator, the problem should be consistent with the electrodynamic one, i.e., this is a problem of the quantum theory of radiation of interacting particles with the thermal fluctuations taken into account.

An effect close to the Purcell one consists of super-Planck anisotropic thermal radiation and radiation heat transfer, including that through small gaps, as well as to the far-field zone with the possibility of almost full absorption [18, 22, 27, 31, 36–48, 141, 142]. In Section 3, the main effects in HMMs are considered in more detail. It should be noted that such effects as negative refraction, spatial dispersion, waves with large \mathbf{k} components (High- k), the Purcell effect, and a number of others are also inherent in biaxial metallic and dielectric PCs, bianisotropic PCs, and plasmon polariton structures. The HMMs here act like the most vivid and simple representatives of AMs clearly demonstrating the above effects. In particular, the negative refraction is largely dependent on the direction and magnitude of the wave vector in the medium, from which a wave is incident on the PC relative to the normal to the interface (Fig. 3), as well as on the direction of this normal and the normal to the isofrequency surface in the \mathbf{k} -space \mathbf{v}_g/v_g .

The negative refraction manifests itself in AMs both with magnetic properties and without them. For example, if the axis of an HMM is directed obliquely to the interface, then, in the case of normal incidence of a plane wave, the transmitted wave declines towards the axis. A displacement of the incident ray towards the axis leads to positive refraction and a backward displacement to a negative one (see Fig. 3 and Ref. [8]). In this case, backward waves are possible in a nonideal HMM. In the presence of dissipation, one should consider the Poynting vector as a direction of the ray. For plane wave incidence, the component k_x in the environment and in the HMM is similar, so that the direction of the transmitted wave is determined by the crossing of the line $k_x = \text{const}$ and the hyperboloid. For the incidence from an optically dense medium, $k_x^2 + k_z^2 = k_0^2 \varepsilon$.

In an ideal HMM, $\mathbf{k}\mathbf{v}_g > 0$, and $\mathbf{k}\mathbf{v}_g \rightarrow 0$ at $k_0 \rightarrow 0$, i.e., there are no backward bulk waves. However, at the HMM boundary there can be Dyakonov-type backward surface plasmon polaritons. If dissipation is present, then the isofrequency surface is not a hyperboloid, and the direction of the transmitted ray is determined by the Poynting vector, but the component k_x tangent to the boundary is real and coincides with its value in a plane wave in a vacuum. In the absence of reflection, the input impedance of an HMM at the boundary plane must coincide with the impedance of an E-wave (for p-polarization) or H-wave (for s-polarization) in a vacuum, where it is real-valued.

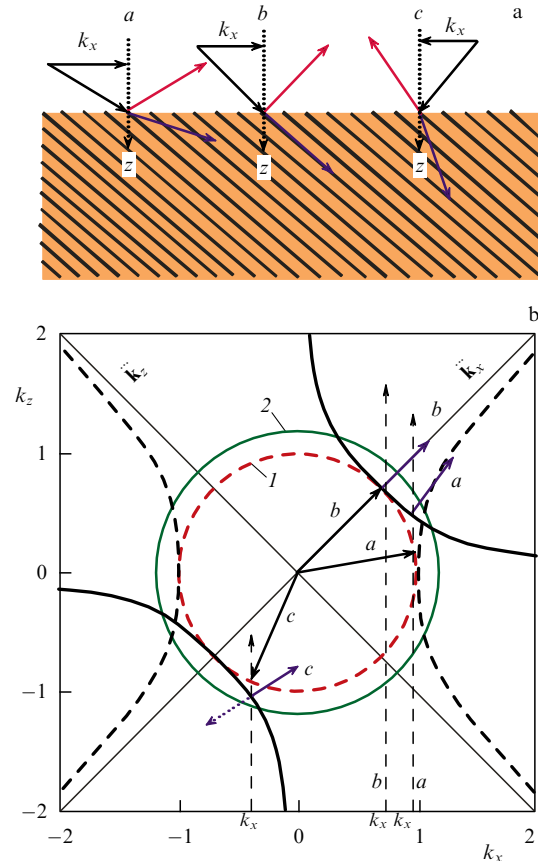


Figure 3. (Color online.) (a) Positive (a, b) and negative (c) refraction for a hypothetical asymmetric (45% cut) planar layered HMM with $\varepsilon_{zz} = -\varepsilon_{xx} = 1$ under the incidence of a plane wave from a vacuum and (b) a \mathbf{k} -diagram. The thick solid hyperboloid corresponds to the isofrequency surface in the \mathbf{k} -space, and the dashed hyperboloid in the \mathbf{k} -space rotated by -45° (for a symmetric HMM); the dashed circle 1 corresponds to the diffraction from the vacuum, the solid circle corresponds to the diffraction from an isotropic dielectric with $\varepsilon = 1.44$. Thick blue arrows in the diagram show the directions of the transmitted wave.

Generally, the incidence of a wave with one polarization excites waves with both polarizations. It is clear that due to this reason the dissipation of total absorption is impossible, since the dissipative AM has a complex impedance. A small reflection coefficient can occur at a certain incidence angle and small dissipation, when the impedances are close to each other (e.g., as shown in Fig. 4). For the fulfilment of the Ewald–Oseen principle in the far-field zone, the PC should have many periods. The dispersion equation for Dyakonov plasmon polaritons should be derived with this fact taken into account using the effective $\hat{\varepsilon}$ matching method. Generally, the normal component k_z and the tangent one k_x are complex-valued, the latter determining the plasmon polariton. The situation here is similar to that for Zenneck plasmon polaritons and the incidence of a plane wave at the Brewster angle. When a p-polarized wave is incident on a dielectric at such an angle that the reflected ray makes a right angle with the transmitted one, the Brewster angle is absent (David Brewster, 1815). Since at least a weak dissipation is always present, a fast surface Zenneck wave ($k_x' < k_0$) is rapidly excited. In a metal, the same Zenneck dispersion equation $k_x = k_0[\varepsilon/(\varepsilon + 1)]^{1/2}$ leads to a slow wave, $k_x' > k_0$, in the case of $\varepsilon' < -1$; therefore, its efficient excitation is possible only from an optically denser medium, and it is

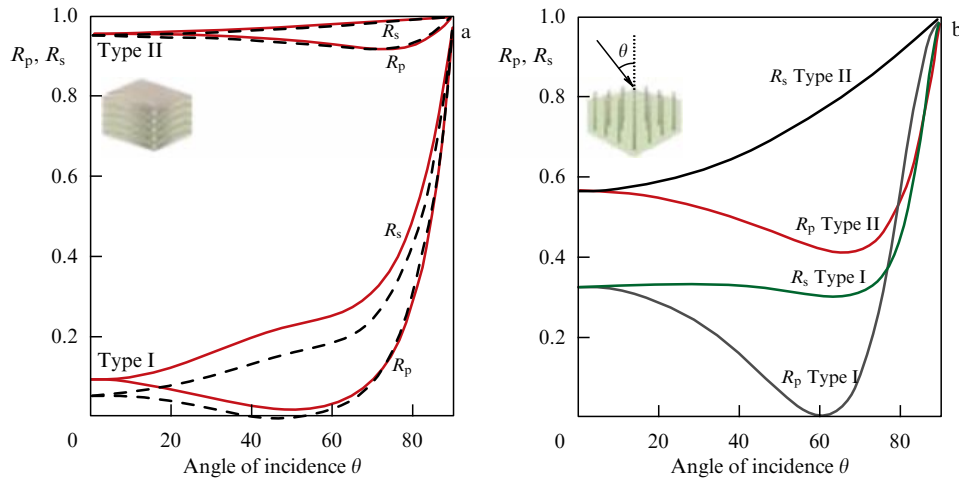


Figure 4. Magnitudes of reflection coefficients versus the angle θ . (a) Ag-TiO₂ planar parallel HMM: R_p and R_s versus the incidence angle for type I and II HMMs based on the effective medium theory. Type I ($\lambda = 360$ nm) and II ($\lambda = 750$ nm) hyperbolic regimes take place for structures of 40 periods with 50% filling by metallic fraction 320 nm thick with the period of 8 nm. (b) R_p and R_s versus the incidence angle for type I ($\lambda = 850$ nm) and II ($\lambda = 390$ nm) wire Ag-Al₂O₃ HMMs 500 nm thick at 15% filling with metallic fraction. (Data from [39].)

necessary to use the Otto or Kretschmann excitation schemes. A plasmon polariton can also be excited from a vacuum at the HMM boundary by means of prisms or matching layers.

3. Fabrication and properties of ideal hyperbolic metamaterials

The simplest HMMs have a planar layered structure of 1D periodic PCs, which can contain two or more layers per period. The alteration of a metallic or semiconductor layer (film) and a dielectric layer is used most frequently. Since a large number of periods is needed, the manufacturing of micro- and nanostructures requires multiple technological operations and is a long and expensive process of sequential deposition of layers.

Metallic films are deposited using electrolytic methods, electrophoresis, electric arc-discharge and gas-plasma sputter deposition, magnetron sputtering in low-pressure plasma, chemical metallization, vacuum metallization on cold and heated substrates, cathode sputtering, laser sputtering, deposition of pure metals from carbonyl compounds in the gas phase, and a number of other methods. It is possible to obtain metallic films having a thickness from 2 nm to a few hundred micrometers and thicker. Thin films of a few nanometers, the most interesting of HMMs, are easily implemented using the methods of magnetron sputtering from low-pressure plasma. The HMMs were implemented using bilayer doped InGaAs/AlInAs semiconductor PCs [161] and metal-dielectric and metal-semiconductor two-layer and three-layer PCs, such as Ag/Al₂O₃, Ag/polymethyl methacrylate, Ag/LiF, Si/Ge, Au/Al₂O₃, Si/SiC/SiO₂, and many other structures [40, 66, 67, 162–171].

As dielectric layers, SiO₂, SiO, Al₂O₃, BeO, BN, and a number of other materials are used. The most often used material is SiO₂, obtained by forming epitaxial layers of silicon followed by their oxidation in dry oxygen, aqueous vapors, humid oxygen at high pressure, and thermal oxidation in dry and humid oxygen. Using oxidation, it is easiest to obtain films 3–7 nm thick. Silicon layers are usually obtained by gas phase epitaxy implemented in two main ways: hydrogen reduction of silicon tetrachloride

(SiCl₄) (chloride method), trichlorosilane (SiHCl₃) or dichlorosilane (SiH₂Cl₂) (silane method). When using the silane method, the decomposition occurs at $T = 1050^\circ\text{C}$, which slows down the diffusion compared to that in the chloride method and reduces the harmful effect of autodoping, which makes it possible to produce sharper junctions between the layers. As HMMs, it is possible to use graphene sheets between layers of SiO₂ or another insulator. Here, it is possible to use both the micromechanical assembling and epitaxial growing of graphene sheets on a substrate. The transfer of graphene and multigraphene (up to 10 sheets), grown from the gas phase by the method of chemical vapor deposition (CVD) on SiO₂/Si or hexagonal BN substrates, is executed using polymer films [172]. For the low-frequency range, it is possible to assemble HMMs from thin sheets of graphene obtained by mechanical exfoliation.

Another type of HMM is represented by wire media, i.e., PCs made of nanowires [2–21, 28–31, 47, 49, 173–179]. The methods of growing periodic structures of nanowires are presented in monograph [180, chapter 9]. Template synthesis of nanowires is a conceptually simple and intuitively clear method of nanostructure fabrication [181–183]. The templates, having cylindrical pores or cavities, are filled with a material that takes the shape of the pore and forms nanowires. Ref. [180] describes frequently used templates and methods of their filling for making nanowires. They use electrochemical deposition and vacuum deposition. Many modern methods of semiconductor nanowire synthesis are based on the mechanism of anisotropic growth of crystals with vapor–liquid–solid (VLS) phases.

For applications requiring homogeneous arrays of oriented nanowires with size control, methods of controlled etching are used, such as reactive ion etching and chemical etching using metals, as well as laser processing. Arrays of nanowires are made of Ag, Au, Bi, BiSb, Bi₂Te₃, CdS, CdSe, Cu, Fe, GaN, GaAs, Ge, InAs, MgO, Mo, Ni, Pb, PbSe, Pd, Si, W, Zn, and ZnO. Figures 5–9 present a view of some nanowire HMMs according to [180]. Dissertation [184] describes technologies of manufacturing nanowire structures using the methods of pulsed laser sputtering and carbo-thermal and thermal synthesis. The same paper presents the

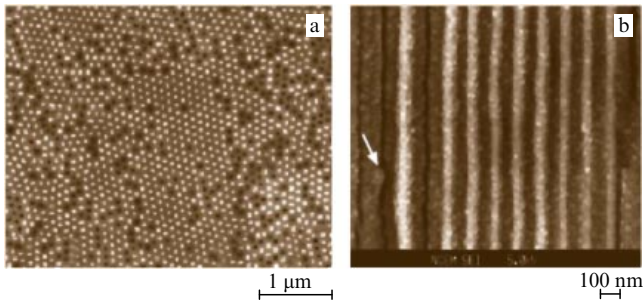


Figure 5. (a) Cross-sectional scanning electron microscopy (SEM) image of an array of Bi_2Te_3 nanowires, demonstrating a relatively high porosity factor. (b) SEM image of a nanowire Bi_2Te_3 array along the axis of the wires. (From [180].)

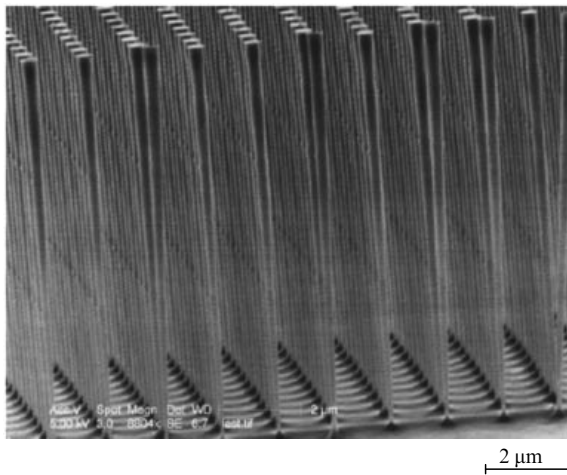


Figure 6. Examples of patterned reactive ion etching (RIE) of nanowires. In these examples, RIE was executed by electron lithography using a template [180].

results of creating planar layered HMMs. The technologies of growing arrays of oriented ZnO nanorods and ZnO films, as well as lattices of ZnO, ZnO:Mg, ZnO:Co, ZnO:Mn nanorods are being developed (see Figs 8, 9). To obtain HMMs, metallic films of nanoscale thickness, e.g., of silver, are sputtered on the above arrays of semiconductor rods.

Carbon nanotubes are also used in HMMs [15, 17, 26, 31], which can be arranged in arrays [185, 186]. Using photolithography, HMMs are obtained in the form of periodic

metallic strips on thin dielectric substrates with sequential layer-by-layer growth. In such HMMs, the use of graphene strips is also possible. HMMs consisting of graphene sheets and nanostrips were considered in Refs [34, 36, 187–191]. Commonly, the length of nanowires and nanostrips is assumed to be very large compared to the wavelength. However, short nanowires, periodically translated in the transverse plane and along the axis, also form an HMM [69]. Such a uniaxial crystal is 3D periodic. HMMs are possible in the form of cylindrical cavities in a metal (semiconductor) or multilayer meshes [40]. To satisfy the condition $\epsilon_{xx} \approx \epsilon_{yy}$, the mesh should be fine. Sometimes curved layered metal-dielectric structures are considered to be HMMs [38–40], which do not support plane waves but are used as lenses. Although in such structures large values of wave vectors are possible, they are not 1D-periodic uniaxial PCs.

To obtain a magnetic HMM, the excitation of ring currents is necessary to create a magnetic moment along the axis, for which it is convenient to use layered structures with 2D periodic ring strip resonators on substrates, made using photolithography, with a subsequent 1D periodic arrangement of the layers. In the low-frequency region, such structures exhibit diamagnetism, since the ring current opposes the magnetic field change. For negative μ_{zz}^{-1} , current resonance is necessary, for which the contribution to polarization is in antiphase with the field. In this case, an electric polarization in the plane of the ring also arises. The losses hamper the occurrence of negative μ_{zz} . To get large μ_{zz} , it is reasonable to apply periodically arranged planar spirals or strongly coupled double rings. In this case, it is possible to ignore the components ϵ_{xx} and ϵ_{yy} , since they are small compared to μ_{zz} . Split-ring resonators create a longitudinal magnetization and two transverse components of electric polarization, i.e., the PC is described by diagonal tensors $\hat{\epsilon}$ and $\hat{\mu}$. The PC of volume spirals is a strongly bianisotropic AM.

HMM properties were first considered in monograph [192] in application to a source (point dipole) in an infinite medium like plasma with a diagonal permittivity tensor (7), in which $\epsilon_{xx} = 1$, and the values of $\epsilon_{zz} = \epsilon$ can be negative. For the dipole radiation, the solution to the problem is obtained in the form of a Green's function. In the case of $\epsilon_{zz} < 0$, it is shown that the radiation power and impedance are infinite, the radiation is anisotropic, and there is a conical surface of a shadow, at the boundary of which the fields turn into infinity,

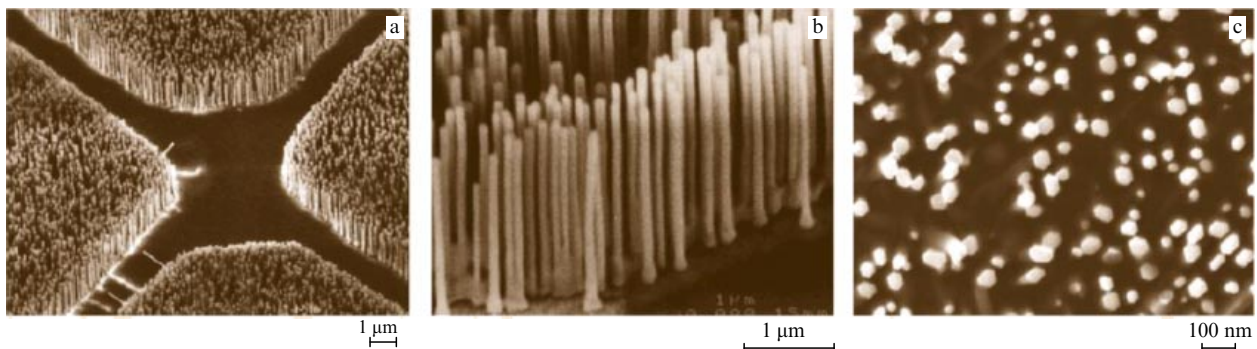


Figure 7. SEM images of an array of ZnO nanowires grown on a sapphire substrate. Image (a) shows patterned growth, image (b) demonstrates high resolution and parallel equalizing of nanowires, image (c) shows faceted sidewalls and a hexagonal cross section of nanowires. For the growth of nanowires on sapphire substrates, a drawing was formed by a layer of Au catalyst 1.0–3.5 nm thick, the role of a shadow mask played by the grid of a transmission electron microscope. (From [180].)

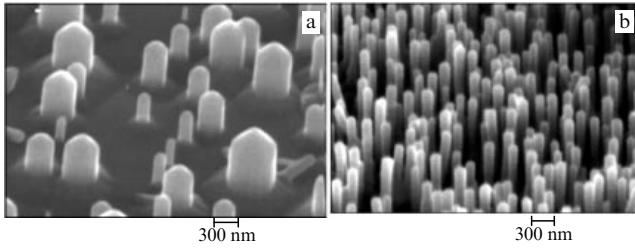


Figure 8. (a) SEM image of ZnO nanocrystals on (1120) sapphire ($P_{\text{ar}} = 100$ mbar, $T_w = 580^\circ\text{C}$, $L = 20$ mm) at the frequency $f_{\text{foil}} = 1$ Hz. (b) The growth of nanorods ($P_{\text{ar}} = 100$ mbar, $T_w = 580^\circ\text{C}$, $L = 20$ mm) at the frequency $f_{\text{foil}} = 10$ Hz. (Results from [184].)

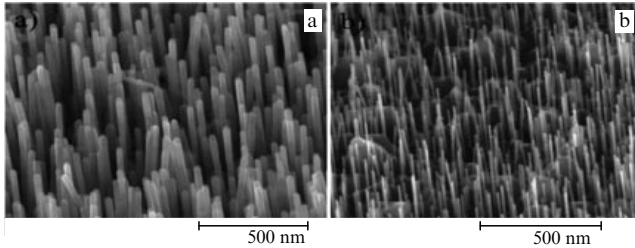


Figure 9. (a) SEM image of ZnO nanorods (manufacturing parameters: laser pulse energy $E_p = 500$ mJ, repetition rate $f_{\text{foil}} = 10$ Hz, pressure $P_{\text{ar}} = 100$ mbar, $L = 20$ mm) at $T_w = 580^\circ\text{C}$ (diameter of nanorods 30–35 nm). (b) SEM image of ZnO nanorods ($E_p = 500$ mJ, $f_{\text{foil}} = 10$ Hz, $P_{\text{ar}} = 100$ mbar, $L = 20$ mm) at $T_w = 550^\circ\text{C}$ and nanorod diameter of 8–15 nm. (Results from [184].)

and inside which there is no radiation. The dipole orientation along and across the axis are considered. The directional pattern in the first case is given by the formula

$$A(\theta) = \frac{\sin^2 \theta}{N^5(\theta)}, \quad N(\theta) = \sqrt{\cos^2 \theta + \varepsilon \sin^2 \theta}.$$

The Helmholtz wave equation becomes hyperbolic at negative permittivity components. The characteristics of hyperbolic equations are known to have discontinuities. Particularly, in the process of propagation of pulses (wave packets) in a dispersive medium, the discontinuity surfaces move with the speed of light. In HMMs, there are static spatial discontinuity surfaces. For nonstationary processes, the HMM behavior is complex. It is necessary to study the spectral integrals involving $\hat{\varepsilon}(\omega, \mathbf{k})$. The considered properties manifest themselves under the long-term action of a quasi-monochromatic pulse. Analogous properties are inherent in a gyrotropic medium with the permittivity tensor (8). Reference [192] considers linear sources. In the presence of losses and for distributed sources, infinity is shown to be eliminated.

3.1 Super-Planck radiation, channeling and stimulation of radiation, and image processing

The change in photonic DOS is an important property. The radiation becomes anisotropic with the possibility of a spacial increase in photonic DOS. This phenomenon is investigated in [18, 27, 35–46, 48, 127, 141, 175–180]. The increasing number of quasi-photons with High k (Hk-states) giving rise to an increase in their DOS and a reduction in the lifetime of excited atoms causes an increase in the radiative heat conductivity, thermal radiation [194–198], and heat flow from a unit area substantially exceeding that determined by

the Stephan–Boltzmann law at certain orientations [27, 193]. This is due to the increase in DOS (ideally, up to infinity) and the anisotropy. Actually, the maximal density of photon states $\rho(\omega)$ is bounded and increases compared to that of a black body by $\alpha = k_{\text{max}}^2/k_0^2$ times, where the quantity $k_{\text{max}} \sim \pi/a$ is bounded by the lattice constant. For the energy flux density along the HMM symmetry axis, the excess coefficient β was found in [193] for the observed radiation, as opposed to the Stephan–Boltzmann radiation: $S_T \approx \beta S_T^{\text{SB}}$, where $\beta = 5(k_p \alpha)^2 / (4\pi k_T)^2$ for HMMs of the first type (here, $k_T = k_B T / (\hbar c)$) and $\beta = (\alpha/2)^2 \varepsilon_d / (1-p)$ for HMMs of the second type, where p is the factor of filling with a conductor, and k_p is the plasma wave number. At $a \sim 10$ nm, an estimate of $\beta \sim 10^3 - 10^5$ has been obtained.

The emission rate (Einstein's spontaneous emission coefficient) for the dipole \mathbf{d} oriented normally to the layers of an HMM and placed at a distance $d_0 < \lambda$ (in the near field) is given by the expression [38, 41]

$$P_{\text{Hk}} \approx \frac{|\mathbf{d}|^2 \sqrt{|\varepsilon_{xx} \varepsilon_{zz}|}}{16\pi \varepsilon_0 \hbar d_0^3 (1 + |\varepsilon_{xx} \varepsilon_{zz}|)}.$$

The effective medium approximation for the radiation of a dipole was considered also in [16, 38, 40, 135–137]. For the energy density of the thermal radiation in the near-field zone at a distance $z \ll \lambda$ in the approximation of the effective medium [38], the following expression is found:

$$u(z, \omega, T) = \frac{U_{\text{BB}}(\omega, T)}{8} \left[\frac{2\sqrt{|\varepsilon'_{xx} \varepsilon'_{zz}|}}{(k_0 z)^3 (1 + |\varepsilon'_{xx} \varepsilon'_{zz}|)} - \varepsilon'' \frac{2(\varepsilon'_{xx} + \varepsilon'_{zz})}{(k_0 z)^3 (1 + |\varepsilon'_{xx} \varepsilon'_{zz}|)^2} \right],$$

in which the dissipation is taken into account, $\varepsilon'' = \varepsilon''_{xx} = \varepsilon''_{zz}$, U_{BB} is the radiation energy density for an absolutely black body. The approach proposed by S M Rytov for the generation of electromagnetic radiation by thermal fluctuations, the fluctuation-dissipation theorem, and the tensor Green's function of the HMM from [27] were used.

In Ref. [48], the effect of a DOS increase in a complex cavity with an asymmetric HMM (see Fig. 3) is evaluated. In such an HMM, the axis does not coincide with the normal to its surface, and the permittivity matrix [7] is transformed by a rotation of axes into a nondiagonal symmetric one. Direct calculations of the modal field and dispersion equation were carried out allowing for the anisotropy of the hyperbolic medium layer. The Berreman transfer matrix method (4×4 transfer matrix method) was used. The super-Planck emission is due to anisotropy. The directed thermal radiation exceeds the radiation from a black body, either within a certain angle along the axis or in a perpendicular direction, depending upon the HMM type. The effect is used in photovoltaics (in solar batteries for the transfer of radiation from the matching structure to rectifying elements [18, 28]), for control of the density of optical states and radiation switching in nanostructured optical schemes [194–198], for channeling radiation with an increase in its aperture [163, 179, 199], for transferring radiation and images over small distances, for creating waveguide structures, for subwavelength resolution, and for enhancing evanescent modes [200–219].

Physically, HMMs of the first type operate like multiwire lines and those of the second type like sets of plane-parallel waveguides. The fabrication of HMMs with diverging nano-

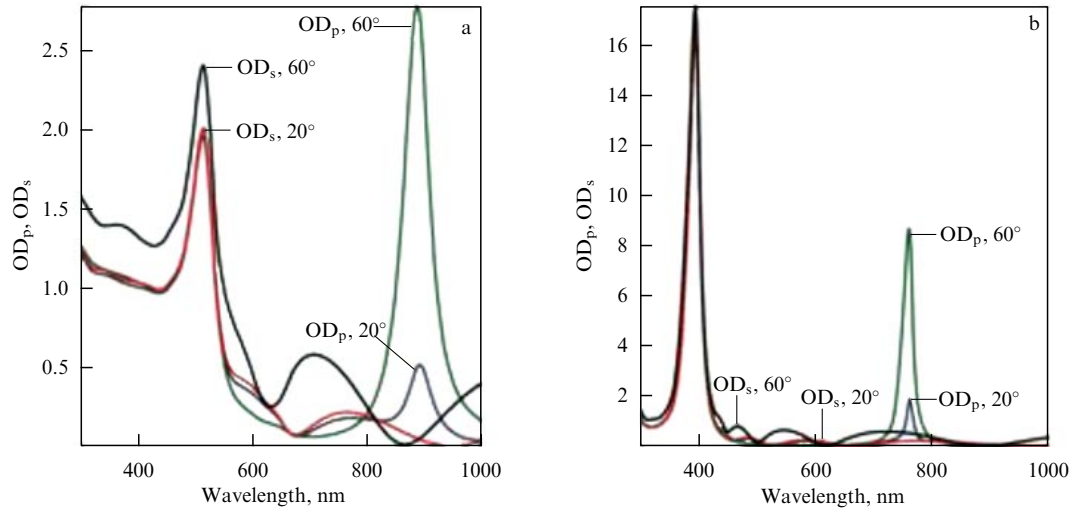


Figure 10. Optical density (OD) as a function of wavelength for p- and s-polarizations in (a) an Au-Al₂O₃ HMM and (b) an Ag-Al₂O₃ HMM at 10% metallic filling in both and the layer thickness of 500 nm. Resonances take place (a) at $\lambda = 500$ nm and $\lambda = 900$ nm, as well as (b) at $\lambda = 400$ nm and $\lambda = 775$ nm. Low-frequency resonances occur only for p-polarization; the resonances are stronger in silver, since the dissipation is smaller. Such resonances are absent in a planar layered structure. (Results according to [39].)

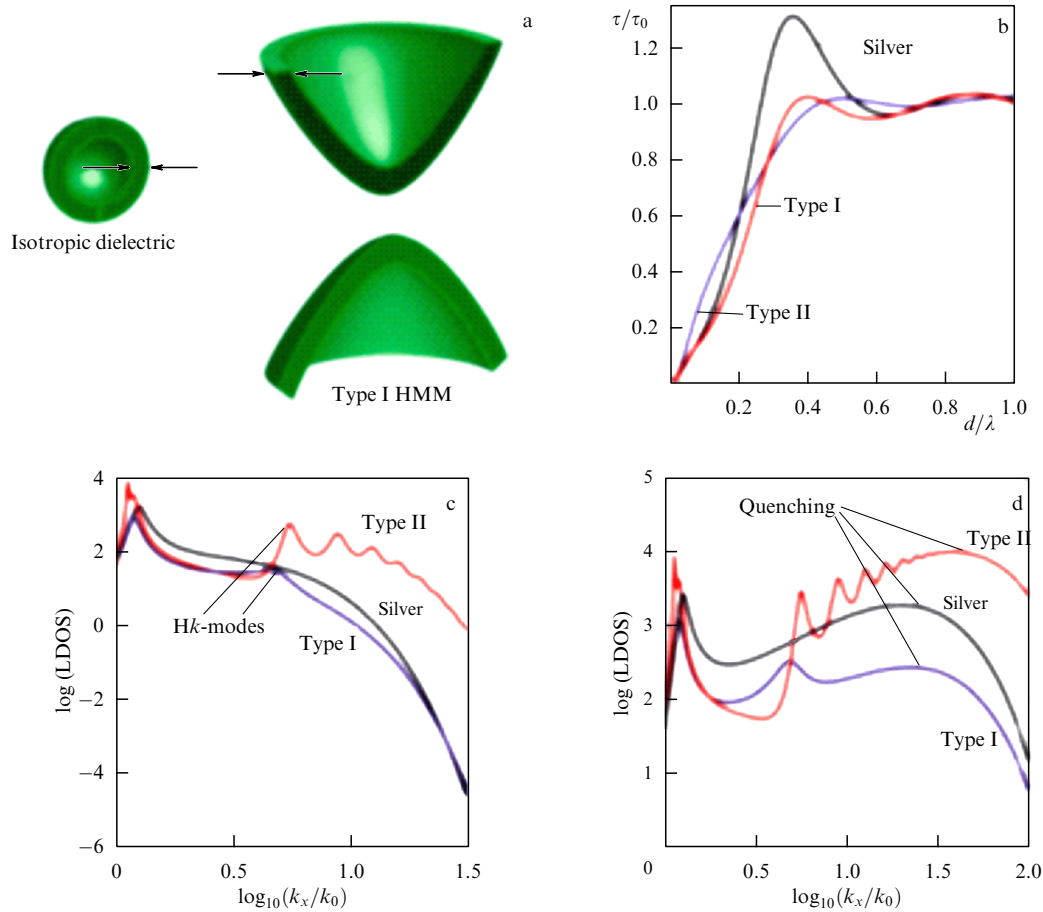


Figure 11. Local density of states (DOS) in HMMs. (a) The isofrequency surface at slightly different energies for an isotropic dielectric and type I HMM. The closed volume between two isofrequency surfaces is a measure of photonic density of the system states. An ideal HMM has a diverging closed volume and, thus, in the ideal limit has an infinite photonic density of states. (b) Lifetime of a dipole, normalized to the lifetime in free space, versus the distance d above the HMM surface. An Ag-TiO₂ structure with 35% filling in the regions of type I HMM ($\lambda = 350$ nm) and type II HMM ($\lambda = 645$ nm). For comparison, we also show the results for a thick silver film ($\lambda = 372$ nm). LDOS versus the wave vector for a 200-nm layer of Ag-TiO₂ (with 35% filling) and 200-nm silver film for the radiators, placed at the distance of (c) 20 nm and (d) 3 nm from the structure. High- k regimes exist in both (c) and (d) cases, but in case (c), a distinct broad peak is seen. (Results according to [39].)

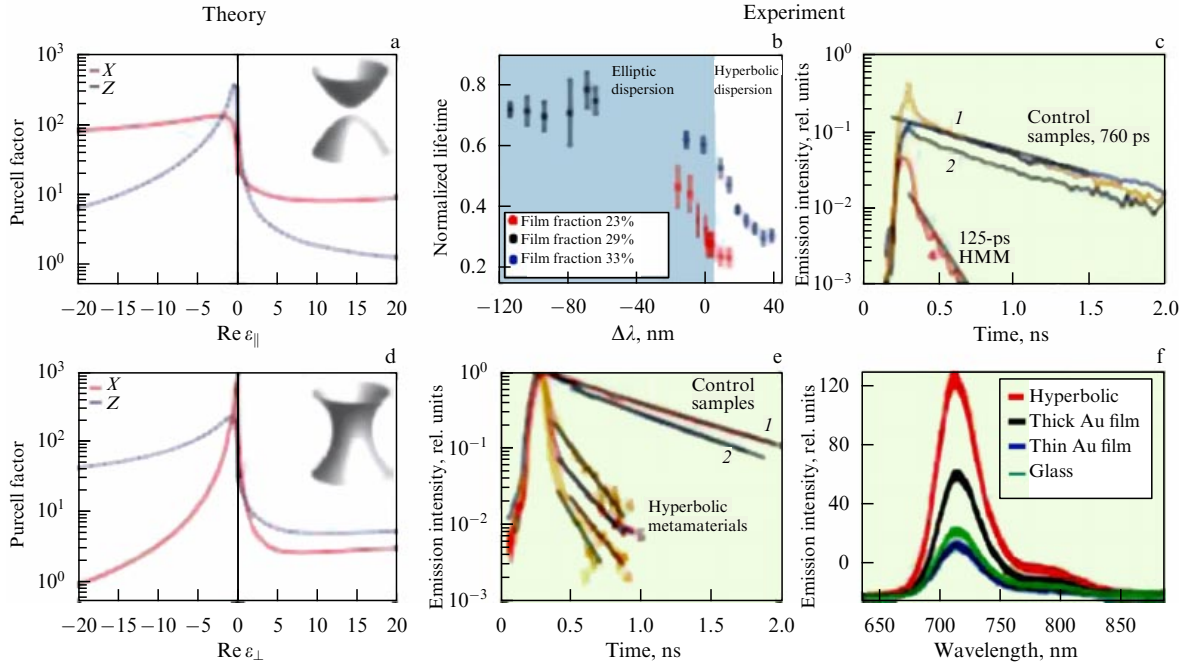


Figure 12. (Color online.) Enhancement of spontaneous emission in HMMs. The Purcell factor in the transition from the elliptic to hyperbolic regime with (a) $\varepsilon_{\parallel} > 0$ and (d) $\varepsilon_{\perp} < 0$. Experiments on spontaneous emission enhancement: (b) dependence of radiation lifetime on wavelength near the transition from the elliptic to hyperbolic regime in a planar layered HMM; (c) photoluminescence kinetics for a dye applied above a silver wire HMM; (e) photoluminescence kinetics for a dye in a layered metal-dielectric HMM; (f) enhancement of photoluminescence kinetics for a dye applied above a layered metal-dielectric material relative to that of a dye on homogeneous films of gold and glass. (Results presented according to [40].)

wires or a fan arrangement of conducting planes or stripes allows magnifying images and overcoming the diffraction limit [279, 217].

Figure 10 presents the results of calculating the DOS for a layer of a nanowire medium under the incidence of p- and s-polarized waves in a layer of HMM. Figures 11 and 12 show the results of calculating the DOS and Purcell effect in HMMs of both types according to the data in [39]. The calculations were carried out for an effective size of the source $a = 0.1k_0^{-1}$, $\text{Im } \varepsilon_{\parallel} = \text{Im } \varepsilon_{\perp} = 0.1$, $\text{Re } \varepsilon_{\perp} = 1$ (Fig. 12a), and $\text{Re } \varepsilon_{\parallel} = 1$ (Fig. 12d). In Fig. 12b, c, curve 1 corresponds to a dye over a pure aluminum membrane, curve 2 to a dye over a gold film on glass, curve 3 to a dye on a silver film on glass, and curve 4 to a dye over a silver coating of an aluminum membrane. Figure 12e shows the dye photoluminescence kinetics in a layered metal-dielectric HMM. Curves 1 and 2 correspond to control samples, in which the dye is applied on the glass and silver substrates, respectively. Curves 3–6 correspond to different samples of metamaterials and different conditions of excitation. Figure 12f shows the enhancement of photoluminescence of a dye applied on a layered metal-dielectric metamaterial with respect to photoluminescence of the dye on homogeneous films of gold and glass.

3.2 Absorbers, screens, lenses, and metasurfaces

An HMM comprising metallic layers 20–40 nm thick between layers of SiO_2 or SiO 50–300 nm thick deposited on glass is an electromagnetic thermal screen, i.e., it reflects more than 90% of the energy of infrared and terahertz radiation and transmits visible light waves well [27]. The optical reflection coefficient oscillates from small values corresponding to the plasmon-polariton excitation to values of the order of 0.1–0.2; therefore, from the side of the incident light, the surface

gradually changes colors as the view angle varies. Applied to window glass, such a thermal screen prevents cooling of a dwelling in winter and heating in summer.

HMMs are anisotropic absorbers whose reflection coefficient strongly depends on the orientation of the axis with respect to the surface, so that almost complete absorption is possible [22, 25, 43–46, 48, 132, 187], as is the electric and optical control of impedance properties, absorption, and reflection. This is possible in HMMs based on graphene by changing the chemical potential [187] or optical pumping, as well as in HMMs based on semiconductor structures. Besides control using an external electric field, control using a magnetic field is convenient, leading to the occurrence of Landau levels and a change in the energy spectrum. Spherically curved layered HMMs and their other configurations acquire the properties of controllable lenses [40, 163, 164, 204, 206, 219] with subwavelength resolution and image transfer to the far-field and near-field zones. In principle, incomplete focusing in the near field by planar layered and curved PCs using evanescent modes is possible.

The HMM surface is an anisotropic impedance surface, along which the propagation of Dyakonov plasmon polaritons is possible. The properties of such a metasurface, in particular, the diffraction of light by it, depend on the cut. If the surface normal to the cut makes an arbitrary angle with the HMM axis, then the tensor (7) is transformed by the rotation matrix. The surfaces of HMMs and other PCs are considered a new class of structure—metasurfaces—with which a new class of devices is associated [220]. Thin two-dimensional metasurfaces are also possible [221]. HMM-based metasurfaces were considered in [36, 37, 222, 223]. In Refs [36, 37, 45, 46], approximate homogenization was carried out based on the Kubo model formula for conduc-

tance and the Bloch equation for the graphene-dielectric HMM. The model calculation of diffraction of p- and s-polarized plane waves by interface and a layer of asymmetric HMMs is carried out. For homogenization, the transverse wave vector was specified to be real-valued. The approximate method of 2×2 transfer matrices was applied, and the possibility of almost complete absorption was shown. The absorption corresponds to the excitation of bulk plasmons along the layers that are almost completely absorbed in a sufficiently thick plate of an HMM, the axis of which is rotated with respect to the surface normal. The considered layer should be described using the 4×4 transfer matrix. If the incident wave is s- or p-polarized, the reflected wave possesses both polarizations.

In the case of bulk plasmon polaritons in an Hk PC, the longitudinal propagation constant is determined, generally, from the Fresnel equation of the fourth order, and only in uniaxial PCs is it separated into two equations, when it is possible to get simple equations for bulk plasmon polaritons [40–49, 118–121]. Note that the Fresnel equation involves two other components and the permittivity tensor that depends on \mathbf{k} . Therefore, to determine the bulk plasmon-polariton equations, additional conditions are required. To determine Dyakonov-type plasmon polaritons along an HMM surface, its input tensor impedance should be known [221]. Such plasmon polaritons are considered in Refs [224, 225].

3.3 Sensors, nanoantennas, waveguides, and control of fluorescence and Raman spectroscopy

The property of image transfer by nanowire lenses [200–219] was proposed for use in sensors [158], including biosensors [226]. When a nanoobject is placed on an HMM surface and exposed to laser radiation, the surface allows ‘finger-printing’ of the object image and identifying the object. Hk structures with plasmon polaritons were used to enhance fluorescence and Raman spectroscopy response in high-sensitivity phase measurements [154, 194], near-field microscopy, and enhanced resolution photolithography. Layered and wire periodic structures have been used as elements of antennas, controlling the directional pattern, and they are promising.

Recently, a number of waveguiding structures with HMM elements have been considered. There is an analogy with terahertz and optical waveguides having a layered cladding and a PC cladding. Instead of a dielectric PC, an HMM is used for the cladding. In the microwave range, wire media and metallic grids were used to manipulate the directional pattern and the polarization (see Fig. 2) in phased array antennas. It is interesting that, beginning in the 1960s, wire AMs were used to simulate the plasma generated by space rocket engines for ground-based optimization of antenna parameters. In Section 5, we will consider a number of applications used and those showing promise in more detail.

4. Methods of analyzing hyperbolic metamaterials

For the structures considered, it is necessary to solve eigenvalue (eigenwave) problems with the dispersion equation in the form $F(\omega, \mathbf{k}) = 0$ or the dispersion band structure; the homogenization problem, i.e., determination of effective permittivity $\hat{\varepsilon}(\omega, \mathbf{k})$; as well as the problem of plane wave diffraction and excitation of the structures by point and other sources. Of importance are the problems of dipole radiation in HMMs and the problems of oscillations in resonators

made of HMMs. The explicit form of $\hat{\varepsilon}(\omega, \mathbf{k})$ is necessary for solving problems of diffraction, excitation, and oscillation, since their direct solution for nanostructures is often unreal and unproductive. Note that the simplest diffraction problems were directly applied to homogenization [56, 57].

4.1 Electrodynamic dispersion equations

Rigorous methods of electrodynamic analysis of PCs (and, in particular, HMMs) can be divided into a few categories (approximate methods are not considered). The first category is based on the solution of Maxwell’s differential equations. Commercial packages of applied software are directly used, a few types of which are currently available. These software packages commonly use the finite element method or finite difference method in space-time or the space domain. For PCs described by a periodic permittivity, the plane wave method is convenient, based on the Floquet–Bloch condition and the Fourier decomposition of permittivity. Indeed, a PC without inclusion of ferromagnetic particles (ferrites) can be described by a periodic permittivity $\varepsilon(\mathbf{r})$. The dispersion equation $F(\omega, \mathbf{k}) = 0$ reduces to the calculation of the determinant of a homogeneous system of linear algebraic equations, obtained by projecting the Fourier transform of Maxwell’s equations.

The second category of programs is based on matrix methods. For one-dimensional PCs representing planar layered HMMs, the method of transfer matrices is rather convenient [23, 69, 123]. For two- and three-dimensional PCs, the formulas can be derived based on the Green’s function method, but they are rather complicated. The Helmholtz wave equation takes the same form as the steady-state Schrödinger equation if we perform the replacements $\mathbf{E} \rightarrow \Psi$ and $k_0^2 \varepsilon(\omega, \mathbf{r}) \rightarrow (2m/\hbar^2)(E - U(\mathbf{r}))$. This allows applying the methods used to calculate the electronic band structure in crystals, in particular, the Corringa–Kohn–Rostoker Green’s function method [227, 228].

Here, we will consider in detail the methods of integral equations based on electrodynamic periodic tensor Green’s functions [33, 229]. Such methods, like the Green’s function methods, can be considered to belong to the third category. Actually, in general, these are integro-differential equations, in which the desired fields are subjected to the action of both differential and integral operators. The reason why this approach is quite convenient is that the homogenization on its base is carried out in the simplest, most efficient, and clearest way, and the analytical results can be obtained by integration. In particular, the dispersion equation derived using the transfer matrix method in a one-dimensional PC follows from the integral equation [229]. The scalar Green’s function for the dielectric base is described by the expression

$$\tilde{G}(\mathbf{r} - \mathbf{r}', k_0, \mathbf{k}) = \frac{1}{\Omega} \sum_{\mathbf{n}=-\infty}^{\infty} \frac{\exp\{-i[(\mathbf{k} + \boldsymbol{\chi}_{\mathbf{n}})(\mathbf{r} - \mathbf{r}')]\}}{(\mathbf{k} + \boldsymbol{\chi}_{\mathbf{n}})^2 - k_0^2 \tilde{\varepsilon}}. \quad (12)$$

Here, \mathbf{a}_l are the vectors of primitive translations (direct lattice vectors), $\mathbf{a}_l \mathbf{b}_m = 2\pi \delta_{lm}$, where \mathbf{b}_l is the reciprocal lattice vector, $\boldsymbol{\chi}_{\mathbf{n}} = n_1 \mathbf{b}_1 + n_2 \mathbf{b}_2 + n_3 \mathbf{b}_3$, $\mathbf{n} = (n_1, n_2, n_3)$, and $\Omega = (\mathbf{a}_1 \mathbf{a}_2 \mathbf{a}_3)$. This is a Green’s function of periodically arranged point sources with a phase shift. 2D and 3D HMMs of the first type can have a cubic lattice with the rotation axis C_4 , and HMMs of the second type can be 1D with the rotation axis C_{∞} . Wire media with a hexagonal lattice and rotation axis C_6 (point group C_{3v} , as in graphene), with the axis C_2 (rectangular section of a wire arrangement) and other

arrangements of wires along the principal dielectric axis z can have the value $\varepsilon'_{zz} < 0$, but they are not HMMs, because they have two optical axes and a more complex Fresnel equation (2). However, they can be considered Hk media. In the case of a 3D HMM consisting of finite-length wires, $l < b/2$, we have

$$\tilde{G}(\mathbf{r}, k_0, \mathbf{k}) = \frac{1}{a^2 b} \sum_{n,l,m=-\infty}^{\infty} \frac{\exp[-i(k_{xn}x + k_{yl}y + k_{zm}z)]}{k_{xn}^2 + k_{yl}^2 + k_{zm}^2 - k_0^2 \tilde{\varepsilon}}. \quad (13)$$

Here, a is the transverse size of a cell, and b is the longitudinal size. In the case of infinite-length wires ($b \rightarrow \infty$), the sum over m transforms into an integral. For a one-dimensional PC, we get

$$\begin{aligned} \tilde{G}(\mathbf{r}, k_0, \mathbf{k}) &= \frac{1}{(2\pi)^2 a} \int_{-\infty}^{\infty} \int_{-\infty}^{\infty} \sum_{m=-\infty}^{\infty} \frac{1}{k_{xn}^2 + k_{yl}^2 + k_{zm}^2 - k_0^2 \tilde{\varepsilon}} \\ &\times \exp\{-i[(k_x + \chi_1)x + (k_y + \chi_2)y + k_{zm}z]\} d\chi_1 d\chi_2. \end{aligned} \quad (14)$$

Such a Green's function is convenient for planar layered PCs and allows, in particular, considering nonuniform layers. In the above relations, $k_{xn} = k_x + 2n\pi/a$, $k_{yl} = k_y + 2l\pi/a$, $k_{zm} = k_z + 2m\pi/b$, and $\tilde{\varepsilon}$ corresponds to the permittivity of the base substance. This Green's function satisfies the inhomogeneous wave Helmholtz equation

$$(\nabla^2 + k^2)\tilde{G}(\mathbf{r} - \mathbf{r}') = -\delta(\mathbf{r} - \mathbf{r}') \exp[-i\mathbf{k}(\mathbf{r} - \mathbf{r}')],$$

and for a delta-source at the point \mathbf{r}' determines the vector potential \mathbf{A} with the phase shift $\mathbf{k}(\mathbf{r} - \mathbf{r}')$ at the observation point \mathbf{r} . It can also be obtained by periodic continuation of the phased Green's function $G = (4\pi R)^{-1} \exp(-ikR)$, $R = |\mathbf{r} - \mathbf{r}'|$, $k = k_0\sqrt{\tilde{\varepsilon}}$. The equivalence is obtained by Poisson summation. It is sufficient to solve the integral equation within the only (zero) cell (Fig. 1c).

Let us place the origin of the coordinate system at the center of a cylinder. The electric vector potential satisfies the equation $(\nabla^2 + k^2)\mathbf{A} = -\mathbf{J}_p^e$, and the fields are presented as $\mathbf{E} = -iZ_0(k + k^{-1}\nabla \otimes \nabla)\mathbf{A}$, $\mathbf{H} = \nabla \times \mathbf{A}$, where

$$\mathbf{A}(\mathbf{r}) = \int_V \tilde{G}(\mathbf{r} - \mathbf{r}', k_0, \mathbf{k}) \mathbf{J}_p^e(\mathbf{r}') d^3r', \quad (15)$$

$Z_0 = \sqrt{\mu_0/\varepsilon_0}$, $\nabla \otimes \nabla \equiv \text{grad}(\text{div})$, and d^3r' is the volume element. For 2D pillar HMMs, the integration is executed over the pillar volume. For a PC, the electric polarization current density $\mathbf{J} = \mathbf{J}_p^e = i\omega\varepsilon_0(\varepsilon - \tilde{\varepsilon})\mathbf{E}$ acts as the most general source. This is an additional current density, as opposed to the displacement current density in a dielectric of the matrix. The integral representation (15) will be written for brevity as $\mathbf{A} = \hat{G}(\mathbf{J}_p^e)$, where \hat{G} is the integral operator in Eqn (15). Then, the electric field will take the form $\mathbf{E} = (k^2 + \nabla \otimes \nabla)\tilde{G}(\chi\mathbf{E})$, where $\chi(\mathbf{r}') = \varepsilon(\mathbf{r}')/\tilde{\varepsilon} - 1$. This hypersingular volume integral equation can be transformed into a number of forms, loaded with surface integrals [230]. Such forms are not convenient in the case of complex-shaped boundaries. We assume that the pillars are homogeneous and use the volume integral equation for the electric field [230],

$$\mathbf{E} = \left(1 + \frac{\chi}{3}\right)^{-1} (k^2 + \nabla \otimes \nabla)\tilde{G}^{\text{V.p.}}(\chi\mathbf{E}), \quad (16)$$

as well as the equation for the magnetic field. Equation (16) follows from the previous one by extracting a spherical

δ -vicinity of the source point \mathbf{r}' and calculating the integral over it analytically at $\delta \rightarrow 0$. As a result, the integrated term $-\chi\mathbf{E}/3$ is extracted, and the integral is calculated in the Cauchy principal value sense, which is denoted by the upper index V.p. (Valeur principal) of the integral operator. For a magnetic field, we have $\mathbf{H} = i\omega\varepsilon_0\nabla \times \hat{G}((\varepsilon - \tilde{\varepsilon})\mathbf{E})$. Inside the pillar, according to the Maxwell's equation $\nabla \times \mathbf{H} = i\omega\varepsilon_0\varepsilon\mathbf{E}$, so that the equation takes the form

$$\mathbf{H} = \nabla \times \tilde{G} \left[\left(1 - \frac{\tilde{\varepsilon}}{\varepsilon}\right) \nabla \times \mathbf{H} \right]. \quad (17)$$

Equation (16) cannot be solved for $\varepsilon = -2\tilde{\varepsilon}$. This condition at $\tilde{\varepsilon} = 1$ determines the accumulation point of the frequencies of localized plasmons [231, 232]: $\varepsilon = \varepsilon_L - \omega_p^2/\omega^2 = -2$, from where we get the accumulation frequency $\omega = \omega_p/\sqrt{\varepsilon_L + 2}$. Therefore, in this case, from a Fredholm equation of the second kind, Eqn (16) turns into a Fredholm equation of the first kind for the frequencies of localized plasmons. In this case, it is better to use the equation in the form of (17) or in another form. The electric field is presented in the form of (15) with replacements $\mathbf{A} \rightarrow \mathbf{E}$, $\mathbf{J}_p^e \rightarrow \mathbf{M}^e = -i\omega\mu_0\mathbf{J}_p^e + (i\omega\varepsilon_0\tilde{\varepsilon})^{-1}\nabla \otimes \nabla \mathbf{J}_p^e$ [233]. Such equations give rise to a surface integral due to the jump in permittivity at the boundary of the body from the value ε inside to $\tilde{\varepsilon}$ outside, namely

$$\nabla \left(\frac{\varepsilon}{\tilde{\varepsilon}} - 1 \right) \mathbf{E} = \mathbf{E} \mathbf{v} \delta(v) \left(1 - \frac{\varepsilon}{\tilde{\varepsilon}} \right) + \frac{\varepsilon}{\tilde{\varepsilon}} \nabla \mathbf{E}.$$

Here, \mathbf{v} is the external normal, and v is the coordinate along it, counted from the surface.

The expansion of the field \mathbf{E} in (16) or the field \mathbf{H} in (17) using N basis functions followed by application of the Galerkin method allows solving the problem. Namely, a homogeneous system of equations $\hat{A}\mathbf{E} = 0$ arises, where the matrix $\hat{A} = \hat{I} - \hat{G}$ is defined according to (16), \hat{I} is the unit matrix, the matrix \hat{G} is determined by the right-hand side of Eqn (16), and \mathbf{E} is a column of the coefficients of the field expansion. The matrices have a block form with the blocks $\hat{A}_{nm}^{vv'}$. The superscripts take the values x, y, z , and the subscripts $1, 2, \dots, N$. Due to (12)–(14), the determinant depends on \mathbf{k} and $k = k_0\sqrt{\tilde{\varepsilon}}$. We have the dispersion equation $\Omega(\mathbf{k}, k_0) = \det \hat{A}(\mathbf{k}, k_0) = 0$. A more detailed consideration can be found in [49, 122]. When solving Eqn (17) numerically, it is necessary to use differentiable volume finite elements.

The task of determining the fields is related to the dispersion problem. When the dispersion is determined, an arbitrary value of the field at some point (or one of the expansion coefficients) is specified, one of the equations is removed, and the field is calculated using the resulting matrix. Such an approach is not very convenient for analytical studies.

Let us consider an approach based on deriving the dispersion equations in the form of functionals. For this purpose, we perform scalar multiplication of Eqn (16) in the form $\mathbf{E} = \hat{L}\mathbf{E}$ by the vector function \mathbf{F}^* and integrate over the volume: $\mathcal{A}(\mathbf{F}, \mathbf{E}) = (\mathbf{F}, \mathbf{E}) - (\mathbf{F}, \hat{L}\mathbf{E}) = 0$. In the solution of Eqn (16), the quantity $\mathcal{A}(\mathbf{F}, \mathbf{E})$, i.e., the steady-state value of the bilinear functional, determines the dispersion equation of the problem in the form $\Phi(k_0, \mathbf{k}) = \mathcal{A}(\mathbf{F}, \mathbf{E}) = 0$. We do not explicitly present the integrals that enter the dispersion equation or other forms of dispersion equations based on

combined integro-differential equations for the magnetic and electric fields. From Eqn (16), it is possible to express k^2 ; however, this quantity nonlinearly enters the integral operator, and then for $\mathbf{F} = \mathbf{E}$ the dispersion equation takes the form

$$k^2 = \frac{(\mathbf{E}, \mathbf{E})(\chi^{-1} + 1/3) - (\mathbf{E}, \nabla \otimes \nabla \tilde{\mathbf{G}}^{\text{V.D.}} \mathbf{E})}{(\mathbf{E}, \tilde{\mathbf{G}} \mathbf{E})}. \quad (18)$$

Here, the scalar products of vector functions (\mathbf{F}, \mathbf{E}) mean integration over the meta-atom volume of common scalar products $\mathbf{F}^* \mathbf{E}$. Obviously, the operator ∇ in (18) can be transferred to \mathbf{E} . Since inside the volume $\nabla \mathbf{E} = 0$, the volume integral reduces to a surface one. In the low-frequency range, one can use the model of ideally conducting metallic meta-atoms [6, 23, 29], which leads to a surface integral equation. The finite-impedance model also yields a similar equation. In the presence of metallic and dielectric meta-atoms, combined volume-surface integro-differential equations generally appear. An analysis of ferrite inclusions is possible by taking into account the electric $\mathbf{J}_p^e = i\omega\epsilon_0(\epsilon - \tilde{\epsilon})\mathbf{E}$ and magnetic $\mathbf{J}_p^m = i\omega\mu_0(\hat{\mu} - \hat{I})\mathbf{H}$ polarization currents based on either coupled integral equations for \mathbf{E} and \mathbf{H} or integro-differential equations with respect to any of the fields. It should be noted that analyses of thin films with thickness t is possible by introducing the electric $\sigma = i\omega\epsilon_0 t(\epsilon(\omega) - \tilde{\epsilon})$ and magnetic $\hat{\sigma}^m = i\omega\mu_0 t(\hat{\mu} - \hat{I})$ surface conductivities.

Planar layered 1D HMMs are most simply and exactly described based on matrix methods. In the case of isotropic layers, it is convenient to introduce the normalized transfer matrix of the layer with thickness t : $a_{11} = a_{22} = \cos \vartheta$, $a_{12} = a_{21}/\rho^2 = i\rho \sin \vartheta$, $\vartheta = k_z t$, $k_z = (k_0^2 \epsilon \mu - k_\perp^2)^{1/2}$. These expressions involve the layer permittivity and permeability, as well as the wave impedance in the normal direction z . For E- or H-type waves, $\rho = k_z/(k_0 \epsilon)$ and $\rho = \mu k_0/k_z$, respectively. If conducting sheets are present (graphene, etc.), they are described by the matrix $a_{11} = a_{22} = 1$, $a_{21} = \sigma Z_0$, $a_{12} = 0$, where $Z_0 = \sqrt{\mu_0/\epsilon_0}$ is the vacuum impedance. For each layer, the matrix \hat{a}_k is introduced, and for several layers matrices \hat{a}_k are multiplied. Let \hat{A} be the result of such multiplication for an HMM of two or more layers in a period. The Floquet–Bloch condition yields the dispersion equation $\cos \psi = X$ or $\psi = \arccos X$. Here, $X = (A_{11} + A_{22})/2$, and ψ is the phase shift by the period d . It is convenient to write $k_z d = \pm i \ln(X \pm \sqrt{X^2 - 1})$.

Let there be a metallic (d_1) and a dielectric (d_2) layer, so that $d = d_1 + d_2$. From the dispersion equation, we determine $k_z = \arccos(X)/d$. This is just the component that also enters dispersion equation (1). Besides it, both dispersion equations contain k_\perp^2 . However, these are different equations: Eqn (1) corresponds to a homogeneous medium, i.e., it is macroscopic, while the derived equation involves permittivities and thicknesses of layers, so that it is an exact microscopic dispersion equation. Given the magnitude of k_\perp^2 determines the angle $\theta = \arctan(k_\perp/k_z)$ of the direction of wave propagation with respect to the axis, this equation allows numerical construction of an isofrequency surface (Fig. 13). Just this surface should be considered the main one. Such a surface consists of identical closed surfaces periodically arranged in the \mathbf{k} -space, corresponding to Brillouin zones [50]. It is possible to construct such surfaces in the higher-frequency zones. At the same time, the surface obtained from Eqn (1) is a model one, based on homogenization. It corresponds to low frequencies and the condition $a \ll \lambda$. For homogenization, one should use the microscopic dispersion

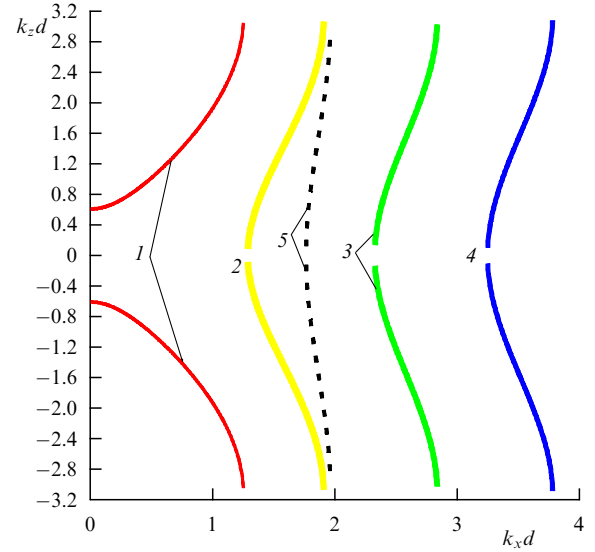


Figure 13. (Color online.) First Brillouin zone of a planar layered dissipation-free HMM based on the rigorous dispersion equation at $d = 200$, $\lambda_p = 100$, $\epsilon_L = 10$, $\epsilon_d = 3.5$, $t_m = 50$ (curves 1–4) and $t_m = 100$ (curve 5) for the wavelengths 680 nm (curve 1), 650 nm (curve 2), 600 nm (curve 3), 550 nm (curve 4), and 500 nm (curve 5).

equation. If there is no dissipation, then in Eqn (1) an arbitrary value of k_\perp^2 can be specified, which corresponds to the possibility of propagation of very slow plasmon polaritons. In this case, by specifying the amplitude and the propagation direction of the Bloch wave, we get all the information about the exact fields in the layers, based on which we can carry out the homogenization, i.e., determine $\hat{\epsilon}(\omega, k_\perp, k_z)$ [69]. However, the isofrequency surface based on the microscopic dispersion equation for Bloch waves does not exactly correspond to Eqn (1), since at $k_\perp \gg k_0$ we get $k_{zz}^2 < 0$, and at $k_\perp < k_0$ the value of k_{zz}^2 is bounded from above. Indeed, consider an E-plasmon polariton in an HMM consisting of metallic layers in a base with the permittivity $\tilde{\epsilon}$, corresponding to an extraordinary wave. Let this plasmon be very slow along the layers: $k_x > k_0 \sqrt{\tilde{\epsilon}}$, $\epsilon < -1$. We have [36, 69]

$$X = \cos \vartheta_1 \cos \vartheta_2 - W \sin \vartheta_1 \sin \vartheta_2.$$

Here, $\vartheta_1 = -id_1(k_x^2 + k_0^2|\epsilon|)^{1/2}$, $\vartheta_2 = -id_2(k_x^2 - k_0^2\tilde{\epsilon})^{1/2}$, and $2W = \rho_1/\rho_2 + \rho_2/\rho_1$. In this nondissipative case, $X = \cosh |\vartheta_1| \cosh |\vartheta_2| - W \sinh |\vartheta_1| \sin |\vartheta_2|$. For propagation along the z -axis, the condition $-1 < X < 1$ must hold, which is possible only if $W > 0$. However, $W < 0$, so that k_z is an imaginary quantity and corresponds to a band gap.

Now let the plasmon be slow, but $k_0 < k_x < k_0 \sqrt{\tilde{\epsilon}}$. Then, the metallic medium is nontransparent, and the dielectric medium, on the contrary, is transparent:

$$X = \cosh |\vartheta_1| \cos \vartheta_2 + iW \sinh |\vartheta_1| \sin \vartheta_2,$$

$$2W = i \left(\frac{d_2 |\vartheta_1|}{d_1 |\epsilon| \vartheta_2} - \frac{d_1 |\epsilon| \vartheta_2}{d_2 |\vartheta_1|} \right).$$

From the inequality, a condition follows:

$$1 - \frac{1}{\cosh |\vartheta_1| \cos \vartheta_2} < |W| \tan \vartheta_2 < 1 + \frac{1}{\cosh |\vartheta_1| \cos \vartheta_2}.$$

If the dielectric layer is nonresonant, the cosine and the tangent are positive. If both layers are electrically thin, then

$$1 - \frac{1}{1 + (|\vartheta_1|^2 - \vartheta_2^2)/2} < |W|\vartheta_2 < 1 + \frac{1}{1 + (|\vartheta_1|^2 - \vartheta_2^2)/2}.$$

Now,

$$2|W| = \sqrt{\frac{k_x^2 + k_0^2|\varepsilon|}{k_0^2\tilde{\varepsilon} - k_x^2}} - \sqrt{\frac{k_0^2\tilde{\varepsilon} - k_x^2}{k_x^2 + k_0^2|\varepsilon|}}.$$

The maximal deceleration of the plasmon polariton means that $k_x \approx k_0\sqrt{\tilde{\varepsilon}}$, $|\varepsilon| \approx 1$ [69, 122]; therefore, a region always exists where the above condition is fulfilled. If the polariton is fast along the layers, then in the perpendicular direction wave propagation takes place. This means that Eqn (1) should be used for homogenized PCs without considering periodic microstructure, in which the component k_z is defined to $2n\pi/d$ and in this sense can take arbitrarily large values at $k_0d \ll 1$, which corresponds to the homogenization. However, Eqn (1) can be applied to the determination of one of the components of the permittivity, if another component and the wave vector are found from independent equations. The ordinary H-wave for metal-dielectric HMMs is of no interest.

In matrix approaches, it is possible to consider wave matrices coupling the amplitudes of waves in two directions, as well as to use the Berreman-type 4×4 matrices that appear in the case of anisotropic conducting surfaces, like graphene, and anisotropic layers. The dimension of this matrix is due to the presence of four tangent field components in a general case. The fourth order of the Fresnel equation generally yields four waves (with both directions taken into account) for a homogeneous anisotropic layer. The problems of diffraction by finite and semi-infinite planar layered structures are also easily solved using the transfer matrices [69, 123]. They allow determining the input impedance Z_{in} at the HMM boundary. Equating Z_{in} to the impedance of vacuum, we get the dispersion equation for surface plasmons $k_{\perp} = k_0(1 - Z_{in}^2)^{1/2}$ along the HMM. The strongly reactive (almost imaginary) impedance leads

to slow plasmons. The inductive impedance leads to a forward surface plasmon polariton, and the capacitive impedance to a backward one [123].

4.2 Homogenization, methods of averaging, and isofrequency surfaces

Homogenization is a procedure that determines the material parameters of a homogeneous (uniform) medium based on the solution to the electrodynamic problem. Correspondingly, the waves in a homogeneous medium and in a structured PC should be in some sense equivalent, as should the corresponding structures with respect to diffraction. For diffraction, the Ewald–Oseen extinction theorem must hold; therefore, the structure must have many periods and the fields should be considered in the far-field zone (compared to the period).

Several methods of introducing material parameters are known [89]. The simplest homogenization of a layered bilayer-periodic AM including the HMM in the low-frequency limit without considering the spatial dispersion is described by the equations [62–69]

$$\varepsilon_{\perp} = \varepsilon_{xx} = \frac{\varepsilon_1 d_1 + \varepsilon_2 d_2}{d}, \quad \varepsilon_{zz} = \varepsilon_{\parallel} = \left(\frac{\varepsilon_1^{-1} d_1 + \varepsilon_2^{-1} d_2}{d} \right)^{-1}, \quad (19)$$

where ε_1 is the permittivity of the metal and ε_2 is the permittivity of the dielectric. If the layers possess magnetic properties, then for the permeability tensor equations like (19) can also be written. With dissipation considered, the components of (19) are complex-valued.

Figure 14 presents the results of permittivity calculations based on (19) according to Ref. [39] (where the notations $\varepsilon_{\parallel} = \varepsilon_{xx}$, $\varepsilon_{\perp} = \varepsilon_{zz}$ are accepted). The homogenization with the spatial dispersion taken into account was considered in [67–69, 234]. In particular, consideration of the fields in the layers and the two Fresnel equations for ordinary and extraordinary waves yields [69]

$$\varepsilon_{xx} = k_0^{-2} [k_x^2 + k_{1z}^2 d^{-2} (d_1^2 + d_1 d_2) + k_{2z}^2 d^{-2} (d_2^2 + d_1 d_2)], \quad (20)$$

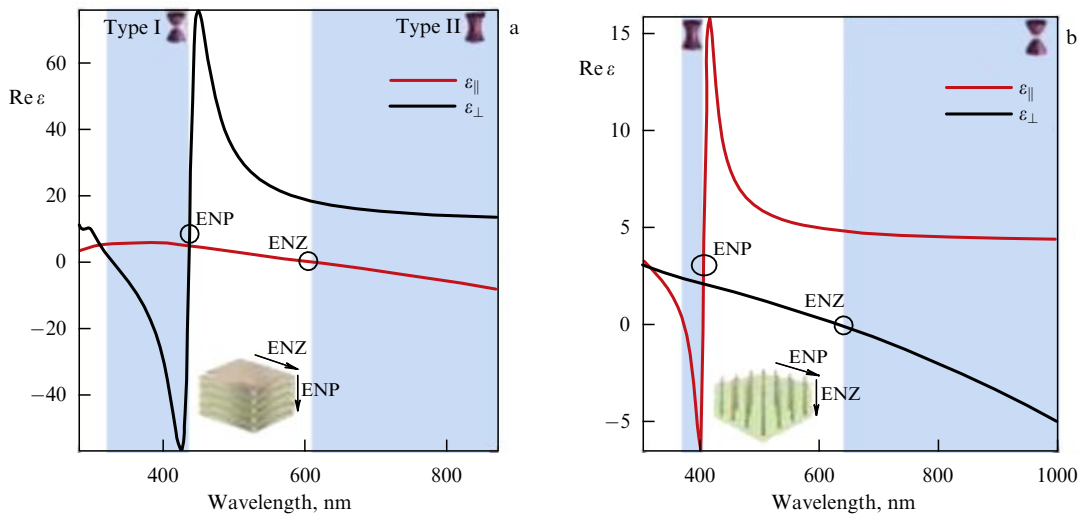


Figure 14. (Color online.) Dielectric permittivities. (a) Planar layered HMM: real parts of permittivity for a planar layered Ag-TiO₂ structure with 35% silver, calculated based on the effective medium theory. (b) Wire HMM: real parts of permittivity for Ag-Al₂O₃ with 15% silver. Hyperbolic regimes of type I and II and the ENZ (epsilon near zero) regions are highlighted. (Data from [39].)

$$\varepsilon_{zz} = k_0^{-2} k_x^2 \times \left[1 - \frac{k_{1z}^2 d^{-2} (d_1^2 + d_1 d_2 \varepsilon_2 / \varepsilon_1) + k_{2z}^2 d^{-2} (d_2^2 + d_1 d_2 \varepsilon_1 / \varepsilon_2)}{k_x^2 + k_{1z}^2 d^{-2} (d_1^2 + d_1 d_2) + k_{2z}^2 d^{-2} (d_2^2 + d_1 d_2)} \right]^{-1}. \quad (21)$$

In the simplest case $d_1 = d_2$, from both (19) and (20), (21), it follows that $\varepsilon_{xx} = (\varepsilon_1 + \varepsilon_2)/2$, $\varepsilon_{zz} = 2\varepsilon_1 \varepsilon_2 / (\varepsilon_1 + \varepsilon_2)$. It is interesting that the same result with the depolarization taken into account is obtained by Garnett–Bruggeman homogenization. The ENZ region for ε_{zz} arises at $\varepsilon_1 \approx 0$, while for the component ε_{xx} the corresponding condition is $\varepsilon_1 \approx -\varepsilon_2$. For a dissipative metal with $\varepsilon_1 = \varepsilon(\omega)$ and a nondissipative dielectric with $\varepsilon_2 = \tilde{\varepsilon}$ we have

$$\varepsilon'_{xx} = \frac{1}{2} \frac{\varepsilon_L + \tilde{\varepsilon} - \omega_p^2}{\omega^2 + \omega_c^2}, \quad \varepsilon'_{zz} = \frac{2\tilde{\varepsilon}[\varepsilon'_{xx}(\varepsilon'_{xx} - \tilde{\varepsilon}) + \varepsilon''_{xx}{}^2]}{\varepsilon'_{xx}{}^2 + \varepsilon''_{xx}{}^2}.$$

It follows that the condition for the existence of such an HMM is the inequality $\varepsilon'_{xx} < 0$ or $\omega = (\omega_p^2 / (\varepsilon_L + \tilde{\varepsilon}) - \omega_c^2)^{1/2}$, since in this case always $\varepsilon'_{zz} > 0$. The condition $\varepsilon'_{zz} < 0$, $\varepsilon'_{xx} > 0$ is also possible, and it means a transition from an HMM of the second type to an HMM of the first type. In this case, $-\tilde{\varepsilon} < \varepsilon' < 0$, which is valid in the region $\omega_p / \sqrt{\varepsilon_L + \tilde{\varepsilon}} < \omega < \omega_p / \sqrt{\tilde{\varepsilon}_L}$. It is possible to obtain the hyperbolicity regions from the general relations (19)–(21), the result depending on k_x , i.e., on the spatial dispersion. The corresponding results are presented in Fig. 15 for real-valued k_x . In the case of diffraction of a plane wave incident from a vacuum, $k_x < k_0$. For the emission of a dipole in an infinite HMM, there is no such restriction, and k_x is complex-valued. Since the signs of $\pm k_x$ and $\pm k_z$ can be chosen independently, bulk plasmon polaritons in four directions take place. The above components are related by the dispersion equation. Having calculated the Poynting vector, we can determine the complex-valued components. In particular, $\langle S_x \rangle$ determines k_x'' . On the other hand, the Green's function for the HMM is found by expansion in plane waves, where the integration is performed over real components [131, 233]. Figure 4 presents the results of the p- and s-polarized wave diffraction for layers of wire and planar layered HMMs according to [39]. Analogous results for the diffraction and homogenization in a wire HMM are presented in Ref. [235].

Consider an approach to homogenization based on the effective medium theory, determining the permittivity of the composition in the low-frequency limit [95, 96, 235–238]. The Maxwell models or formulas (weak scattering approximation) [96] $\varepsilon^{\text{eff}} = \tilde{\varepsilon} [1 + 3\delta(\varepsilon - \tilde{\varepsilon}) / (2\tilde{\varepsilon} + \varepsilon)]$ are often used, as are the J K M Garnett and D A G Bruggeman models (effective field model) and a number of other models. In our case, $\delta = d_1 l d$ is the concentration of metallic layers. Commonly, the rigorous formulas are obtained for spherical particles in the low-frequency limit, but they can be extended to ellipsoids and cylinders. Thus, the Garnett formula takes the form

$$\frac{\varepsilon^{\text{eff}} - \tilde{\varepsilon}}{L(\varepsilon^{\text{eff}} - \tilde{\varepsilon}) + \tilde{\varepsilon}} = \delta \frac{\varepsilon - \tilde{\varepsilon}}{\tilde{\varepsilon} + L(\varepsilon - \tilde{\varepsilon})}, \quad (22)$$

and for the Bruggeman formula we have

$$\delta \frac{\varepsilon^{\text{eff}} - \varepsilon}{\varepsilon^{\text{eff}} + L(\varepsilon - \varepsilon^{\text{eff}})} + (1 - \delta) \frac{\varepsilon^{\text{eff}} - \tilde{\varepsilon}}{\varepsilon^{\text{eff}} + L(\tilde{\varepsilon} - \varepsilon^{\text{eff}})} = 0. \quad (23)$$

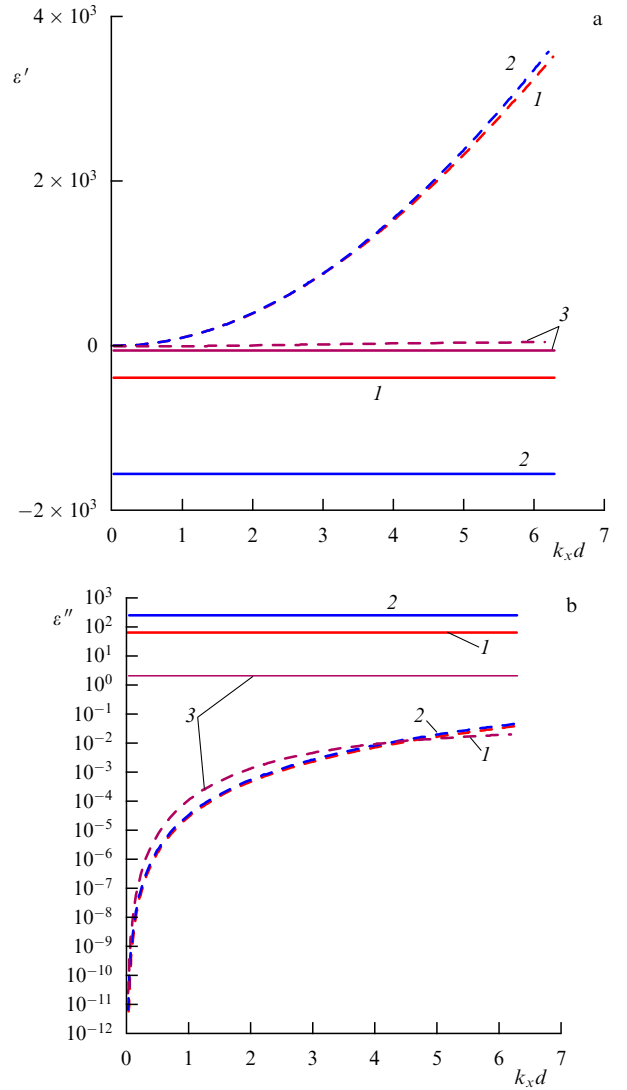


Figure 15. (Color online.) Spatial dispersion: values of (a) real components ε'_{xx} (solid curves) and ε'_{zz} (dashed curves) and (b) imaginary components ε''_{xx} (solid curves) and ε''_{zz} (dashed curves) depending on the normalized component of the wave vector $k_x d$. Curves 1: $k_0 d = 0.1$, $d_1/d = 0.1$; curves 2: $k_0 d = 0.1$, $d_1/d = 0.4$; curves 3: $k_0 d = 0.5$, $d_1/d = 0.4$.

Here, L are the depolarization factors (coefficients) that have different values for different directions of the field. Therefore, formulas (22), (23) determine the components of tensor effective permittivities. For a cylinder, $L_{\parallel} = 0$, $L_{\perp} = 1/2$. In the case of spherical particles, $L_x = L_y = L_z = 1/3$, and formulas (22), (23) turn into formulas well known in the literature [97]. For a metallic layer, one should take $L_z = 1$, $L_x = L_y = 0$. From the Garnett formula, in the case of a layered HMM, we have $\varepsilon_{xx} = \tilde{\varepsilon} + d_1/d(\varepsilon - \tilde{\varepsilon})$, $\varepsilon_{zz} = \tilde{\varepsilon}(\varepsilon - \delta\tilde{\varepsilon}) / (\varepsilon - \delta(\varepsilon - \tilde{\varepsilon}))$, which coincides with (19). As can be easily checked, the same result follows from the Bruggeman formula. For an HMM consisting of metallic cylinders with length l in a lattice $a \times a \times b$ ($l < b$), from both formulas it follows that $\varepsilon_{zz} = \tilde{\varepsilon} + \delta(\varepsilon - \tilde{\varepsilon})$, $\varepsilon_{xx} = \tilde{\varepsilon} [1 + 2\delta(\varepsilon - \tilde{\varepsilon}) / (\varepsilon + \tilde{\varepsilon})]$. Here, the concentration of the cylindrical meta-atoms is $\delta = \pi r^2 l / (a^2 b)$. As above, it is not difficult to derive the conditions under which such an AM is an HMM. The Garnett formula that has the restriction $\delta < 1/3$ is seen to be valid in a planar layered

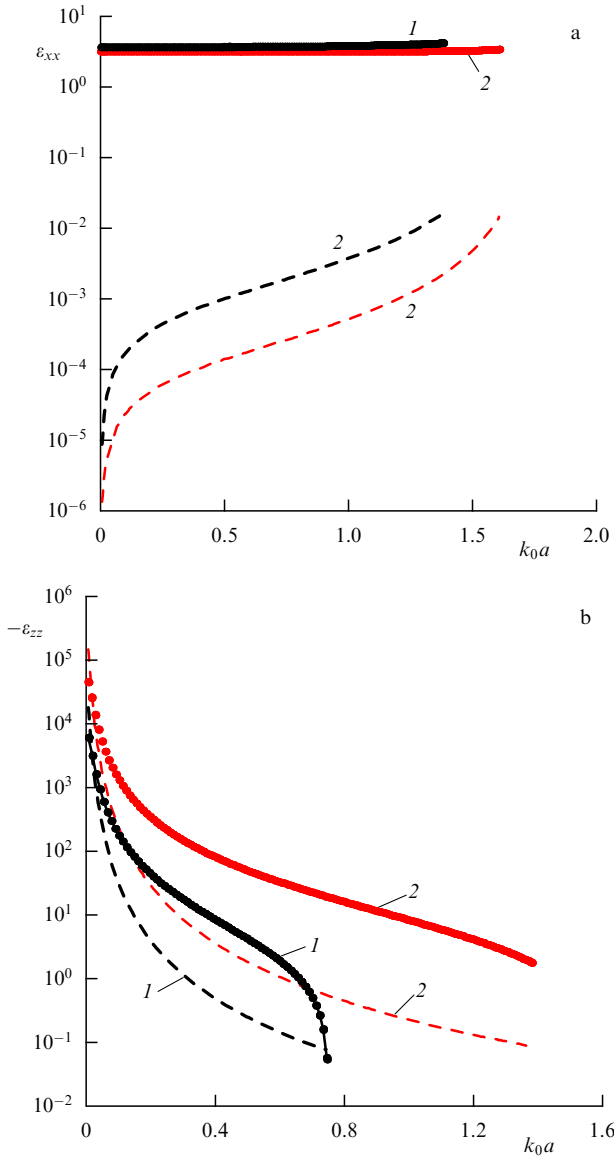


Figure 16. (Color online.) Real values of ε'_{xx} and $-\varepsilon'_{zz}$ (solid curves) and negative imaginary parts ε''_{xx} and ε''_{zz} (dashed curves) of (a) ε_{xx} and (b) ε_{zz} for homogenization based on the Garnett formula: $r/a = 0.1$, $l/b = 0.5$ (curves 1); $r/a = 0.2$, $l/b = 0.9$ (curves 2). The parameters $a = b = 100$ nm, $\omega_p = 1.9 \times 10^{16}$ Hz, $\omega_c = 5 \times 10^{13}$ Hz, $\varepsilon_L = 10$, $\tilde{\varepsilon} = 3$ are used.

HMM and under the condition $1/3 < \delta < 1$. Figure 16 presents the corresponding results of homogenization (dependence of permittivity components on frequency) for an HMM of finite-length wires (see Fig. 1).

If the homogenization is performed, i.e., the tensor $\hat{\varepsilon}(k_0, k_{\parallel}, k_{\perp})$ is determined, then, according to (1) and (9), we have

$$\frac{\varepsilon'_{\parallel}(k_{\perp}^{\prime 2} - k_{\perp}^{\prime\prime 2}) + 2k'_{\perp}k''_{\perp}\varepsilon''_{\parallel}}{\varepsilon'^2_{\parallel} + \varepsilon''^2_{\parallel}} + \frac{\varepsilon'_{\perp}(k_{\parallel}^{\prime 2} - k_{\parallel}^{\prime\prime 2}) + 2k'_{\parallel}k''_{\parallel}\varepsilon''_{\perp}}{\varepsilon'^2_{\perp} + \varepsilon''^2_{\perp}} = k_0^2, \quad (24)$$

$$\frac{\varepsilon''_{\parallel}(k_{\perp}^{\prime 2} - k_{\perp}^{\prime\prime 2}) - 2\varepsilon'_{\parallel}k'_{\perp}k''_{\perp}}{\varepsilon'^2_{\parallel} + \varepsilon''^2_{\parallel}} + \frac{\varepsilon''_{\perp}(k_{\parallel}^{\prime 2} - k_{\parallel}^{\prime\prime 2}) - 2\varepsilon'_{\perp}k'_{\parallel}k''_{\parallel}}{\varepsilon'^2_{\perp} + \varepsilon''^2_{\perp}} = 0. \quad (25)$$

Since the tensor $\hat{\varepsilon}$ must be the same for both the ordinary and the extraordinary waves, the equations

$$k_{\perp}^{\prime 2} - k_{\perp}^{\prime\prime 2} = k_0^2 \varepsilon'_{\perp}(k_0, k_{\parallel}, 0), \quad 2k'_{\perp}k''_{\perp} = k_0^2 \varepsilon''_{\perp}(k_0, k_{\parallel}, 0) \quad (26)$$

should also be valid. Using (26) without dissipation, it is possible to present Eqn (1) in the form

$$\frac{\mathbf{k}_{\perp}^2}{\varepsilon_{\parallel}(k_0, k_{\parallel}, k_{\perp})} + \frac{k_0^2 \varepsilon_{\perp}(k_0, k_{\parallel}, 0)}{\varepsilon_{\perp}(k_0, k_{\parallel}, k_{\perp})} = k_0^2. \quad (27)$$

However, relations (26) follow from (24), (25) when $\mathbf{k}_{\perp} = 0$, so that actually we have two real-valued equations, (24), (25), for four variables, k'_{\perp} , k''_{\perp} , k'_{\parallel} , and k''_{\parallel} . The other two equations are given by the microscopic dispersion equation in the form $\Omega(\mathbf{k}, k_0) = 0$ or in the form $\omega = \omega(\mathbf{k})$. It is necessary to separate both functions into real and imaginary parts and equate them to zero. For four variables, we get four equations, from which, in principle, these variables can be determined for given k_0 , i.e., they cannot be unbounded. In a nondissipative model, substituting the real-valued function $\omega = \omega(\mathbf{k})$ into (1), we get the isofrequency surface on which the components k_{\parallel} , k_{\perp} change independently. However, this surface is no longer an ellipsoid or hyperboloid of revolution even with the frequency dispersion taken into account, and the spatial dispersion bounds the components k_{\parallel} and k_{\perp} . Thus, the dissipation and spatial dispersion lead to the boundedness of the wave vectors. In the first approximation for the spatial dispersion we have [75, 88]

$$\begin{aligned} \varepsilon_{\perp}(\mathbf{k}, k_0) &= \varepsilon_{\perp}(k_0) + \alpha_{\perp jl}(k_0)k_jk_l, \\ \varepsilon_{\parallel}(\mathbf{k}, k_0) &= \varepsilon_{\parallel}(k_0) + \alpha_{\parallel jl}(k_0)k_jk_l, \end{aligned}$$

where summation over the repeating indices is implied. In the above-mentioned papers [36, 37], the component k_{\parallel} was complex and was determined from the complex Bloch dispersion equation, while $k_{\perp} = k_x$ was considered real-valued. Let $k_{\perp} > k_0\sqrt{\tilde{\varepsilon}}$ and the dissipation be absent. Then, the quantity k_z is imaginary. In this case, $\varepsilon_{\perp} < 0$, but the corresponding term in (1) does not change sign.

Thus, the homogenization for HMMs requires determining two scalar complex quantities that should be found based on Maxwell's equations. There are six such scalar equations. In the general case of a complex symmetric ($\varepsilon_{ij} = \varepsilon_{ji}$) non-Hermitian tensor of a nongyrotropic AM with six complex components, the number of equations corresponds to the number of unknown components. In the symmetric Casimir description, if the tensors $\hat{\varepsilon}$ and $\hat{\mu}$ can be simultaneously diagonalized, there are also six complex unknowns. For a nondissipative gyrotropic uniaxial medium, the Onsager–Casimir conditions should be taken in the form $\varepsilon_{ij} = \varepsilon_{ji}^*$. In the presence of dissipation in such a medium, the permittivity tensor becomes non-Hermitian; however, for the off-diagonal elements, the antisymmetry conditions can be written as $\varepsilon_{ij} = -\varepsilon_{ji}$. Here, four complex unknowns are present. In the AM, it is possible to introduce independently the sublattices for meta-atoms contributing to electric and magnetic polarization (which is impossible in systems of natural substances). These sublattices can be rotated (independent of the possibility of technological implementation of such an AM). Generally, the diagonalization of $\hat{\varepsilon}$ and $\hat{\mu}$ is impossible, and then the number of unknowns exceeds the number of equations, which indicates the limited nature of introducing $\hat{\mu}$. A substantial excess occurs in the symmetric bianisotropic model with four tensors (5). Here, it is necessary to use the symmetry conditions [238–240].

If we approximate the material parameters in some way, e.g., by expansion in powers of k_0 and \mathbf{k} , then the

homogenization can be executed by determining the expansion coefficients from the solution to the inverse problem, minimizing the discrepancy between the exact dispersion and the dispersion determined from the Fresnel equation [229]. For homogenization of uniaxial PCs, one can use Eqns (24), (25) and the rigorous microscopic Bloch dispersion equation $\Omega(\mathbf{k}, k_0) = 0$. However, the latter cannot be resolved with respect to two components $k_x(k_0)$ and $k_z(k_0)$. Therefore, it is necessary to formulate two more real-valued equations or determine one of the components of the complex permittivity tensor. It is simpler to specify the real-valued component k_x and to determine k_z from the complex Bloch equation [36, 37]. Such homogenization is possible by solving the inverse problem of plane wave diffraction.

In the optics of homogeneous magnetodielectric media, besides the Fresnel equation $\mathbf{k}^2 = k_0^2 \epsilon \mu$, the wave impedance $Z = Z_0 \sqrt{\mu/\epsilon}$, $\mathbf{H} = Z(\mathbf{k} \times \mathbf{E})/k$ takes place. However, the introduction of impedances for PCs is ambiguous. It is also impossible to manage with one impedance—the matrix of impedances is required, the elements of which depend on the polarizations and wave vectors. Nevertheless, for a planar layered HMM, it is possible to choose the polarization so that there will be only three components, for which the wave impedance can be introduced. The use of the impedance for homogenization in [62] led to the appearance of magnetic properties in purely dielectric structures and imaginary permittivities for nondissipative structures. For such PCs, $\mathbf{v}_g = \nabla_{\mathbf{k}} \omega(\mathbf{k})$ coincides in the direction with the averaged Poynting vector $\langle \mathbf{S} \rangle = \langle \text{Re}(\mathbf{E} \times \mathbf{H}^*) \rangle / 2$. However, for dissipative PCs, the coincidence is absent. Instead, $\langle \mathbf{S} \rangle$ coincides in direction with \mathbf{k}'' , since the energy moves towards dissipation. In this case, $\mathbf{k}'/|\mathbf{k}'| \neq \mathbf{k}''/|\mathbf{k}''|$, since the phase and energy move in different directions.

The condition for the existence of a backward wave is the inequality $\mathbf{k}' \cdot \mathbf{k}'' < 0$. Let us denote $\mathbf{n}_E = \langle \mathbf{S} \rangle / |\langle \mathbf{S} \rangle|$. This unit vector becomes known if the dispersion equation is solved: the fields and the Poynting vector are found (to an arbitrary factor). Let us introduce the additional condition as $\mathbf{n}_E(k_0, \mathbf{k}) = \mathbf{k}''/|\mathbf{k}''|$. For E-waves in a planar layered medium, it is always possible to choose such a polarization, for which $k_y = 0$. Then, the normalized impedance of the layer is $E_x/(Z_0 H_y)$. Let us denote it as $\rho_l = (k_0^2 \epsilon_l - k_x^2)^{1/2} / (k_0 \epsilon_l)$. Obviously, the averaged impedance is expressed as $\langle \rho \rangle = (\rho_1 d_1 + \rho_2 d_2) / d$. If we write the fields in the layers, impose the Floquet–Bloch conditions, and average the fields, then the averaged impedance can be presented in the form $\langle \rho \rangle = \langle E_x \rangle / (Z_0 \langle H_y \rangle)$. Such an approach was used to derive Eqns (20) and (21) [69].

Let ϵ_{zz} be determined, e.g., from equations (19) or (21), and let $\epsilon'_{zz} > 0$. Then, from the Bloch equation, we determine k_z , and from (1) we have $\epsilon_{xx} = k_z^2 \epsilon_{zz} / (k_0^2 \epsilon_{zz} - k_x^2)$. It follows that at $\epsilon'_{xx} < 0$ the bulk plasmon along x should be slow, and k_x^2 can be determined from the above relations, thus determining the component ϵ_{xx} that does not coincide with (19). If the component ϵ_{xx} is determined from the homogenization relations, then Eqn (1) determines ϵ_{zz} . The results are different, which again emphasizes the ambiguity of homogenization.

Let us consider the averaging method and calculation of polarizations. In planar layered structures, the electric fields have the form $A_l^+ \exp(-ik_z l z) + A_l^- \exp[ik_z l(z - d_l)]$, and the magnetic fields $\rho_l^{-1} \{A_l^+ \exp(-ik_z l z) - A_l^- \exp[ik_z l(z - d_l)]\}$ (up to Z_0^{-1}). The coefficients are related via the wave transfer

matrices. The averaging means

$$\langle E_x \rangle = d^{-1} \left(\int_0^{d_1} E_{x1} dz + \int_{d_1}^d E_{x2} dz \right).$$

In a similar way, $\langle H_y \rangle$ and $\langle E_z \rangle$ are averaged in the case of PCs described by the Green's function (13). In this case,

$$\langle E_x \rangle = \frac{1}{a^2 b} \int_{-a/2}^{a/2} \int_{-a/2}^{a/2} \int_{-b/2}^{b/2} E_x dx dy dz.$$

Actually, in the process of averaging, it is necessary to calculate integrals of the form

$$\int_{-a/2}^{a/2} \exp(-ikx) dx = \frac{2 \sin(ka/2)}{ka} = \text{sinc}\left(\frac{ka}{2}\right).$$

The averaged fields contain sums of products of certain coefficients with the functions $\text{sinc}(\dots)$. For wires infinite in the z -axis direction, the domain of averaging over the coordinate z should be chosen as $(-L < z < L)$ at $L \rightarrow \infty$. To calculate the polarizations in a general case, one should use volume densities of polarization currents $\mathbf{J}_p^e = i\omega \epsilon_0 (\hat{\epsilon}_a - \hat{I}) \mathbf{E}$ and $\mathbf{J}_p^m = i\omega \mu_0 (\hat{\mu}_a - \hat{I}) \mathbf{E}$. Here, the meta-atoms included in a dielectric base with the permittivity $\tilde{\epsilon}$ have tensor macroscopic permittivity $\hat{\epsilon}_a$ and permeability $\hat{\mu}_a$.

In the case of thin layers, the above permittivities can be related to surface conductivities, considering the currents as surface ones. In the case of impedance integral equations, the surface currents are introduced, and all the results presented below differ from those above only by replacing all volume integrals with surface ones. The use of tensors $\hat{\epsilon}_a$ and $\hat{\mu}_a$ in a planar layered structure or tensor conductivities of the layers leads to the fact that the PC is generally not uniaxial and is not described by effective permittivities like (7), but can support Hk-waves. Although the above densities are directly related to microscopic polarizations, one should introduce macroscopic polarizations, with which the macroscopic (averaged or effective) AM parameters should be related.

The present method of homogenization is equivalent to the derivation of macroscopic equations of electrodynamics by averaging microscopic equations over a physically infinitely small volume.

Below, for simplicity we do not consider magnetic particles or quadrupole and higher-order multipole moments in the polarization and the connection of homogenization models (see [89, 241]). The permittivity of meta-atoms is considered isotropic and homogeneous, $\hat{\epsilon}_a = \epsilon$. In this approximation, the charge density has the form $\rho = -\epsilon_0 (\epsilon - \tilde{\epsilon}) \nabla \cdot \mathbf{E}$. Since $\nabla \cdot [(\epsilon - \tilde{\epsilon}) \mathbf{E}] = 0$, and inside a homogeneous particle $\nabla \cdot \mathbf{E} = 0$, we have $(\epsilon - \tilde{\epsilon}) \nabla \cdot \mathbf{E} = -\nabla \cdot (\epsilon - \tilde{\epsilon}) \mathbf{E}$. Since the particle has a sharp boundary, $\nabla \cdot (\epsilon - \tilde{\epsilon}) = -\mathbf{v} \cdot (\epsilon - \tilde{\epsilon}) \delta(v)$, where \mathbf{v} is the external normal and v is the coordinate along it. Thus, the charge density is a surface one. However, we will integrate over the volume to allow considering inhomogeneous particles, as well as because the field \mathbf{E} in the numerical implementation will be searched for in the form of expansions. The functions in the expansions do not satisfy such conditions separately, but their sum in the limit satisfies them.

Consider a cell with the volume $a^2 b$. The electric dipole moment of a unit volume is defined as

$$\mathbf{P}^e = \frac{1}{a^2 b} \int_V \mathbf{r} \rho(x, y, z) dx dy dz.$$

The magnetic dipole moment of the unit volume (magnetization) is defined as

$$\mathbf{M} = \frac{1}{a^2 b} \int_V \mathbf{r} \times \mathbf{J}_p^e \, dx \, dy \, dz,$$

and the magnetic polarization as $\mathbf{P}^e = \mu_0 \mathbf{M}$. The above quantities should also be averaged. Under homogenization, the equations have the form

$$\begin{aligned} \langle D_i \rangle &= \varepsilon_0 \varepsilon_{ij} \langle E_j \rangle = \varepsilon_0 \tilde{\varepsilon} \langle E_i \rangle + \langle P_i^e \rangle, \\ \langle B_i \rangle &= \mu_0 \mu_{ij} \langle H_j \rangle = \mu_0 \langle H_i \rangle + \langle P_i^m \rangle. \end{aligned} \quad (28)$$

These are two systems of equations. If we suppose that the effective permittivity and permeability tensors can be reduced to a diagonal form, then the components ε_{ij} and μ_{ij} are determined from each system of three equations. In a general case of averaging the constitutive equations (5), the number of unknowns is greater than the number of equations, so it is necessary to impose symmetry conditions or other additional conditions.

As an example, consider the homogenization of an HMM consisting of metallic nanowires (cylinders) with length l and radius r , embedded in a dielectric matrix and forming a lattice of parallelepiped cells with the dimensions a , a , b (see Fig. 1). We consider it following Refs [29, 49, 242]. In the case of infinite wires, we can finally calculate the limit at $b > l \rightarrow \infty$ or consider the appropriate problem with the transformed Green's function (13). To derive a dispersion equation, let us use the volume integral equation method. Consider the field inside the cylinder in a cylindrical coordinate system. For this purpose, we take the expansion of the electric field inside the cylinder and its solution satisfying the Maxwell's equations, boundary conditions at the cylinder's boundary, and Floquet–Bloch conditions. The solution of Eqn (16) provides the fulfilment of all these conditions. To avoid the use of a large number of probe basis functions, it is desirable to subordinate them to the Helmholtz equation. In the case of a long wire, the dominant contribution comes from the component E_z . The component E_ρ barely contributes to the transverse polarization. The component E_φ contributes to P_z^m if the radius of the cylinders is sufficiently large. Consider the decomposition of E_z :

$$E_z = \sum_{n=1}^N E_{zn} \cos \left[\frac{(2n-1)\pi z}{l} \right] J_0(\rho \kappa_n). \quad (29)$$

Here, we have chosen the azimuthally independent decomposition that is well consistent with the problem. In a general case, one should use double summation:

$$E_z(\rho, \varphi, z) = \sum_{m=-N}^M \sum_{n=0}^N E_{znm} J_m(\rho \kappa_m) \cos(k_{nz} z) \exp(-im\varphi).$$

The even decompositions with respect to z are considered, since the odd ones correspond to higher frequencies, and their contribution to the dipole moment is absent. In these decompositions, $k_{nz} = (2n-1)\pi/l$ and $\kappa_m = (k_0^2 \varepsilon - k_{nz}^2)^{1/2}$; therefore, they satisfy the Helmholtz equation. Other components are decomposed analogously. An additional condition that can be imposed on the field inside the cylinder to reduce the number of unknown components is $\nabla \mathbf{E} = 0$, or $\partial \rho E_\rho / \partial \rho + \partial E_\varphi / \partial \varphi + \rho \partial E_z / \partial z = 0$. Ignoring the azimuthal dependence, we obtain the relation between the radial

component and the axial one. The azimuthal dependence is important for large radii. In this case, in addition to P_z^m , it gives rise to P_x^e and P_y^e .

In the first approximation, we express the polarization current as $\mathbf{J}_p^e = i\omega \varepsilon_0 (\varepsilon - \tilde{\varepsilon}) \mathbf{z}_0 E_z(\rho, z)$. For the axial dependence, we take two terms: $E_z(\rho, z) = E_0 J_0(\rho \kappa_0) + E_1 J_0(\rho \kappa_1) \cos(k_{1z} z)$. The lower the frequency, the better this approximation. In the low-frequency limit, the polarization current is determined by the conduction current alone, which vanishes at the ends of the wire. In the model of ideally conducting wires, the surface density of current can be replaced with an axial current, and the boundary conditions can be imposed on the surface, $E_z(r, z) = 0$ [24, 29], which is equivalent to the Pocklington approximation in antenna theory. However, in real metals at low frequencies, $\varepsilon \approx -i\sigma/(\omega \varepsilon_0)$, the penetration depth $\delta > \rho$, and the field is distributed following the law $J_0((1-i)\rho/\delta)$, where $\delta = \sqrt{2/(\omega \mu_0 \sigma)}$, i.e., it does not depend much on ρ . At frequencies where $\varepsilon \approx \varepsilon' < 0$, the distribution has the form $J_0(\rho(k_0^2 |\varepsilon'| + k_{1z}^2)^{1/2})$. In these cases, the volume density of polarization current can be considered constant and approximated by a linear axial current. The equation determining the component $E_z(\rho, z)$ has the form

$$E_z(\rho, z) = \chi \left(\frac{\partial^2}{\partial z^2} + k^2 \right) \int_V \tilde{G}(\rho, z, \varphi | \rho', z', \varphi') E_z(\rho', z', \varphi') \, d^3 r'. \quad (30)$$

Here, the element of volume is $d^3 r' = \rho' \, d\rho' \, d\varphi' \, dz'$. The function \tilde{G} , obtained from (13) by transition to the cylindrical system of coordinates, can be represented as [233]

$$\begin{aligned} \tilde{G}(\rho, z, \varphi | \rho', z', \varphi') &= \frac{1}{a^2 b} \sum_{n=-\infty}^{\infty} \sum_{j=-\infty}^{\infty} \sum_{l=-\infty}^{\infty} \sum_{m=-\infty}^{\infty} \frac{1}{\kappa_{jl}^2 + k_{zm}^2 - k^2} \\ &\times \exp(-ik_{zm}(z-z') - in(\varphi - \varphi')) J_n(\rho \kappa_{jl}) J_n(\rho' \kappa_{jl}). \end{aligned} \quad (31)$$

The integration over φ' eliminates the angular dependence in Eqn (30). Therefore, Eqn (30) can be presented in a more convenient form:

$$\begin{aligned} E_z(\rho, z) &= \chi \int_{-l}^l \int_0^r \tilde{G}_0(\rho, z | \rho', z') E_z(\rho', z') \rho' \, d\rho' \, dz', \\ \tilde{G}_0(\rho, z | \rho', z') &= \frac{2\pi}{a^2 b} \sum_{n=-\infty}^{\infty} \sum_{l=-\infty}^{\infty} \sum_{m=-\infty}^{\infty} \frac{(k^2 - k_{zm}^2) J_0(\rho \kappa_{nl}) J_0(\rho' \kappa_{nl})}{\kappa_{nl}^2 + k_{zm}^2 - k^2} \\ &\times \exp[-ik_{zm}(z-z')]. \end{aligned} \quad (32)$$

In these relations, $\kappa_{nl} = (k_{xn}^2 + k_{yl}^2)^{1/2}$. Let us use two conditions to obtain the dispersion equation. The first one is found by integrating Eqn (32) over the cylinder volume. The second one is obtained by multiplying both sides of this equation by $E_z(\rho, z)$ and integrating over the volume. The second-order determinant of the resulting system of equations should be zero, which yields the desired approximate dispersion equation. An equivalent dispersion equation is derived from the same conditions for Eqn (30) using integration by parts. With the homogeneity kept in mind, to determine the field, we assume $E_0 = 1$, and E_1 is found from any of the equations of the system. Specifying k_0 and k_z , we determine k_x from the dispersion equation. In our simplest case, the effective parameters have the form $\hat{\mu} = \hat{I}$, $\varepsilon_{xx} = \varepsilon_{yy} = \tilde{\varepsilon}$, $\varepsilon_{zz} = \tilde{\varepsilon} + \varepsilon_0^{-1} \langle P_z^e \rangle / \langle E_z \rangle$. To calculate the mean

values, the Green's function representation (13) is convenient. It incorporates functions similar to $g(x, k_{xn}) = \exp(-ik_{xn}x)$. We have

$$\begin{aligned} \langle g(k_{xn}) \rangle &= \frac{1}{a} \int_{-a/2}^{a/2} \exp(-ik_{xn}x) dx = \operatorname{sinc}\left(\frac{k_{xn}a}{2}\right), \\ \langle P_z^e \rangle &= 4E_1 \varepsilon_0 (\varepsilon - \tilde{\varepsilon}) r l a^{-3} \frac{J_1(r\kappa_1)}{\kappa_1}, \\ \varepsilon_{zz} &= \tilde{\varepsilon} + \frac{4E_1 (\varepsilon - \tilde{\varepsilon}) r l J_1 \left(\sqrt{k_0^2 r^2 \varepsilon - (\pi r/l)^2} \right)}{a^2 b \langle E_z \rangle \sqrt{k_0^2 \varepsilon - (\pi/l)^2}}. \end{aligned} \quad (33)$$

In the region of very low frequencies, $k_0^2 r^2 \varepsilon \approx -\sigma Z_0 k_0 r^2 \ll (\pi r/l)^2$ and $|k_0^2 r^2 \varepsilon| \ll (\pi r/l)^2$ if $k_0 l \ll \pi^2/(\sigma Z_0 l)$. Then,

$$J_1 \left(\sqrt{k_0^2 r^2 \varepsilon - \left(\frac{\pi r}{l}\right)^2} \right) = i I_1 \left(\frac{\pi r}{l} \right) \approx i \frac{\pi r}{l}.$$

In plasmonics, $\omega_c \ll \omega < \omega_p/\sqrt{\varepsilon_L + 1}$ with weak dissipation $\varepsilon \approx \varepsilon' < 0$, and for $|k_0^2 r^2 \varepsilon| \ll 1$, the Bessel function equals $i((\pi r/l)^2 + |k_0^2 r^2 \varepsilon|)^{1/2}$. The last quantity can be used in a wide range of frequencies $k_0 r \ll 1$. In the plasmonic range, $\varepsilon'_{zz} = \tilde{\varepsilon} - 4(E_1/\langle E_z \rangle)(|\varepsilon'| + \tilde{\varepsilon}) \times r^2 l/(a^2 b)$. Therefore, the hyperbolicity arises at

$$-\varepsilon' > \tilde{\varepsilon} \left[\frac{a^2 b}{4(E_1/\langle E_z \rangle) r^2 l} - 1 \right] = \tilde{\varepsilon} \gamma. \quad (34)$$

We also have $\varepsilon' = \varepsilon_L - \omega_p^2/(\omega^2 + \omega_c^2) \approx \varepsilon_L - \omega_p^2/\omega^2$, so that the hyperbolicity arises at low frequencies $\omega^2 < \omega_p^2/(\tilde{\varepsilon} \gamma + \varepsilon_L)$, since $\gamma \gg 1$. Moreover, for the hyperbolicity, the losses should be small. That is why HMMs, strictly speaking, are implemented at ultralow temperatures, when ω_c can be reduced by a few orders of magnitude. The limit transition $l \rightarrow \infty, b \rightarrow \infty$ at $l \approx b$ in relation (34) makes it valid in the case of infinitely long wires. For ideally conducting wires, this problem was first considered in Ref. [6], and with the field penetration taken into account in Ref. [49]. Increasing r can soften these requirements, but in this case, a difference between μ_{zz} and unity arises. Consider this case. For this aim, the component E_φ should be taken into account, without which $\langle M_z \rangle \equiv 0$. As the simplest approximation, let us take the component $E_\varphi(\rho, z) = E_3 J_1(\rho \kappa_0)$, which corresponds to $H_z(\rho, z) = i Z_0 \sqrt{\varepsilon} E_3 J_0(\rho \kappa_0)$. We have $\mu_{zz} = 1 + \langle M_z \rangle / \langle H_z \rangle$ and the averaged component of the magnetic moment

$$\begin{aligned} \langle M_z \rangle &= 2\pi i l \omega \varepsilon_0 (\varepsilon - \tilde{\varepsilon}) E_3 a^{-2} b^{-1} \kappa_0^{-3} (r \kappa_0)^2 J_2(r \kappa_0) \\ &\approx \pi r^4 l \kappa_0^2 a^{-2} b^{-1} (\varepsilon - \tilde{\varepsilon}) \frac{E_3}{Z_0} \frac{\sqrt{-\varepsilon}}{4}. \end{aligned}$$

The region of hyperbolicity (indefinite metrics) takes place at $\langle M_z \rangle > \langle H_z \rangle$. For $\mu'_{zz} < 0$ and $\varepsilon'_{zz} < 0$, the PC is not an HMM. In this case, it supports backward waves and Hk waves. The case of large radii $r \gg l$ is also possible. Such conducting discs mainly give rise to μ_{zz} and $\varepsilon_{zz} \approx \tilde{\varepsilon}$. Wire ring structures are simpler to simulate and more exactly correspond to a magnetic HMM [107, 109]. In the Landau–Lifshitz approach, an infinite PC is described by the permittivity tensor $\hat{\varepsilon}$ alone.

The simple relations considered with a few terms in the field approximation taken into account can be improved to be more precise. In particular, considering E_φ requires the

solution of the approximate equation for this component. Then, all components of the vector potential should be taken into account in the cylindrical system of coordinates [233]:

$$\begin{aligned} A_\rho(\rho, z) &= \int_V \tilde{G}(\rho, z, \varphi | \rho', z', \varphi') J_\rho(\rho', z') \sin(\varphi - \varphi') d^3 r', \\ A_\varphi(\rho, z) &= \int_V \tilde{G}(\rho, z | \rho', z') J_\varphi(\rho', z') \cos(\varphi - \varphi') d^3 r', \\ A_z(\rho, z) &= \int_V \tilde{G}(\rho, z, \varphi | \rho', z', \varphi') J_z(\rho', z') d^3 r'. \end{aligned} \quad (35)$$

Integrating over the angle, we find that the integration in (35) is executed over the meridional cross section of the cylinder with the functions $\tilde{G}_\rho(\rho, z | \rho', z')$ and $\tilde{G}_\varphi(\rho, z | \rho', z')$ for the first two relations and with the function $\tilde{G}_z(\rho, z | \rho', z')$ for the last one. Here, $\tilde{G}_\rho = -i\tilde{G}_1$ and $\tilde{G}_\varphi = \tilde{G}_1$, and the function \tilde{G}_1 differs from $\tilde{G}_z = \tilde{G}_0$ by the fact that, instead of the Bessel functions J_0 , it involves the Bessel functions J_1 . We now arrive at the following representation of the components:

$$\begin{aligned} E_z(\rho, z) &= (ik_0 \tilde{\varepsilon})^{-1} Z_0 \left[\rho^{-1} \left(\frac{\partial}{\partial \rho} \right) \left(\rho \left(\frac{\partial A_\rho}{\partial z} \right) \right) + \left(k^2 + \frac{\partial^2}{\partial z^2} \right) A_z \right], \\ E_\varphi(\rho, z) &= -ik_0 Z_0 A_\varphi, \end{aligned}$$

which leads to coupled integral equations for the field components, since $J_z = i\omega \varepsilon_0 (\varepsilon - \tilde{\varepsilon}) E_z$, $J_\varphi = i\omega \varepsilon_0 (\varepsilon - \tilde{\varepsilon}) E_\varphi$. In an equation like (16), an additional term arises, and an equation for E_φ additionally appears. Disregarding E_z and E_ρ , we find

$$E_\varphi(\rho, z) = k^2 \chi \int_{-l/2}^{l/2} \int_0^r \tilde{G}_\varphi(\rho, z | \rho', z') E_\varphi(\rho', z') \rho' d\rho' dz'. \quad (36)$$

A fully rigorous model corresponds to considering the angular dependence for all three components of the field \mathbf{E} . It is possible to construct models based on integro-differential equations for the magnetic field as well.

In [243, 244] and a number of other papers, it is proposed to use meta-atoms of other types in the form of dielectric balls of two radii, embedded in two cubic sublattices with radius a , shifted along each of the coordinates by $a/2$. In the above papers, it was stated that under the coincidence of the frequencies of two resonances in two types of balls, when the first resonance is electric-dipole and the second one is magnetic-dipole, the metamaterial will exhibit the properties of a left-handed medium, i.e., will be described by scalar effective material parameters $\varepsilon^{\text{eff}} < 0$ and $\mu^{\text{eff}} < 0$. Here, to disprove this statement, we consider a simple model PC with the inclusion of dielectric cylinders with the parameters $l \ll r$, in which it is possible to ignore all components of the electric field except E_φ . In an isolated ball or cylinder, only this azimuth-independent component (alongside H_ρ and H_z) is present in the fundamental oscillation $H_{01\delta}$, which is magnetic-dipole [243, 244] and can create a magnetic moment. The field of such a mode is described by one component of the vector potential $A_\varphi = A_{0\varphi} J_1(\rho \tilde{\kappa}) \cos(k_z z)$, $\tilde{\kappa} = (k_0^2 \varepsilon - k_z^2)^{1/2}$. In a PC, no azimuthal symmetry is possible, but the contribution of nonsymmetric terms is small and can be disregarded. The contribution of the component $A_\rho = A_{0\rho} J_1(\rho \tilde{\kappa}) \sin(k_z z)$ at small ratio l/r is smaller than that of the components A_φ and $A_z = A_{0z} J_0(\rho \tilde{\kappa}) \cos(k_z z)$. It is possible to take all three components or two components into account. In the latter case, one should put $A_{0z} = 0$ to ensure the divergence-freedom

property of the field, and in the former case one can introduce one amplitude only, since the continuity equation holds. Indeed, we have

$$\nabla \mathbf{A} = (A_{0\rho}\tilde{\kappa} - k_z A_{0z})J_0(\rho\tilde{\kappa}) \sin(k_z z),$$

and also

$$E_\rho = -iZ_0(k_0\tilde{\epsilon})^{-1} [A_{0\rho}k_z^2 + 2A_{0z}k_z\tilde{\kappa}]J_1(\rho\tilde{\kappa}) \sin(k_z z),$$

$$E_z = -iZ_0(k_0\tilde{\epsilon})^{-1} [A_{0z}(\tilde{\kappa}^2 - k_z^2) + A_{0\rho}\tilde{\kappa}k_z]J_0(\rho\tilde{\kappa}) \cos(k_z z).$$

Imposing the condition $\nabla \mathbf{E} = 0$, we find that $A_{0\rho}$ can be arbitrary and $A_{0z}k^2 = 0$, i.e., $A_{0z} = 0$. If we assume $E_\rho = 0$, i.e., take $A_{0\rho}k_z + 2A_{0z}\tilde{\kappa} = 0$, then the divergence freedom condition $\nabla \mathbf{E} = \partial E_z / \partial z = 0$ leads to the requirement that $E_z = 0$, i.e., the existence of only one nonzero component E_φ . In our case, it is convenient to take arbitrary field amplitudes

$$E_\varphi = E_{0\varphi}J_1(\rho\tilde{\kappa}) \cos(k_z z), \quad E_\rho = E_{0\rho}J_1(\rho\tilde{\kappa}) \sin(k_z z),$$

$$E_z = E_{0z}J_0(\rho\tilde{\kappa}) \cos(k_z z)$$

and impose the divergence-freedom condition $E_{0\rho} = E_{0z}k_z/\tilde{\kappa}$. In this case, Eqn (36) becomes modified and completed with two other equations. The independent components E_{0z} and $E_{0\varphi}$ will determine the components ϵ_{zz} and μ_{zz} .

We assume the absence of dissipation, so that it is necessary to investigate the possibility of satisfying the condition $\mu_{zz} < 0$. In general, $E_\varphi(\rho, z)$ should be decomposed in a series of the form (29)

$$E_\varphi(\rho, z) = \sum_{m=0}^{\infty} E_{\varphi m} J_1(\rho\kappa_m) \begin{pmatrix} \cos(k_m z) \\ \sin(k_m z) \end{pmatrix},$$

and the coefficients should be sought. In this expression, the cosine corresponds to the even oscillations with respect to z , and the sine corresponds to the odd ones. The eigenfrequencies of odd oscillations are higher. We consider a simple approximation of the fundamental oscillation $H_{01\delta}$: $E_\varphi(\rho, z) = E_{\varphi 0}J_1(\rho\tilde{\kappa}) \cos(k_z z)$. In [245, 246], the problem for an isolated cylindrical dielectric resonator is solved numerically, and it is shown that this approximation is in good agreement with the exact solution. The component $E_\varphi(\rho, z)$ is related to the components $H_z(\rho, z) = iE_{\varphi 0}\tilde{\kappa}J_0(\rho\tilde{\kappa}) \cos(k_z z)/(k_0Z_0)$ and $H_\rho(\rho, z) = -ik_zE_{\varphi 0}J_1(\rho\tilde{\kappa}) \cos(k_z z)/(\tilde{\kappa}Z_0)$ by the Maxwell equations.

Note that the electric field, as well as the magnetic one, is divergence-free and satisfies Eqn (36). Such a field creates no electric dipole moment. Due to the homogeneity, we set $E_{\varphi 0} = 1$. The magnetic dipole moment is expressed as

$$\langle M_z \rangle = 2\pi i \omega \epsilon_0 (\epsilon - \tilde{\epsilon}) l r^2 a^{-2} b J_2(r\tilde{\kappa}) \operatorname{sinc}\left(\frac{k_z l}{2}\right).$$

Here, $\operatorname{sinc}(k_z l/2) \approx 1$ if the magnitude of k_z is not too large, i.e., angle θ is not too small. Since it is assumed that $\epsilon > \tilde{\epsilon}$, for a negative component of the magnetic field, the value of $\langle H_z \rangle$ should be imaginary and negative. Note that H_z is the complete internal field, to which the microscopic induction $B_z = \mu_0 H_z$ corresponds (the microparticles possess no magnetic properties). The induction $\langle B_z \rangle = \mu_0 \mu_{zz} \langle H_z \rangle$ is macroscopic, just like the field $\langle H_z \rangle$. The model presented in [243, 244] for the action on a single particle of a plane wave with

subsequent summation of the dipole moment of the particles in the PC, which does not account for the infinite number of spatial harmonics, leads to an incorrect result, since the external field is used. Since $\mathbf{H} = \nabla \times \mathbf{A}$, we have $H_z = \rho^{-1} \partial(\rho A_\varphi) / \partial \rho$ or, according to (35),

$$H_z(\rho, z) = i\omega \epsilon_0 (\epsilon - \tilde{\epsilon}) \int_{-l/2}^{l/2} \int_0^r \left[\rho^{-1} \tilde{G}_1(\rho, z | \rho', z') + \frac{\partial}{\partial \rho} \tilde{G}_1(\rho, z | \rho', z') \right] E_\varphi(\rho', z') d\rho' dz'.$$

For averaging, we use the Green's function representation (13). Then, $H_z(x, y, z) = \partial A_y / \partial x - \partial A_x / \partial y$. Now, in Eqn (15), it is necessary to keep in mind that

$$J_{px}^c = J_{p\rho}^c \cos \varphi - J_{p\varphi}^c \sin \varphi, \quad J_{py}^c = J_{p\rho}^c \sin \varphi - J_{p\varphi}^c \cos \varphi.$$

This corresponds to the relations

$$J_{px}^c = -i\omega \epsilon_0 (\epsilon - \tilde{\epsilon}) \sin \varphi J_1(\tilde{\kappa}\rho) \cos(k_z z),$$

$$J_{py}^c = i\omega \epsilon_0 (\epsilon - \tilde{\epsilon}) \cos \varphi J_1(\tilde{\kappa}\rho) \cos(k_z z).$$

We have

$$H_z(\mathbf{r}) = i\omega \epsilon_0 (\epsilon - \tilde{\epsilon}) \int_V J_1(\tilde{\kappa}\rho') \cos(k_z z') \times \left(\cos \varphi' \frac{\partial \tilde{G}(\mathbf{r} - \mathbf{r}')}{\partial x} + \sin \varphi' \frac{\partial \tilde{G}(\mathbf{r} - \mathbf{r}')}{\partial y} \right) d^3 r'. \quad (37)$$

Let us present the final averaged values (see [242]). For $\langle E_z \rangle$, we get

$$\langle E_z \rangle = \frac{\gamma}{a^2 b} \sum_{n,j,l=-\infty}^{\infty} \frac{1}{k_{xn}^2 + k_{yj}^2 + k_{zl}^2 - k_0^2 \tilde{\epsilon}}$$

$$\times (k^2 - k_{zl}^2) \operatorname{sinc}\left(\frac{k_{xn} a}{2}\right) \operatorname{sinc}\left(\frac{k_{yj} a}{2}\right) \operatorname{sinc}\left(\frac{k_{zl} a}{2}\right) I_{njl}, \quad (38)$$

where I_{njl} denotes the integral

$$I_{njl} = \int_V \exp\left[i(k_{xn}\rho \cos \varphi + k_{yj}\rho \sin \varphi + k_{zl}z)\right] \times [J_0(\rho\kappa_0) + E_1 J_0(\rho\kappa_1) \cos(k_{1z}z)] d^3 r'.$$

To calculate this integral, we make use of formulas [233, 247]:

$$\exp(ik_{xn}\rho \cos \varphi) = \sum_{m=-\infty}^{\infty} i^m \exp(-im\varphi) J_m(k_{xn}\rho), \quad (39)$$

$$\exp(ik_{yj}\rho \sin \varphi) = \sum_{m'=-\infty}^{\infty} \exp(im'\varphi) J_{m'}(k_{yj}\rho), \quad (40)$$

which we substitute into Eqn (38). As a result of angular integration, a factor of $2\pi \delta_{mm'}$ appears. The integration over z yields

$$I_{njl} = 2\pi l \sum_{m=-\infty}^{\infty} i^m \int_0^r J_m(k_{xn}\rho) J_m(k_{yj}\rho) \eta_l(\rho) \rho d\rho, \quad (41)$$

$$\eta_l(\rho) = \operatorname{sinc}\left(\frac{k_{lz} l}{2}\right) J_0(\rho\kappa_0)$$

$$+ E_1 \frac{\operatorname{sinc}[(k_{lz} + k_{1z})l/2] + \operatorname{sinc}[(k_{lz} - k_{1z})l/2]}{2} J_0(\rho\kappa_1). \quad (42)$$

The final averaged component is expressed as

$$\langle H_z \rangle = \frac{i\omega\epsilon_0(\epsilon - \tilde{\epsilon})}{a^2b} \sum_{n,j,l=-\infty}^{\infty} I_{zl} \frac{1}{k_{xn}^2 + k_{yj}^2 + k_{zl}^2 - k_0^2\tilde{\epsilon}} \times \text{sinc}\left(\frac{k_{xn}a}{2}\right) \text{sinc}\left(\frac{k_{yj}a}{2}\right) \text{sinc}\left(\frac{k_{zl}a}{2}\right) I_{\rho nj}. \quad (43)$$

In expression (43), it is necessary to calculate the integrals

$$I_{\rho nj} = \int_0^r [k_{xn}\alpha_{nj}(\rho) + k_{yj}\beta_{nj}(\rho)] J_1(\tilde{\kappa}\rho) \rho \, d\rho. \quad (44)$$

Generally, $\langle H_z \rangle$ depends on k_x and k_z (for polarization with $k_y = 0$), so that it is senseless to speak about a negative value of μ_{zz} at a definite frequency, as well as, generally, about simultaneously negative ϵ^{eff} and μ^{eff} ; this property for a certain AM model at a given frequency can appear only in a certain region of the isofrequency surface. It is more convenient in this case to use the notion of negative refraction, proving which requires the calculation of the averaged Poynting vector and the quantity $p = \mathbf{k} \langle \mathbf{S}(k_0, \mathbf{k}) \rangle$, which can be called an index of the forward wave. The wave is forward if $p > 0$, and backward if $p < 0$. In the presence of dissipation, $\text{Re } p$ should be used, since $\mathbf{k}'' \langle \mathbf{S}(k_0, \mathbf{k}) \rangle > 0$. If we take the first approximation

$$\alpha_{nj}(\rho) \approx 4\pi J_1(k_{xn}\rho) \frac{J_1(k_{yj}\rho)}{k_{yj}\rho}, \quad \beta_{nj}(\rho) \approx 2\pi J_0(k_{xn}\rho) J_1(k_{yj}\rho),$$

then, even in this case, we have

$$I_{\rho nj} \approx 2\pi \int_0^r J_1(k_{yj}\rho) \left[k_{xn} (J_2(k_{xn}\rho) + J_0(k_{xn}\rho)) + k_{yj} J_0(k_{xn}\rho) \right] J_1(\tilde{\kappa}\rho) \rho \, d\rho. \quad (45)$$

The integrals (44) should be calculated numerically. Note that both in ϵ_{zz} and in μ_{zz} the dependence on $\epsilon - \tilde{\epsilon}$ vanishes because of cancellation. However, in Eqn (38), there are quantities $k^2 - k_{zj}^2 = k_0^2\epsilon - (k_z + 2\pi l/a)^2$, which can be negative, in particular, they are always negative when $\epsilon < 0$. The above decompositions converge, but clarification of the μ_{zz} sign issue requires significant computational costs to calculate the integrals (44) in double series. The asymptotic estimates at great n and j indexes are difficult to obtain, since the arguments of the Bessel functions vary in a wide range. This difficulty is related to the cylindrical geometry of the problem. To overcome this difficulty, we constructed a similar model with square cylinders, for which the series summation can be carried out analytically. Calculations based on this model have shown that the condition of negative μ_{zz} is not valid. In the case of spherical inclusions considered in [243], the PC has a body-centered cubic lattice. A ball of one sort (size) is located in the crystal cell center, and in the corners of the cube are balls of the other size. Each such ball belongs to eight adjacent cells, while only one eighth of each corner ball belongs to an elementary cell. As a result, a rather complicated configuration appears, which is difficult for analytical investigation, while the numerical analysis allows clarifying the structure of the fields only. The problem is solved much more simply with cubes. The question about negative refraction is much more easily answered by constructing dispersion surfaces (see [248]).

For the averaging procedure, the initial equation is used. For example, Eqn (38) follows from acting on Eqn (15) by the

operator $-iZ_0(k + k^{-1}\nabla \otimes \nabla)$. The averaging leads to smoothing and singularity reduction, which is due to the $\text{sinc}(\dots)$ function. However, series of the (38) type still converge slowly. To make use of Eqn (16), it is necessary to exclude the small ball from the domain of integration over dashed coordinates (source point coordinates), which is inconvenient. In the model with ideally conducting particles, the field does not penetrate into them. Correspondingly, the model is constructed for a surface current density with the surface equations [24, 29]. In this case, in performing the field averaging, one has to omit the domain occupied by the particle. If the problem is solved with sufficient precision, the field inside such particles should be obtained as zero or very small. Commonly, the size of the particles is small, and the effect of such omitting is small even more so. Solving the dispersion equation in the dissipative case requires the calculation of the averaged Poynting vector $\langle \mathbf{S} \rangle$. Without dissipation, $\langle \mathbf{S} \rangle$ can be obtained by calculating the total density of energy stored in the cell and the group velocity $\langle \mathbf{S} \rangle = \mathbf{v}_g(\epsilon_0\epsilon\langle \mathbf{E}^2 \rangle + \mu_0\langle \mathbf{H}^2 \rangle)/4$. In both cases, it is necessary to average the quantities $\mathbf{E}\mathbf{H}^*$, $\mathbf{E}\mathbf{E}^*$, and $\mathbf{H}\mathbf{H}^*$. In these quantities, the oscillating functions associated with spatial harmonics are mutually canceled, which is why it is important from the very beginning to use equations that have no nonintegrable singularities. In the case of dissipation, the cancellation of complex-valued exponential functions is not complete: the factor $\exp(-2\mathbf{k}''\mathbf{r})$, which describes the decrease in the energy flux towards the damping, remains.

4.3 Correspondence between rigorous and model approaches

The rigorous approach does not allow determining dispersion and exact isofrequency surfaces, including those in resonance regions, at higher frequency branches or at any values of \mathbf{k} , including complex ones. The homogenization allows determining a type (1) model surface. The homogenization results are valid for small k_0d and kd , i.e., they should agree with the rigorous approach in this limit. A better correspondence is possible with several terms in the decomposition of permittivity in k_0d and kd taken into account.

One of the homogenization methods consists of solving the inverse problem of determining the coefficients in such decompositions by minimizing the discrepancy for the above surfaces or dispersions. This is also valid for two other methods of homogenization, based on solving the inverse diffraction problem and calculating the mean electric and magnetic polarization. Also of importance is the model of a homogeneous medium, namely, whether it accounts for the magnetic permeability, the tensor character of permittivity and permeability, the spatial dispersion, and cross-polarization. The last is determined from physical considerations. In particular, at low frequencies, where ϵ^{eff} and μ^{eff} make sense, the metallic structures of meta-atoms with ring currents exhibit induced diamagnetism, i.e., $0 < \mu^{\text{eff}} < 1$. This result is demonstrated by the formulas presented in [59], which yield for a PC of metallic balls having radius r in a cubic lattice at low frequencies the value of $\mu = 1 - 3\delta/(2 + \delta)$, where $\delta = 4\pi r^3/(3a^3) \ll 1$.

The conclusion in [75] about the absence of noticeable magnetic properties in the optical range is disputed in many recent papers on artificial magnetism of metamaterials. The introduction of such magnetism is a method of homogenization, and if it is not used, an infinite PC is quite describable as a dielectric AM only. Only some diffraction problems are an

exception, in which the use of effective permeability is convenient for describing the jumps of \mathbf{H} . One cannot manage without the tensor permeability (11) when describing magnon ferrite HMMs (10).

A rigorous description requires special consideration of the role played by dissipation and spatial dispersion. As mentioned above, the frequency (temporal) and the spatial dispersion, as well as the related dissipation, substantially affect the properties of metamaterials. The first manifests itself already in the macroscopic properties of meta-atoms. We will consider the role of spatial dispersion and dissipation by the example of the HMM of graphene sheets studied in [36, 37, 44], where it was not taken into account. The dispersion equation has the same form as above, namely, $\cos \Psi = X = \cos \vartheta + i\rho Z_0 \sigma (\sin \vartheta)/2$. The model of graphene conductivity without spatial dispersion within the framework of the Kubo–Greenwood approach and the method of nonequilibrium Green’s functions [249–251] is considered in a number of publications [252–267]; in HMM modeling, it was taken in the form $\sigma = \sigma_{\text{inter}} + \sigma_{\text{intra}}$, where the intraband σ_{intra} and interband σ_{inter} conductivities depend on the chemical potential μ_c and temperature T . For interband conductivity, the temperature dependence (at $k_B T \ll |\mu_c|$) can be ignored, and then [263–267]

$$\sigma_{\text{intra}}(\omega, \mu, \omega_c, T) = \frac{-ie^2 k_B T}{\pi \hbar^2 (\omega - i\omega_c)} \varphi(\mu_c, T) = \frac{\sigma_{0\text{intra}}}{1 + i\omega/\omega_c}, \quad (46)$$

$$\sigma_{\text{inter}}(\omega, \mu, \omega_c, 0) = \frac{-ie^2}{4\pi \hbar} \ln \left(\frac{2|\mu_c| - (\omega - i\omega_c)\hbar}{2|\mu_c| + (\omega - i\omega_c)\hbar} \right), \quad (47)$$

$$\begin{aligned} \varphi(\mu_c, T) &= \frac{\mu_c}{k_B T} + 2 \ln \left[1 + \exp \left(-\frac{\mu_c}{k_B T} \right) \right] \\ &= \ln \left[2 + 2 \cosh \left(\frac{\mu_c}{k_B T} \right) \right]. \end{aligned}$$

From the Drude-type formula (46), it follows that the intraband conductivity is inductive, and it corresponds to the DC conductance

$$\sigma_{0\text{intra}} = \frac{e^2 k_B T}{\pi \hbar^2 \omega_c} \ln \left\{ 2 \left[1 + \cosh \left(\frac{\mu_c}{k_B T} \right) \right] \right\}. \quad (48)$$

For $k_B T \ll |\mu_c|$ in Eqn (46), one should take $\sigma_{0\text{intra}} = (e^2/h)[2|\mu_c|/(\hbar\omega_c)]$, and for $k_B T \gg |\mu_c|$, respectively, $\sigma_{0\text{intra}} = 2(\ln 2)(e^2/h)k_B T/(\hbar\omega_c)$. Let the frequency not be very high, $|\omega - i\omega_c|\hbar \ll |\mu_c|$, which is true when $\omega\hbar \ll |\mu_c|$ and $\omega_c\hbar \ll |\mu_c|$. Then, the interband conduction is due to capacitive susceptance

$$\begin{aligned} \sigma_{\text{inter}} &\approx \frac{e^2 \omega_c (1 + i\omega/\omega_c)}{4\pi |\mu_c|} \left[1 + \frac{i(1 + i\omega/\omega_c)\omega_c \hbar}{|\mu_c|} \right] \\ &\approx \frac{e^2 \omega_c (1 + i\omega/\omega_c)}{4\pi |\mu_c|}. \end{aligned}$$

In this case, at low temperatures and low frequencies, we have the total conductivity

$$\sigma = \frac{e^2 |\mu_c|}{2\pi \hbar^2 \omega_c (1 + i\omega/\omega_c)} + \frac{e^2 \omega_c (1 + i\omega/\omega_c)}{4\pi |\mu_c|}. \quad (49)$$

This is inductive susceptance if

$$\omega^2 < \omega_c^2 (2\mu_c^2/(\omega_c \hbar)^2 - 1),$$

and capacitive otherwise. The real part of σ (49) has the form

$$\sigma' = \frac{e^2}{h} \frac{2\mu_c^2 + (\omega_c \hbar)^2 (1 + \omega^2/\omega_c^2)}{2\hbar\omega_c |\mu_c| (1 + \omega^2/\omega_c^2)}. \quad (50)$$

For $\omega/\omega_c \ll 1$ (high collision rate),

$$\sigma' \approx \frac{e^2}{h} \frac{2\mu_c^2 + (\omega_c \hbar)^2}{2\hbar\omega_c |\mu_c|} \approx \frac{e^2}{h} \frac{|\mu_c|}{\hbar\omega_c} \gg \frac{e^2}{h},$$

and for $\omega/\omega_c \gg 1$ (low collision rate),

$$\sigma' \approx \frac{e^2}{h} \frac{2\mu_c^2 + (\omega \hbar)^2}{2\hbar\omega_c |\mu_c| \omega^2/\omega_c^2} \approx \frac{e^2}{h} \frac{|\mu_c|}{\hbar\omega} \frac{\omega_c}{\omega}.$$

If the frequency is high ($|\mu_c| \ll |\omega - i\omega_c|\hbar$), the interband conductivity is the inductive susceptance

$$\sigma_{\text{inter}} \approx \frac{e^2}{4\hbar} + \frac{e^2 |\mu_c|}{\pi \omega_c \hbar^2 (1 + i\omega/\omega_c)}. \quad (51)$$

For $\omega/\omega_c \gg 1$, we have its real part $\sigma'_{\text{inter}} = e^2/(4\hbar)$, and for $\omega/\omega_c \ll 1$, it increases: $\sigma'_{\text{inter}} \approx (e^2/h)(\pi/2 + 2|\mu_c|/(\omega_c \hbar))$. Thus, in doped graphene at low dissipation in the frequency band $\omega_c(2\mu_c^2/(\omega_c \hbar)^2 - 1)^{1/2} < \omega \ll |\mu_c|/\hbar$, the conductivity is capacitive susceptance, and the slow E-plasmon along the single film is backward [123]. Adding (46) and (51), we present the dynamic conductivity in the form

$$\sigma = \frac{e^2}{4\hbar} + \frac{\sigma_0}{1 + i\omega/\omega_c} = \sigma' + i\sigma''. \quad (52)$$

The cases of weak and strong spatial dispersion were considered in [260]. To account for the spatial dispersion, one should use the tensor conductivity. Such conductivity was obtained in a general form [259–267], in the approximation of relaxation time, and in the Bhatnagar–Gross–Kruk approximation [267]. In the last case, we have the component $\sigma_{xx}(\omega)$:

$$\begin{aligned} \sigma_{xx}(\omega) &= \sigma_{\text{intra}}(\omega) \left[1 + \frac{v_F^2}{4(\omega - i\omega_c)^2} \left(3 - \frac{2i}{\omega/\omega_c} \right) k_x^2 \right] \\ &\quad + \sigma_{\text{inter}}(\omega). \end{aligned} \quad (53)$$

Here, $v_F \approx c/300$. The component $\sigma_{yy}(\omega)$ is obtained by symmetric replacement, and for $\sigma_{xy}(\omega) = \sigma_{yx}(\omega)$ we have

$$\sigma_{xy}(\omega) = \sigma_{\text{intra}}(\omega) \frac{v_F^2}{2(\omega - i\omega_c)^2} \left(1 - \frac{i}{\omega/\omega_c} \right) k_x k_y.$$

Now, the dispersion equation should be written using the 4×4 transfer matrix and imposing the Floquet–Bloch conditions. In the transfer matrix, both E-waves and H-waves must be allowed for. We do not present the corresponding cumbersome result. If the wave is considered to have $k_y = 0$, it is sufficient to deal with E-waves and the above dispersion equation $\cos \Psi = X$, in which $\rho = (k_0^2 \tilde{\epsilon} - k_x^2)^{1/2}/(k_0 \tilde{\epsilon})$. According to Eqn (19) and the relation between the permittivity and conductivity $\epsilon_{\perp} = \tilde{\epsilon} + i\sigma Z_0$, $\epsilon_{zz} = \tilde{\epsilon}$; therefore, $\epsilon'_{\perp} < 0$ if the conductivity of graphene is inductive. Considering Eqn (53), we can see that at large k_x^2 the quantity $-\epsilon'_{\perp}$ increases, limiting the growth of $k_x'^2$. However, here, we have put $k_y = 0$ and simplified the dispersion equation. Generally, such an AM can no longer be described by the diagonal tensor (7). The real values of $\epsilon_{zz} = \tilde{\epsilon}$, k_x , and

under the condition $k_0^2 \tilde{\varepsilon} > k_x^2$ of ρ , too, follow from the fact that the homogenization based on Eqn (19) for them means the normal motion of a T-wave at an angle of $\theta = \pi/2$ to the axis, when the electric field is transverse and there is no longitudinal component of the current and losses. A T-wave propagates freely (exciting no currents) through a set of planes perpendicular to the electric field. However, in reality, a T-wave in a system of such plane-parallel waveguides of dissipative conducting sheets possesses dissipation and becomes a quasi-T wave, which leads to complex k_x with $k_x'' \approx 1/(dZ_0\sigma')$.

In the considered models of graphene HMMs, the conductivity of an isolated graphene sheet was used. Actually, it is necessary to allow for environment (substrate) and adjacent layers, e.g., in a graphene bilayer or the edges of nanostripes [181–191, 253–269]. The corresponding quantum problem is commonly solved numerically within the framework of the density functional formalism, the molecular dynamics method, and modifications of the strong coupling method. In Refs [264, 265], for epitaxial graphene on a metal and semiconductor, analytical expressions are obtained based on the Anderson–Newns model Hamiltonian. Note that relations like (46), (47) are based on the approximate calculation of integrals in the vicinity of Dirac points of the Brillouin zone. The conductivity of graphene is studied in external electric and magnetic fields, e.g., in [252, 253, 261, 265].

In recent times, a new line of research and manufacturing of controlled metasurfaces [220–223] is being developed, including hyperbolic ones [222], for which it is important to consider the spatial dispersion. Metasurfaces are convenient for easy implementation of backward surface plasmon polaritons with the possibility of focusing a laser-induced diverging plasmon polariton, if it appears in the region, where it is backward. The metasurface impedance, controllable electrically, magnetically, or optically, allows replacing a forward plasmon polariton with a backward one. A sample of several metasurfaces connected in sequence with backward surface plasmon polaritons allows, in principle, supporting backward bulk plasmon polaritons. For photonics, the metasurfaces that support slow Hk-surface plasmon polaritons are interesting.

Let us consider the effect of dissipation and spatial dispersion on the boundedness of the values of wave vector components and on the change in the isofrequency surface shape in the \mathbf{k}' -space for HMMs. To construct the isofrequency surface (1) in a 3D \mathbf{k}' -space, the two real equations (24) and (25) are insufficient (the vector $\mathbf{k} = \mathbf{k}' - i\mathbf{k}''$ has four real parameters). The situation becomes more complex if homogenization is not performed. In this case, it is necessary to determine four more real-valued parameters for $\hat{\varepsilon}$. One of the equations may be the Bloch dispersion equation, from which two real equations follow. Let us write the Bloch dispersion equation in the form resolved with respect to the frequency $\omega = \omega(\mathbf{k})$. This dispersion equation can be obtained as a condition of resonance at a given (generally, complex-valued) phase shift on the PC faces. The second equation has the form $\text{Im} \omega(\mathbf{k}) = 0$. If the phase shifts are specified to be real, then the resonance frequency in the presence of dissipation will be complex. Expressing in a general case $\Omega(k_{\parallel}, k_{\perp}, k_0) = 0$ from the dispersion equation and the quantities k_{\parallel}'' , k_{\perp}'' from Eqn (25) and substituting them into (24), we get the desired surface. In this case, the components of the vector \mathbf{k}' are independent. This is a consequence of $\hat{\varepsilon}$ being independent of \mathbf{k} without the spatial

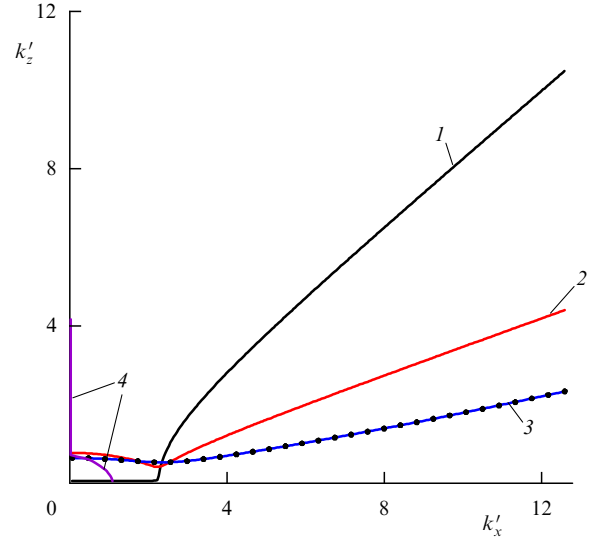


Figure 17. First-quadrant section of isofrequency surface (k'_{\parallel} and k'_{\perp} , in the units [10^7 m^{-1}]) for a homogenized planar layered HMM (curves 1–3) and a wire HMM (4) under the effect of dissipation. Parameter values: $a = d = 100 \text{ nm}$, $\omega_p = 1.9 \times 10^{16} \text{ Hz}$, $r/a = 0.1$, $\varepsilon_L = 10$, $\tilde{\varepsilon}' = 3$, $k_0 d = 0.5$. Curve 1: $\tilde{\varepsilon}'' = 0.003$, $\omega_c = 5 \times 10^{13} \text{ Hz}$; curve 2: $\tilde{\varepsilon}'' = 0.03$, $\omega_c = 5 \times 10^{15} \text{ Hz}$; curves 3 and 4: $\tilde{\varepsilon}'' = 0.3$, $\omega_c = 5 \times 10^{16} \text{ Hz}$.

dispersion taken into account. In the case of a first-type HMM, its dispersion equation is derived in the form resolved with respect to k_z . Calculating the vector $\mathbf{n}_E = \langle \mathbf{S} \rangle / |\langle \mathbf{S} \rangle| = k'' / |k''|$, we get one more real equation. In this case, the components of the vector \mathbf{k}' are coupled, which leads to their bounding. Imagine that the dispersion equation is formulated, the Brillouin zones (dispersion diagrams) are constructed, and the homogenization problem is solved. The quantities k'_{\parallel} and k'_{\perp} determine the angle θ at which the wave propagates with respect to the z -axis: $\theta = \arctan [(k_x'^2 + k_y'^2)^{1/2} / k_z']$. From Eqn (25), it follows that

$$k_{\perp}''^2 + 2 \frac{\varepsilon'_{\parallel}}{\varepsilon''_{\parallel}} k_{\perp}'' k'_{\perp} - k_{\perp}''^2 = \chi^2,$$

where

$$\chi^2 = \frac{(\varepsilon_{\parallel}''^2 + \varepsilon_{\perp}''^2) [\varepsilon_{\parallel}'' (k_{\parallel}''^2 - k_{\parallel}'^2) - 2\varepsilon'_{\perp} k_{\parallel}' k_{\parallel}'']}{\varepsilon_{\parallel}'' (\varepsilon_{\perp}'^2 + \varepsilon_{\perp}''^2)}. \quad (54)$$

We assume that $\varepsilon_{\perp}'' / \varepsilon_{\perp}' > 2k_{\parallel}'' / k_{\parallel}'$. Since $k_{\perp}'' > 0$, the positive root of the quadratic equation should be taken:

$$k_{\perp}'' = \sqrt{k_{\perp}'^2 \left[1 + \left(\frac{\varepsilon_{\parallel}'}{\varepsilon_{\parallel}''} \right)^2 \right] + \chi^2 - \frac{\varepsilon'_{\perp}}{\varepsilon_{\parallel}''} k'_{\perp}}. \quad (55)$$

As a result of these substitutions, Eqn (24) takes the form

$$k_{\perp}''^4 (\varepsilon_{\parallel}'^2 + \varepsilon_{\parallel}''^2) + k_{\perp}''^2 \varepsilon_{\parallel}''^2 \chi^2 = [\varepsilon_{\parallel}''^2 f(k_0, k'_{\parallel}, k_{\parallel}'') + \varepsilon_{\parallel}' k_{\perp}'^2]^2, \quad (56)$$

where the function

$$f(k_0, k'_{\parallel}, k_{\parallel}'') = \frac{1}{2} \left[k_0^2 + \frac{\chi^2 \varepsilon_{\parallel}'}{\varepsilon_{\parallel}'^2 + \varepsilon_{\parallel}''^2} - \frac{\varepsilon_{\parallel}' (k_{\parallel}'^2 - k_{\parallel}''^2) + 2k_{\parallel}' k_{\parallel}'' \varepsilon_{\perp}'}{\varepsilon_{\perp}'^2 + \varepsilon_{\perp}''^2} \right].$$

At large $k_{\perp}''^2$, it follows from (56) that $k_{\perp}''^2 (1 + \varepsilon_{\parallel}''^2 \chi^2 / k_{\perp}'^2) / 2 = \varepsilon_{\parallel}' f(k_0, k'_{\parallel}, k_{\parallel}'')$, from where the possibility of the boundedness

of $k_{\perp}^{\prime 2}$ is seen if the function f is bounded. For this function at small dissipation, we get

$$2f(k_0, k_{\parallel}^{\prime}, k_{\parallel}^{\prime\prime}) \approx k_0^2 + \varepsilon_{\perp}^{\prime -2} \left[k_{\parallel}^{\prime 2} \left(\frac{\varepsilon_{\perp}^{\prime\prime}}{\varepsilon_{\parallel}^{\prime\prime}} - \varepsilon_{\perp}^{\prime} \right) - \frac{2k_{\parallel}^{\prime} k_{\parallel}^{\prime\prime} \varepsilon_{\perp}^{\prime} \varepsilon_{\parallel}^{\prime\prime}}{\varepsilon_{\parallel}^{\prime\prime}} \right];$$

therefore, the expression in square brackets must be bounded. The left-hand side of (56) is a quadratic function of k_{\perp}^{\prime} . It is also quadratic in k_{\parallel}^{\prime} , as is the function $f(k_0, k_{\parallel}^{\prime}, 0)$ if the dissipation is ignored for motion along the axis ($k_{\parallel}^{\prime\prime} = 0$). For an HMM of the first type in this approximation, we get an equation biquadratic in k_{\perp}^{\prime} :

$$k_{\perp}^{\prime 4} + \frac{k_{\perp}^{\prime 2} \varepsilon_{\parallel}^{\prime\prime} \varepsilon_{\perp}^{\prime\prime} k_{\parallel}^{\prime 2}}{\varepsilon_{\perp}^{\prime 2} + \varepsilon_{\perp}^{\prime\prime 2}} = \frac{[\varepsilon_{\parallel}^{\prime\prime 2} f(k_0, k_{\parallel}^{\prime}, 0) + \varepsilon_{\parallel}^{\prime} k_{\perp}^{\prime 2}]^2}{\varepsilon_{\parallel}^{\prime 2} + \varepsilon_{\parallel}^{\prime\prime 2}},$$

which allows constructing an isofrequency surface. If $k_x = 0$ (the axial wave), then the propagation in a wire HMM is analogous to a wave in a dissipative multiwire line with a quasi-T wave. For a wire HMM, $k_{\parallel}^{\prime\prime} \approx -\text{Im}(k_0 \sqrt{\varepsilon_{\perp}^{\prime}})$. This value can be used as an initial one for iterations. Determining k_{\perp}^{\prime} from (56), we find $k_{\parallel}^{\prime\prime} = -\text{Im}(k_0 (\varepsilon_{\perp}^{\prime\text{eff}})^{1/2}) \cos \theta$ and repeat the iterations (56).

In the case of a layered HMM of the second type, we put $k_y = 0$, $k_x^{\prime\prime} = 1/(dZ_0 \sigma')$, $\varepsilon_{zz} = \tilde{\varepsilon}$, $k_z = d^{-1} \arccos X$, and $\varepsilon_{\perp} = \tilde{\varepsilon} + i\sigma Z_0$. Here, we use the simplest homogenization based on thin-layer conductivity $\sigma = \gamma d_1$ ($d_1 \ll d_2$), where γ is the bulk (specific) conductance. It is also possible to use the more rigorous relations (20), (21). Using (1) or (24), (25), let us express k_x^{\prime} and $k_x^{\prime\prime}$ (and, therefore k_z) as functions of frequency. The periodicity of k_z^{\prime} corresponds to different Brillouin zones; therefore, in the first zone at a given frequency the vector \mathbf{k} is bounded. Imposing additional conditions like $k_x^{\prime\prime} = 1/(dZ_0 \sigma')$ or $\mathbf{n}_E = \langle \mathbf{S} \rangle / \langle \mathbf{S} \rangle = \mathbf{k}'' / |\mathbf{k}''|$ can lead to unsolvability of the system of equations. If the HMM has a finite structure and the diffraction problem is considered for a plane wave penetrating into it, then k_z for a wire HMM and k_x for a planar layered one can be taken as corresponding to the incident wave. In a finite sample under such excitation, edge waves arise.

Executing homogenization, specifying the values of $k_{\parallel}^{\prime\prime}$ independent of the angle θ , determining k_{\perp}^{\prime} from (25), and substituting everything into (24), one can construct the isofrequency surface without addressing the rigorous Bloch dispersion equation and other relations. Using these relations leads to the fixation of the components, since they can be considered to be functions of frequency (generally, multi-sheet). Just this dependence is given by the rigorous microscopic dispersion equation that yields dispersion diagrams. The quantities in dispersion equation (1) can be considered independent only in the case of diffraction of waves by HMM samples in the long-wave approximation. In the first-order approximation of the spatial dispersion theory, we have [75]

$$\begin{aligned} \varepsilon_{\perp}(\mathbf{k}, k_0) &= \varepsilon_{\perp}(k_0) + \alpha_{\perp jl}(k_0) k_j k_l, \\ \varepsilon_{\parallel}(\mathbf{k}, k_0) &= \varepsilon_{\parallel}(k_0) + \alpha_{\parallel jl}(k_0) k_j k_l, \end{aligned}$$

where the summation over the repeating indices is implied. In our case, j and l take the values \perp and \parallel . In particular, in a number of papers [6, 7, 9, 24], for wire HMMs, the results of homogenization were obtained:

$$\varepsilon_{\parallel}(\mathbf{k}, k_0) \approx \tilde{\varepsilon} - \frac{\tilde{k}_p^2}{k_0^2 \tilde{\varepsilon} - k_z^2}, \quad \varepsilon_{\perp} \approx \tilde{\varepsilon},$$

which at small k_z^2 yields

$$\varepsilon_{\parallel} \approx \tilde{\varepsilon} - \frac{\tilde{k}_p^2}{k^2} + \frac{k_z^2}{k^2},$$

where $k^2 = k_0^2 \tilde{\varepsilon}$, $\tilde{k}_p^2 = 2\pi a^{-2} / (\ln(a/r) - 1.31)$ is a square of some plasma wave number determined by the configuration of the wire 'plasma'. The quantity ε_{\parallel} is negative only when the longitudinal component is bounded: $k_z^2 < k_0^2 \tilde{\varepsilon}$. Moreover, for $\varepsilon_{\parallel} < 0$ the necessary condition $\tilde{k}_p^2 + k_z^2 \tilde{\varepsilon} - k_0^2 \tilde{\varepsilon}^2 > 0$ should be satisfied. Under these conditions, for the transverse component we have

$$k_x^2 = k_0^2 + \frac{k_z^2 (k_0^2 \tilde{\varepsilon} - k^2)}{k^2 + k_z^2 \tilde{\varepsilon} - k_0^2 \tilde{\varepsilon}^2}.$$

The transverse component is bounded if $\tilde{k}_p^2 > k_0^2 \tilde{\varepsilon}^2$, in this case $k_z^2 = 0$ and $k_z^2 = k_0^2 \tilde{\varepsilon}$ yield the values $k_x^2 = k_0^2$. Differentiating this expression with respect to k_z^2 and equating the derivative to zero, we get the value at the maximum,

$$k_x^2 = \sqrt{\frac{\alpha^4}{\tilde{\varepsilon}} + k_0^2 \tilde{\varepsilon} \alpha^2} - \frac{\alpha^2}{\tilde{\varepsilon}},$$

where $\alpha^2 = \tilde{k}_p^2 - k_0^2 \tilde{\varepsilon}^2$. The maximal value of k determined from the equation $k_x^2 + \tilde{\varepsilon}^{-1} k_z^2 = k_0^2 + \tilde{\varepsilon}^{-1} k_p^2 k_z^2 / (\alpha^2 + k_z^2 \tilde{\varepsilon})$ is bounded. An additional limitation follows from considering losses. In Ref. [157], as a result of homogenization, an additional contribution to k_z^2 (see also [40]) in the form $k_p^2 a / \sqrt{\pi r (1 - \varepsilon(\omega))}$ is obtained. In Ref. [49], using the averaging method, the following expression is obtained for \tilde{k}_p^2 :

$$\begin{aligned} \tilde{k}_p^2(\omega, \mathbf{k}) &= \left[\sum_{m=-\infty}^{\infty} \frac{1}{k_0^2 \tilde{\varepsilon} - k_z^2 - k_{xm}^2 - k_{yn}^2} \right. \\ &\times \left. \left(\text{sinc} \left(\frac{k_{xm} a}{2} \right) \text{sinc} \left(\frac{k_{yn} a}{2} \right) - \text{sinc}(k_{xm} \pi r) \text{sinc}(k_{yn} \pi r) \right) \right]^{-1}, \end{aligned}$$

which depends on the frequency and spatial dispersion. The frequency dependence can be eliminated by considering the dispersion law. The above result is obtained in the approximation according to which the field does not penetrate into the wires. A rigorous result that considers the field distribution inside the wires is rather cumbersome.

Figure 17 presents the sections of the appropriate surfaces in the first quadrant under dissipation ($\tilde{\varepsilon} = \tilde{\varepsilon}' - i\tilde{\varepsilon}''$ and at different ω_c) for a planar layered (curves 1–3) and wire (curve 4) HMM. In the first case, the expressions of \tilde{k}_p^2 and ε_{zz} from [7] were used, and $\varepsilon_{xx} = \tilde{\varepsilon}(1 - \pi r^2/a^2) + \varepsilon \pi r^2/a^2$. A real value of k_z was specified and then replaced with a complex one, $k_z \rightarrow k_z(1 - i\varepsilon_{xx}''/\varepsilon_{xx}')$, and k_x was determined. In the case of the planar layered HMM, a real k_x was specified, after which the homogenization was performed based on (20), (21), and then the value was refined by iterations $k_x \rightarrow k_x(1 - i\varepsilon_{zz}''/\varepsilon_{zz}')$ with repeated homogenization. Then, k_z was determined. In Ref. [242] a similar surface was constructed for an HMM of finite-length wires with spatial dispersion (33). It is worth noting that for a considerable domain of large values of k in Fig. 17 the limitation related to the incorrectness of homogenization comes into effect.

Thus, the spatial dispersion most strongly bounds the homogenized isofrequency surface. The rigorous isofre-

quency surface is always bounded (see Fig. 13). In the examples considered, the real part of one of the components was considered unbounded. Actually, it is limited by the maximal deceleration of bulk plasmon polaritons caused by dissipation. The dissipation leads to the boundedness of both components. Another physical limitation related to homogenization has the form $k \ll \pi/a$ and is determined by the lattice constant. One more limitation (for metallic HMMs) is due to the plasma wave number k_p .

To construct a homogenized isofrequency surface, it is convenient to use the iteration approach, since the effective permittivity is a nonlinear function of k^2 . It can be presented in the form of expansion $\hat{\epsilon}(\omega, \mathbf{k}) \approx \hat{\epsilon}(\omega) + \hat{\alpha}(\omega)\mathbf{k}^2 + \hat{\beta}\alpha(\omega)\mathbf{k}^4$ with diagonal positive (in the absence of dissipation) matrices. However, for HMMs of the first and the second types, expansion in k_z^2 and k_\perp^2 , respectively, takes place. The substitution of this relation into (1) at $\epsilon_\perp(\omega)\epsilon_\parallel(\omega) < 0$ yields a bounded homogenized isofrequency surface, which at small k^2 is close to a hyperboloid and at large k^2 is bounded. Restricting ourselves to two terms, we arrive at an equation of the sixth order. Disregarding the spatial dispersion for the positive component of permittivity, we get a biquadratic equation for k_z^2 and k_x^2 , respectively. Its real-valued solutions are bounded; there can be no real solutions at all if the discriminant is negative. The limitation of the other component is due to periodicity and related to dispersion surface bending. However, the real limitation may occur much earlier because of the condition $k \ll \pi/a$, since for small k^2 the expansion is asymptotic. In particular, for the above homogenization of a wire HMM, we take $\epsilon_\parallel \approx -\bar{\epsilon} + k_z^2/(k_0^2\bar{\epsilon})$, $\epsilon_\perp \approx \bar{\epsilon}$ and get

$$k_z^4 - k_z^2[\tilde{k}_p^2 - 2k_0^2\bar{\epsilon}(\bar{\epsilon} + 1^2)] + k_0^2\bar{\epsilon}(\tilde{k}_p^2 + k_\perp^2\bar{\epsilon} - k_0^2\bar{\epsilon}^2) = 0.$$

For large k_\perp^2 , there are no solutions. It is interesting that in ideal HMMs the maximal angle between \mathbf{k} and \mathbf{S} is acute and tends to $\pi/2$, i.e., there are no backward waves. However, they must be present in any PC, and in the case of the above limitation take place due to the bending of the surface.

The exact surface is constructed in the first Brillouin zone (see Fig. 13). From the dispersion equation for a planar layered HMM, the component $k_z = k_z(k_0, k_x)$ is determined (to $2m\pi/d$) as $k_z = \pm(\arccos X)/d$. Here, $X = \cosh \theta_m \cos \theta_d - \rho \sinh \theta_m \sin \theta_d$. Denoting the permittivity of the metal as $\epsilon_m = \epsilon_L - k_p^2/k_0^2$ and the dielectric as ϵ_d with the thicknesses $t_m + t_d = d$, we have

$$\rho = \frac{\alpha - \alpha^{-1}}{2}, \quad \alpha = \frac{\epsilon_d k_{mz}}{k_{dz} |\epsilon_m|}, \quad \theta_m = k_m t_m, \quad \theta_d = k_{dz} t_d,$$

$$k_{mz} = k_0 \sqrt{n^2 + |\epsilon_m|}, \quad k_{dz} = k_0 \sqrt{\epsilon_d - n^2},$$

where $n = k_x/k_0$ is the coefficient of plasmon polariton deceleration along the layer. If $n > \sqrt{\epsilon_d}$, then $\rho = i(|\alpha| + |\alpha|^{-1})/2$, $\sin \theta_d = -i \sinh |\theta_d|$. The region $-1 < X < 1$ corresponds to the waves propagating along the axis, and the region $-\pi/d < k_z < \pi/d$ corresponds to the isofrequency surface in the first Brillouin zone (see Fig. 13). The surface touches the axis k_z at a certain frequency. At lower frequencies, the surface breaks and becomes doubly connected, and with a further decrease in frequency completely vanishes. This happens because $k_{mz} \approx (k_x^2 + k_p^2)^{1/2}$, and the value of $|\rho| \sim k_0^{-2}$ infinitely increases. Although at low frequencies homogenization (19) yields $\epsilon_\perp \approx t_m \epsilon_m/d < 0$, $\epsilon_\parallel \approx \epsilon_d/t_d > 0$ and the HMM is not realized. To implement

the HMM, slow plasmon polaritons along the layers are necessary, i.e., the condition $n \gg 1$ must be fulfilled. On the other hand, homogenization based on (20) and (21) allows obtaining rather complicated expansions in k_x^2 . In the simplest case, $t_d = t_m$ for the transverse component, we get $\epsilon_\perp = -[k_p^2/k_0^2 - (\epsilon_L + \epsilon_d) - k_x^2/k_0^2]/2$, and the longitudinal component is independent of k_x^2 :

$$\epsilon_\parallel = \frac{2\epsilon_d(k_p^2/k_0^2 - \epsilon_L)}{k_p^2/k_0^2 - (\epsilon_d + \epsilon_L)}.$$

The limitation yields the condition $k_x^2 < k_p^2 - k_0^2(\epsilon_L + \epsilon_d)$. If it is violated, there are no solutions, as seen from Fig. 13, i.e., HMMs with infinitely decelerated plasmon polaritons do not exist.

The dispersion equation for a wire HMM is written in the form of a functional, depending on k_0 and \mathbf{k} . Having found its stationary value and resolved with respect to k_x , we can also formally write $k_x = k_x(k_0, k_z)$. Here, k_x is defined to $2n\pi/a$. To find the complex waves in a dissipative HMM, one more equation is necessary. It is not possible to choose one of the complex components arbitrarily. It is also impossible to use Eqn (1) for this purpose, since it is derived by primitive homogenization. However, it is possible to calculate $\langle \mathbf{S} \rangle$ and used the relation $\mathbf{k}'' = k'' \langle \mathbf{S} \rangle / |\langle \mathbf{S} \rangle|$. The unit vector \mathbf{k}''/k'' determines the direction of damping, coincident with the direction of the energy flux $\langle \mathbf{S} \rangle$. In a dissipative PC, the direction of the flux $\langle \mathbf{S} \rangle$ does not coincide with that of group velocity. Specifying the direction of phase motion with respect to the axis (e.g., specifying k_z'), it is now possible to determine the components k_z'', k_x', k_x'' and construct the isofrequency surface $\omega(k_\perp, k_z)$. However, it is forbidden to apply the isofrequency method. In particular, the backward wave is determined by the condition $\mathbf{k}'\mathbf{k}'' < 0$ rather than the condition $\mathbf{k}'\mathbf{v}_g < 0$. In uniaxial PCs, one can introduce averaged wave impedances and use them as additional relations. Namely, for $k_y = 0$ for a wire HMM,

$$Z^e = \frac{\langle E_x \rangle}{\langle H_y \rangle} = \frac{\langle S_z \rangle}{2\langle H_y \rangle}, \quad Z^e = \frac{Z_0(\bar{\epsilon} - k_z^2/k_0^2)^{1/2}}{\bar{\epsilon}}.$$

In a general case, the spatial dispersion manifests itself in the dependence of Z^e on two angles, $\varphi = \arctan(k_y'/k_x')$ and $\theta = \arctan((k_x'^2 + k_y'^2)^{1/2}/k_z')$. In this sense, dispersion equation (1) corresponds to the limit $a/\lambda \rightarrow 0$ or $d/\lambda \rightarrow 0$ with the possibility of waves with large k . The physical limitations for the vector \mathbf{k}' are dissipation [123] and the spatial dispersion $|\mathbf{k}'|d < 1$. Therefore, the dissipation and the spatial dispersion limit the hyperbolicity. For HMMs of graphene with d of a few nanometers, the minimal wavelengths appear to be a few tens of nanometers.

5. Possible effects, applications, and prospects

In real HMMs, the observed waves are bulk Hk plasmon polaritons with $k \gg k_0$, and the dispersion close to the hyperbolic one takes place at limited k . This is what should be considered the main property of HMMs. This property, first demonstrated as early as 1963 for a strongly magnetized plasma [270], is related to the propagation of very slow bulk and surface plasmons along metallic or conducting structures [270]. Slow-light quasi-photons play a crucial role in nano-image formation by nanolenses in overcoming the optical diffraction limit [271–291]. Divergent wire and layered fan,

curved and plane-parallel structures are promising. Fan HMM structures, which are an analog of the scanning optical microscope, have already been used to transfer the near-field image to the far-field zone with great magnification, overcoming the diffraction limit [292]. The resolution of such an optical microscope depends on the manufacturing capabilities of the nanotechnology and can reach a few nanometers, while considerable magnification can be achieved using extensive structures. Extension and deceleration are limited by the dissipation of plasmon polaritons. At the maximal deceleration frequency (the frequency of plasmon resonance), the plasmon polariton losses are also maximum and inversely proportional to the losses in the material [122, 123]: $k'_x \approx k''_x = 1/\sqrt{2\varepsilon''}$, which is characteristic of both the Zenneck plasmon along the metal boundary and the plasmon polariton along the thin metallic layers and wires. This universal relation means that the smaller the dissipation ε'' , the higher the plasmon polariton losses near the resonance. It is valid for waveguides near the cutoff frequency, for PCs and slow-wave structures near the nontransmission band edge, for plasmon polaritons near the bandgap boundary, and for Lorentz dispersion near the resonance frequency [229]. The physical reason is that in all such ideal nondissipative structures, the waves in the band gaps are evanescent and their propagation constants are imaginary. Small dissipation makes them complex and the propagation losses greater. This is a resonance effect. Therefore, one should operate at frequencies slightly lower than the plasmon resonance frequency $\omega_p/\sqrt{\varepsilon_L + 1}$ and reduce the collision rate. At the liquid helium temperature, the collision rate is reduced by nearly 150 times. At ultralow temperatures, its reduction by several orders of magnitude is possible. In this case, the mean free path substantially exceeds all characteristic dimensions: layer thicknesses, radii and lengths of nanowires, wavelength. The transport of carriers becomes ballistic and quantum mechanical [249–269], the surface impedance, permittivity, and conductance lose their local sense, and such notions as kinetic inductance and quantum capacitance arise.

Dynamical electrophysical parameters of HMM-type structures should be determined using the methods of quantum and nonequilibrium statistical mechanics for quantum wires (nanowires) and quantum wells (thin conducting layers) [293–298]. For calculating DOS and the number of conductivity modes in a film a few nanometers thick (2D electron gas), the Landauer model (in which the number of conductivity modes is equal to the number of de Broglie half-waves in the dimension) requires specification based on the solution to the quantum mechanical problem. Of interest are graphene ribbon quantum wires [188–191], graphene structures, including those strongly coupled to quantum dots in the form of gold and silver particles [298–301], and structures consisting of quantum dots [299–303]. A review of hybrid nanostructures based on metal-2D nanomaterial like graphene, boron nitride, and other conducting films for improved plasmonics is presented in [300, 301]. Such AMs already require rigorous quantum mechanical calculation [189–191, 302], as well as the functionalization of graphene HMMs by atoms [302].

The creation of promising HMMs and Hk -AMs is associated with loss reduction. One of the ways for loss compensation is to use atomically smooth surfaces with a large mirror reflection coefficient and ultrapure materials. Another method of loss compensation is related to using

active (pumped) semiconductor or graphene structures [117, 303–316]. Optical [310], diffusion [312–316], electric, and magnetic [311] pumping is possible. Omitting consideration of the vast literature on such structures (see, e.g., [117]), we note that in graphene HMMs optical and diffusion pumping can give rise to the negative real part $\sigma'(\omega) < 0$ of the dynamic conductivity [310], which is possible in the range from nearly one to a few THz, and the external slow electric and magnetic fields change the band structure and the conductivity [262, 311]. The diffusion pumping implies the injection of charge carriers from the pumped semiconductor layer [316]. For graphene, $\sigma'(\omega) < 0$ means an excess of the negative real part of interband conductivity $\sigma'_{\text{inter}}(\omega) = (e^2/4\hbar) \tanh[(\hbar\omega - 2\varepsilon_F)/(k_B T)]$ over the positive real part of the intraband conductivity related to scattering by phonons [310]. For pumped HMMs, 2D monolayer structures analogous to graphene (borophene, germanene, boron nitride, etc.) and semiconductor nanofilms (e.g., InSb) are promising.

Note that, for the implementation of HMMs, compensation by spasers [117] and directly by pumping should be high-precision to avoid the appearance of a gain medium. Otherwise, for the gain medium, similar problems of boundedness of the wave vector components arise.

From the point of view of the electrodynamic approach to the analysis, the quantum calculation of the coupled active structures of spasers should lead to the determination of their electrophysical parameters. The simplest models of active and passive layers or passive nanowires in an active medium can be based on the inverse negative effective collision rate. If the structure is completely active, then the index $p = \mathbf{k} \cdot \mathbf{S}(k_0, \mathbf{k})$ can be calculated as $p = \mathbf{k} \cdot \mathbf{k}''$, in which case $p > 0$ corresponds to a backward wave and $p < 0$ to a forward one. However, a combination of active and dissipative layers requires a classification based on the Poynting vector. This also relates to plasmon polaritons along active-dissipative meta-surfaces. Consideration of active resonance structures requires more complex modeling.

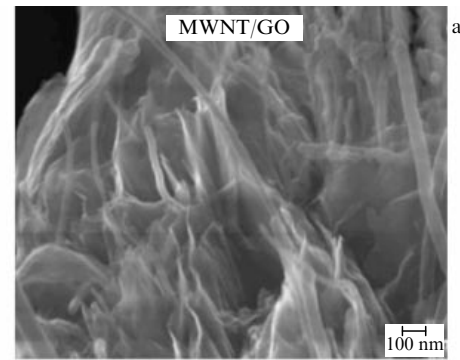
As mentioned above, the fields of application of HMMs and devices based on them are already rather diverse. They are waveguides (from the microwave to optical range), microresonators, attenuators, metasurfaces, optical nano-antennas, ultrasensitive and high-efficiency terahertz and optical detectors, sensors, focusing and magnifying super-lenses, solar batteries, switches and absorbers (loads), and thermal and terahertz screens. Magnetic HMMs [317–325], strongly exhibiting magneto-optical properties, electrically, magnetically, and optically controlled HMM-based devices [319], including nonreciprocal ones [324], graphene-metallic structures [298], and a number of other ones have interesting prospects. It is promising to use HMMs in GHz and THz traveling-wave amplifiers, in transistors and transistor amplifiers, for radiation-based heat transfer, and for heat removal devices and modulators. Hk -states open the way to obtaining high-contrast fluorescence images, as well as allowing creating multifunctional nanophotonic materials for ultra-fast optical switching and signal processing and instruments for near-field microscopy and photolithography with enhanced resolution. HMMs and Hk -AMs are convenient and have been used to control fluorescence, amplify the Raman spectroscopy response, and design directed antennas, waveguides, and resonators of the terahertz (THz) and infrared (IR) ranges (including controllable ones), attenuators, and modulators.

AMs with metallic layers are described by the permittivity tensor (8). If a magnetic field is directed at an angle to the normal, then the tensor transforms by the rotation matrix and comprises no zero components. If ferrite layers are added to such an AM, it will be described by two tensors, the permittivity and permeability (11). In this case, the simultaneous occurrence of negative components in both tensors is possible. This AM supports bulk spatial waves. To operate with it in the infrared and visible ranges, it is necessary to apply strong magnetic fields with induction of the order of 1 T. Hollow THz and IR waveguides with HMM walls and HMM-layer waveguides that recently became a subject of study [326, 327] are promising. Unidirectional leaky waves are possible along a layer of asymmetric HMMs with an applied magnetic field and noncoincident optical and waveguide axes, which allows creating optical leaky-wave narrow-beam antennas. Plasmon polaritons on both sides of such a layer are different, so that a plasmon polariton moving to the right along one side corresponds to the one moving to the left along the other side with a change of sign of k_x and k_z . In thick layers, such coupling vanishes, and the dispersion equation in the absence of a magnetic field takes the form

$$k_z = \pm k_0 \sqrt{\frac{\varepsilon_{xx}\varepsilon_{zz} - \varepsilon_{xz}^2 - \varepsilon_{xx}}{\varepsilon_{xx}\varepsilon_{zz} - \varepsilon_{xz}^2 - 1}}.$$

This equation describes a plasmon polariton along the surface of a semi-infinite sample in the direction of the z -axis and comprises components of the effective permittivity tensor of the asymmetric HMM [36]. In the presence of the k_y component, the equation becomes more complicated. It is simplified when $\varepsilon_{xz} = 0$ (the optical axis is parallel or perpendicular to the surface). In this case, $k_z = \pm k_0 \sqrt{\varepsilon_{xx}(\varepsilon_{zz} - 1)/(\varepsilon_{xx}\varepsilon_{zz} - 1)}$. Slow plasmon polaritons are possible at $\varepsilon_{xx}\varepsilon_{zz} \rightarrow 1$ or at $\varepsilon_{xx} \rightarrow \infty$; in the latter case, a region with backward plasmon polaritons exists. This distinguishes the HMM from a metal, on the surface of which plasmon polaritons are forward, and offers new possibilities for designing waveguiding structures. Dipole radiation near the surface gives rise to bulk and surface modes; therefore, antennas located near the surface of controlled HMMs or directly using HMMs are of interest.

Observable effects in HMMs are the super-Planck radiation, negative refraction, the Purcell effect, enhancement of fluorescence, and the Raman effect in and near the volume inside the HMM. The Purcell effect manifests itself in a different way for a source of radiation inside and outside the HMM sample. Inside, damping is enhanced, because the Hk -modes do not go beyond the sample boundaries and are absorbed. Radiation enhancement in the far zone is possible for a dipole located outside the HMM structures. In the infrared and terahertz ranges, this fact offers possibilities of creating materials with anisotropic absorption and emission properties and anisotropic emissivity. As a possible effect, we mention the dynamic Casimir effect, experimentally discovered in 2011 in a waveguide with a squid [328], and the optical Compton effect (direct and inverse). To possibly observe the former, one should use high-power modulated laser radiation to switch the elliptic mode of dispersion to the hyperbolic one in a layered semiconductor-dielectric HMM in a cavity tuned to the modulation half-frequency. In the second case, the hyperbolic properties are to be obtained in the ultraviolet range. In both cases, ultralow temperatures and ultrasensitive instrumentation are needed. HMMs exhibit the properties of



Carbon nanotube-graphene composite

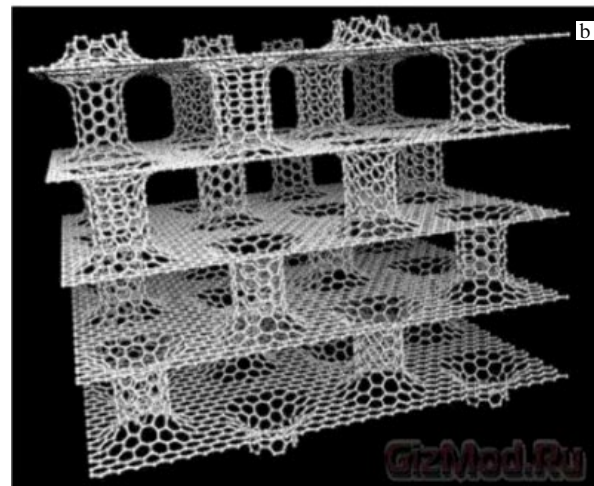
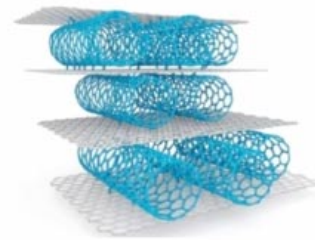


Figure 18. (a) Photograph obtained using an atomic force microscope and a model of 2D films of a hybrid carbon nanotube-graphene composite with nanotubes parallel to each other covalently bound to graphene monolayers [352]. (MWNT/GO—Multi-Walled carbon NanoTubes/Graphene Oxide sheets). (b) Multilayer graphene sheets linked by carbon nanotubes (columnar graphene) [353, 354].

ENZ materials, which offer the possibility of using it in image processing and other fields [329].

From the constructive point of view, multiperiodic PCs [330] operating in various ranges, hyperlenses operating based on Dyakonov plasmons [205, 206, 331, 332], instruments of near-field microscopy [291, 292], HMMs based on Bragg polariton structures [75, 333], plasmon polariton-based amplifiers and attenuators [334–337], diffraction supergratings [338], microresonators [339, 340], waveguiding structures [341–347], almost ideally absorbing surfaces [348], and planar superlenses [271] are of great interest. Amplification of plasmon polaritons in Hk -semiconductor and dielectric grating structures with graphene and resistors in the form of graphene nanostripes is considered in [312–316].

Apparently, the research and technology of manufacturing the considered structures will develop towards higher

miniaturization with the progress in nanotechnologies to the level of a few atoms or even individual atoms, incorporated in nanostructures, with a reduction in the a/λ ratio and application of quantum-mechanical methods of analysis. Problems of manufacturing PCs with the size of meta-atoms of the order of 1 nm or less (i.e., consisting of a few atoms) arise. The improvement of analysis methods for such structures with quantum dots requires the development of quantum mechanics, density functional theory, methods of molecular dynamics, nonequilibrium statistical mechanics, and nonequilibrium Green's function in combination with PC electro-dynamics.

For HMMs operating in different ranges, it is necessary to measure the plasma frequencies. In perfect metals, they are in the ultraviolet range, but in semiconductor structures, their variation in a wide range is possible by doping, optical, and electric control. Magnetic layered MSW-based HMMs operate in the microwave range. Graphene and other carbon structures, as well as n -InSb HMMs, are ideal for the THz range. From the point of view of application, both traditional HMM structures and complex 3D PCs are possible, including those controlled by external fields (magnetic and electric), layered structures with thin conducting and/or ferrite films, and structures of semiconductor and dielectric nanowires coated with metallic films. Graphene HMMs are applicable in ranges from the terahertz to ultraviolet.

Control by laser radiation allows modifying the film properties from those typical for high-resistance semiconductors (dielectrics) to, practically, metal properties, as well as creating active structures, which changes the frequency properties and makes amplification possible. Another promising line of development is using nonlinear properties [3, 177, 340], including harmonic generation. Since the formal HMM model (1) actually reduces to obtaining large values of the wave vector components, this property is implemented in structures with slow plasmons, whose analysis requires methods of quantum plasmonics. In this sense, HMMs demonstrate effects that occur in quantum structures, in particular, the van Hove effect [346].

The van Hove singularities observed in DOSs of the local near field, mainly related to slow plasmon polaritons, may be used in quantum defect-based instruments, in sensors, in photovoltaics, for Raman scattering enhancement on the HMM surface or in the presence of an HMM, and for diffraction-grating nanophotolithography [119]. Possible applications of slow Dyakonov-type plasmon polaritons along HMM surfaces as waveguiding structures may underlie the construction of active devices in the terahertz range, including solid-state and vacuum traveling-wave amplifiers with the possibility of electric, magnetic, and laser control. Of interest is the analogy between HMMs and models of space-time, also described by indefinite metrics [347–353]. In particular, Ref. [348] considers a model of the physical vacuum in magnetic fields of the order of 10^{16} T and above, accompanied by the creation of ρ -mesons from the vacuum and considering the vacuum to be an HMM. In these papers, it is proposed to model four-dimensional processes in the space-time of the early Universe based on the model consideration of optical 3D HMMs.

Natural graphite also demonstrates HMM properties [354]. Recently, new carbon structures of oriented carbon nanotubes and nanotube/graphene hybrid structures (columnar graphene) have been synthesized [355–357] (Fig. 18), which can also be considered HMMs. From the

point of view of controlling the modification of properties in graphene and other HMMs, functionalizing technologies are possible, such as hydration, oxidation, etching, and laser polishing. In turn, this requires the development of methods for energy band calculations, such as the strong coupling method, density functional theory (including that allowing for the effect of external fields on the band structure), and consideration of structure functionalization by individual atoms or quantum dots. The appearance of sp^3 hybridized states in graphene under hydration strongly enriches the spectrum of optical excitation [302]. Electrophysical parameters of thin films and nanowires in an external magnetic field should be determined using quantum methods with the Landau levels taken into account. The quantum-mechanical method of analysis is also necessary to account for the compensation of losses in active dissipative HMMs.

Recently, technologies have appeared for gold electro-deposition into silicon grooves with a submicron width, an aspect ratio above 35, and a structure area of a few square centimeters for optical, X-ray, and other applications [358], as well as a number of other technologies for HMMs.

In the above description, we used electrophysical parameters characteristic of bulk samples. Actually, the electrophysical parameters depend on the dimensions (film width, radii and lengths of cylinders, etc.) and quantum-dimensional effects, including the environment [268, 269]. It is promising to use planar layered structures consisting of lattices of graphene strips on a layer. In this case, a possibility arises to control the electrophysical parameters by changing the topology (width, edge shape, chirality). For example, the quantization of the strip width leads to sharp variations in both conductivity and optical transparency; the width modulation allows obtaining heterostructures and manipulating the electronic parameters [191]. The method of cutting the strip from a graphene monolayer (shaping of the strip edges), its bending, and other mechanical deformations determines the intensity of hydration and thus allows controlling the electronic properties. Note also that plasmon-exciton mixed states [75, 330] arising in strongly coupled nanosystems can give rise to new unique properties. The homogenization considered above (see also [271, 359–362]) is valid in the far-field zone, since in the near-field zone the Ewald–Oseen theorem does not hold [363], requiring a rigorous consideration of the near field with the environment microstructure taken into account. This is the sense in which one should approach the modeling of HMMs comprising ultrathin layers.

6. Conclusion

The present review considers an electrodynamic approach to the analysis of the properties and homogenization of uniaxial metallic (plasmonic) and magnetic (magnonic) PCs demonstrating in certain ranges of ω and \mathbf{k} different-sign real parts of diagonal components of the effective permittivity and permeability tensors. The roles of dissipation and spatial dispersion are investigated. It is shown that both frequency and spatial ranges are limited. Mutual features of such PCs are that they support slow bulk Hk -plasmons and on their surfaces plasmon-polaritons exist. The principle boundedness of k due to spatial dispersion is determined by the technological limit of the obtained thickness of layers, i.e., by the order of 1 nm^{-1} . Practically, to increase k it is also necessary to

reduce the dissipation using optical or electric pumping and low temperatures.

Naturally, the review does not cover all papers, a large number of which demonstrate considerable interest in the problem considered [364]. The basic properties of HMMs, their present-day applications, and their prospects are described. An approach based on macroscopic material parameters is presented. Promising nanodimension Hk-HMMs require quantum mechanical methods of analysis.

This study was supported by the Ministry of Education and Science of Russia within the Project Part of the State Assignment in the field of research activity no. 3.1155.2014/K and the Russian Science Foundation (project no. 16-19-10033).

References

- Pendry J B et al. *Phys. Rev. Lett.* **76** 4773 (1996)
- Pendry J B et al. *J. Phys. Condens. Matter* **10** 4785 (1998)
- Pendry J B et al. *IEEE Trans. Microwave Theory Tech.* **47** 2075 (1999)
- Smith D R et al. *Phys. Rev. Lett.* **84** 4184 (2000)
- Shelby R A, Smith D R, Schultz S *Science* **292** 77 (2001)
- Belov P A, Tretyakov S A, Viitanen A J *J. Electromagn. Waves Appl.* **16** 1153 (2002)
- Belov P A et al. *Phys. Rev. B* **63** 113103 (2003)
- Smith D R, Schurig D *Phys. Rev. Lett.* **90** 077405 (2003)
- Nefedov I S, Viitanen A J, Tretyakov S A *Phys. Rev. E* **71** 046612 (2005)
- Engheta N, Ziolkowski R W *Metamaterials: Physics and Engineering Explorations* (New York: J. Wiley and Sons, IEEE Press, 2006)
- Narimanov E E, Shalaei V M *Nature* **447** 266 (2007)
- Yao J et al. *Science* **321** 930 (2008)
- Nefedov I S, Viitanen A J, in *Theory and Phenomena of Metamaterials* (Metamaterials Handbook, Ed. F Gapolino) (Boca Raton, FL: CRC Press. Taylor and Francis, 2009) p. 15
- Noginov M A et al. *Opt. Lett.* **35** 1863 (2010)
- Nefedov I S *Phys. Rev. B* **82** 155423 (2010)
- Poddubny A N, Belov P A, Kivshar Yu S *Phys. Rev. A* **84** 023807 (2011)
- Nefedov I, Tretyakov S *Phys. Rev. B* **84** 113410 (2011)
- Nefedov I S, Simovski C R *Phys. Rev. B* **84** 195459 (2011)
- Nefedov I S, Tretyakov S A *Photon. Nanostruct. Fundament. Appl.* **9** 374 (2011)
- Liberal I et al. *J. Appl. Phys.* **110** 104902 (2011)
- Liberal I et al. *J. Appl. Phys.* **110** 064909 (2011)
- Narimanov E E et al., arXiv:1109.5469
- Davidovich M V et al. *Fiz. Volnovykh Protsesov Radiotekh. Sistemy* **15** (2) 19 (2012)
- Davidovich M V, Stepukh J V, Shilovskii P A *Tech. Phys.* **57** 320 (2012); *Zh. Tekh. Fiz.* **82** (3) 7 (2012)
- Biehs S A, Tschikun M, Ben-Abdallah P *Phys. Rev. Lett.* **109** 104301 (2012)
- Nefedov I S *Mater. Phys. Mech.* **13** 1 (2012)
- Guo Y et al. *Appl. Phys. Lett.* **101** 131106 (2012)
- Simovski C R et al. *Adv. Mater.* **23** 4229 (2012)
- Davidovich M V, Shilovskii P A *Tech. Phys.* **57** 1687 (2012); *Zh. Tekh. Fiz.* **82** (12) 79 (2012)
- Liberal I et al. *IEEE Trans. Antennas Propag.* **60** 1921 (2012)
- Hashemi S M, Nefedov I S *Phys. Rev. B* **86** 195411 (2012)
- Baranov D G et al. *JETP* **114** 568 (2012); *Zh. Eksp. Teor. Fiz.* **141** 650 (2012)
- Davidovich M V, Shilovskii P A *Tech. Phys.* **58** 1173 (2013); *Zh. Tekh. Fiz.* **83** (8) 90 (2013)
- Iorsh I V et al. *Phys. Rev. B* **87** 075416 (2013)
- Drachev V P, Podolskiy V A, Kildishev A V *Opt. Express* **21** 15048 (2013)
- Nefedov I S, Valagiannopoulos C A, Melnikov L J *Opt.* **15** 114003 (2013)
- Nefedov I S et al. *Sci. Rep.* **3** 2662 (2013)
- Guo Y et al. *Adv. Optoelectron.* **2012** 452502 (2012)
- Shekhar P, Atkinson J, Zubin J *Nano Convergence* **1** 14 (2014)
- Poddubny A et al. *Nature Photon.* **7** 958 (2013)
- Cortes C L et al. *J. Opt.* **14** 063001 (2012)
- Flory F, Escoubas L, Berginc G J. *Nanophoton.* **5** 052502 (2011)
- Valagiannopoulos C A, Nefedov I S *Photon. Nanostruct. Fundament. Appl.* **11** 182 (2013)
- Nefedov I S et al. *Sci. Rep.* **3** 2662 (2013)
- Nefedov I S, Melnikov L A, Nefedov E I *Proc. SPIE* **8771** 87710K (2013)
- Nefedov I S, Melnikov L A *Appl. Phys. Lett.* **105** 161902 (2014)
- Davidovich M V, Nefedov I S *Proc. SPIE* **9031** 903115 (2014)
- Kozina O, Melnikov L, Nefedov I *AIP Conf. Proc.* **1936** 020007 (2018)
- Davidovich M V, Nefedov I S *JETP* **118** 673 (2014); *Zh. Eksp. Teor. Fiz.* **145** 771 (2014)
- Belov P A, Simovskii K R, Tretyakov S A *Radiotekh. Elektron.* **49** 1285 (2004)
- Simovski C R, Sauviac B *Radio Sci.* **39** RS2014 (2004)
- Simovski C P *Opt. Spectrosc.* **107** 726 (2009); *Opt. Spektrosk.* **107** 766 (2009)
- Simovski C R *J. Opt.* **13** 013001 (2011)
- Silin R A *Phys. Usp.* **49** 542 (2006); *Usp. Fiz. Nauk* **176** 562 (2006)
- Veselago V G *Phys. Usp.* **54** 1161 (2011); *Usp. Fiz. Nauk* **181** 1201 (2011)
- Lewin L *Proc. IEE* **94** 65 (1947)
- Brown J *Proc. IEE* **100** 51 (1953)
- Brown J, Jackson W *Proc. IEE* **102** 11 (1955)
- Lewin L *Advanced Theory of Waveguides* (London: Wireless Engineer by Iliffe, 1951); Translated into Russian: *Sovremennaya Teoriya Volnovodov* (Moscow: IL, 1954)
- Seeley J S, Brown J *Proc. IEEE* **105C** 93 (1958)
- Brown J *Prog. Dielectrics* **2** 195 (1960)
- Rytov S M *Sov. Phys. JETP* **2** 466 (1956); *Zh. Eksp. Teor. Fiz.* **29** 605 (1955)
- Brekhovskikh L M *Waves in Layered Media* (New York: Academic Press, 1960); Translated from Russian: *Volny v Sloistykh Sredakh* (Moscow: Izd. AN SSSR, 1957)
- Brekhovskikh L *Waves in Layered Media* 2nd ed. (New York: Academic Press, 1980)
- Levin M L *Zh. Tekh. Fiz.* **18** 1399 (1948)
- Chebykin A V et al. *Phys. Rev. B* **84** 115438 (2011)
- Chebykin A V et al. *Phys. Rev. B* **86** 115420 (2012)
- Elser J et al. *Appl. Phys. Lett.* **90** 191109 (2007)
- Davidovich M V *JETP* **123** 928 (2016); *Zh. Eksp. Teor. Fiz.* **160** 1069 (2016)
- Sivukhin D V *Opt. Spektrosk.* **3** 308 (1957)
- Makarov V P, Rukhadze A A *Phys. Usp.* **54** 1285 (2011); *Usp. Fiz. Nauk* **181** 1357 (2011)
- Woodley J F, Mojahedi M *Phys. Rev. E* **70** 046603 (2004)
- Rytov S M *Zh. Eksp. Teor. Fiz.* **17** 930 (1947)
- Rautian S G *Phys. Usp.* **51** 981 (2008); *Usp. Fiz. Nauk* **178** 1017 (2008)
- Agranovich V M, Gartstein Yu N *Phys. Usp.* **49** 1029 (2006); *Usp. Fiz. Nauk* **176** 1051 (2006)
- Landau L D, Lifshitz E M *Electrodynamics of Continuous Media* (Oxford: Elsevier, 2004); Translated from Russian: *Elektrodinamika Sploshnykh Sred* (Moscow: Nauka, 1982)
- Balabukha N P, Basharin A A, Semenenko V N *J. Commun. Technol. Electron.* **54** 898 (2009); *Radiotekh. Elektron.* **54** 946 (2009)
- Shevchenko V V *J. Commun. Technol. Electron.* **55** 986 (2010); *Radiotekh. Elektron.* **55** 1052 (2010)
- Anenkov V V, Shevchenko V V *J. Commun. Technol. Electron.* **56** 1186 (2011); *Radiotekh. Elektron.* **56** 1194 (2011)
- Grachev G G, Shevchenko V V *J. Commun. Technol. Electron.* **55** 403 (2010); *Radiotekh. Elektron.* **55** 432 (2010)
- Shevchenko V V *Phys. Usp.* **54** 1131 (2011); *Usp. Fiz. Nauk* **181** 1171 (2011)
- Pokrovsky A L, Efros A L *Solid State Commun.* **125** 283 (2002)
- Davidovich M V *Izv. Saratov. Univ. Novaya Ser. Ser. Fiz.* **11** (1) 42 (2011)
- Silin V P, Rukhadze A A *Elektromagnitnye Svoistva Plazmy i Plazmopodobnykh Sred* (Moscow: Gosatomizdat, 1961)

85. Rukhadze A A, Silin V P *Sov. Phys. Usp.* **4** 459 (1961); *Usp. Fiz. Nauk* **74** 223 (1961)
86. Rukhadze A A, Silin V P *Sov. Phys. Usp.* **5** 37 (1962); *Usp. Fiz. Nauk* **76** 79 (1962)
87. Alexandrov A F, Bogdankevich L S, Rukhadze A A *Principles of Plasma Electrodynamics* (Berlin: Springer-Verlag, 1984); Translated from Russian: *Osnovy Elektrodinamiki Plazmy* (Moscow: Vysshaya Shkola, 1978)
88. Agranovich V M, Ginzburg V L *Sov. Phys. Usp.* **5** 675 (1963); *Usp. Fiz. Nauk* **77** 663 (1962)
89. Vinogradov A P *Phys. Usp.* **45** 331 (2002); *Usp. Fiz. Nauk* **172** 363 (2002)
90. Vinogradov A P *Elektrodinamika Kompozitnykh Materialov* (Moscow: Editorial URSS, 2001)
91. Mackay T G, Lakhtakia A *Electromagnetic Anisotropy and Bianisotropy: A Field Guide* (Singapore: World Scientific, 2010)
92. Lakhtakia A *Beltrami Fields in Chiral Media* (Singapore: World Scientific, 1994)
93. Sihvola A H, Lindell I V *Microwave Opt. Technol. Lett.* **4** 8295 (1991)
94. Fisanov V V *Dokl. Tomsk. Gos. Univ. Sistem Uprav. Radioelektron.* **2** (24) 193 (2011)
95. Vinogradov A P, Dorofeenko A V, Zouhdi S *Phys. Usp.* **51** 485 (2008); *Usp. Fiz. Nauk* **178** 511 (2008)
96. Snarskii A A *Phys. Usp.* **50** 1239 (2007); *Usp. Fiz. Nauk* **177** 1341 (2007)
97. Efimova et al. *Infrakrasnaya Spektroskopiya System Ponizhennoi Razmernosti* (St. Petersburg: Lan', 2016)
98. Akhiezer A I, Akhiezer I A *Elektromagnetizm i Elektromagnitnye Volny* (Moscow: Vysshaya Shkola, 1978)
99. Rashevskii P K *Rimanova Geometriya i Tenzornyi Analiz* (Moscow: Nauka, 1967)
100. Nagy K L *State Vector Spaces with Indefinite Metric in Quantum Field Theory* (Groningen: P. Noordhoff, 1966); Translated into Russian: *Prostranstva Sostoyanii s Indefinitnoi Metrikoi v Kvantovoi Teorii Polya* (Moscow: Mir, 1969)
101. Azizov T Ya, Iokhvidov I S *Osnovy Teorii Lineinykh Operatorov v Prostranstvakh s Indefinitnoi Metrikoi* (Moscow: Nauka, 1986)
102. Graglia R D, Uslenghi P L E, Zich R E *IEEE Trans. Antennas Propag.* **39** 83 (1991)
103. Mandel L, Wolf E *Optical Coherence and Quantum Optics* (Cambridge: Cambridge Univ. Press, 1995); Translated into Russian: *Opticheskaya Kogerentnost' i Kvantovaya Optika* (Moscow: Fizmatlit, 2000)
104. Scully M O, Zubairy M S *Quantum Optics* (Cambridge: Cambridge Univ. Press, 1997); Translated into Russian: *Kvantovaya Optika* (Moscow: Fizmatlit, 2000)
105. Ignatov A M, Rukhadze A A *Sov. Phys. Usp.* **24** 759 (1981); *Usp. Fiz. Nauk* **135** 171 (1981)
106. Tikhodeev S G et al. *Phys. Usp.* **52** 945 (2009); *Usp. Fiz. Nauk* **179** 1003 (2009)
107. Davidovich M V, Shilovskii P A *Geteromagn. Elektron.* **13** 45 (2012)
108. Lagarkov A N et al. *Phys. Usp.* **52** 959 (2009); *Usp. Fiz. Nauk* **179** 1018 (2009)
109. Davidovich M V *JETP Lett.* **108** 279 (2018); *Pis'ma Zh. Eksp. Teor. Fiz.* **108** 299 (2018)
110. Vashkovskii A V, Lokk E G *Phys. Usp.* **47** 601 (2004); *Usp. Fiz. Nauk* **174** 657 (2004)
111. Vashkovskii A V, Lokk E G *Phys. Usp.* **49** 537 (2006); *Usp. Fiz. Nauk* **176** 557 (2006)
112. Vashkovskii A V, Lokk E G *Phys. Usp.* **49** 389 (2006); *Usp. Fiz. Nauk* **176** 403 (2006)
113. Kurin V V *Phys. Usp.* **52** 953 (2009); *Usp. Fiz. Nauk* **179** 1012 (2009)
114. Akhiezer A I, Bar'yakhtar V G, Peletminskii S V *Spin Waves* (Amsterdam: North-Holland Publ. Co., 1968); Translated from Russian: *Spinovye Volny* (Moscow: Nauka, 1967)
115. Kaner E A, Skobov V G *Sov. Phys. Usp.* **9** 480 (1967); *Usp. Fiz. Nauk* **89** 367 (1966)
116. Zuev V S, Zueva G Ya *Opt. Spectrosc.* **105** 778 (2008); *Opt. Spektrosk.* **105** 852 (2008)
117. Vinogradov A P et al. *Phys. Usp.* **55** 1046 (2012); *Usp. Fiz. Nauk* **182** 1122 (2012)
118. Ishii S E et al. *Laser Photon. Rev.* **7** 265 (2013)
119. Zhukovsky S V, Kidwai O, Sipe J E *Opt. Express* **21** 14982 (2013)
120. Zhukovsky S V, Lavrinenko A V, Sipe J E *Proc. SPIE* **8915** 891512 (2013)
121. Zhukovsky S V et al. *Phys. Rev. A* **90** 013801 (2014)
122. Davidovich M V *Tech. Phys. Lett.* **43** 1023 (2017); *Pis'ma Zh. Tekh. Fiz.* **43** (22) 55 (2017)
123. Davidovich M V *Quantum Electron.* **47** 567 (2017); *Kvantovaya Elektron.* **47** 567 (2017)
124. Pursell E V *Phys. Rev.* **69** 681 (1946)
125. Alberl G, Chizhov A V *Nanosyst. Phys. Chem. Math.* **8** 559 (2017)
126. Iwase H, Englund D, Vučković J *Opt. Express* **18** 16546 (2010)
127. Jacob Z, Smolyaninov I I, Narimanov E E *Appl. Phys. Lett.* **100** 181105 (2012)
128. Glazov M M et al. *Phys. Solid State* **53** 1753 (2011); *Fiz. Tverd. Tela* **53** 1665 (2011)
129. Kavokin A et al. *Microcavities* (Oxford: Oxford Univ. Press, 2007)
130. Jacob Z, Shalaev V M *Science* **334** 463 (2011)
131. Potemkin A S et al. *Phys. Rev. A* **86** 023848 (2012)
132. Narimanov E et al., in *Quantum Electronics and Laser Science Conf., 16–21 May 2010, San Jose, Calif., United States, 2010, QPDA6*
133. Glazov M M et al. *Phys. Solid State* **53** 1753 (2011); *Fiz. Tverd. Tela* **53** 1665 (2011)
134. Xie H Y, Leung P T, Tsai D P *Solid State Commun.* **149** 625 (2009)
135. Kidwai O, Zhukovsky S V, Sipe J E *Opt. Lett.* **36** 2530 (2011)
136. Kidwai O, Zhukovsky S V, Sipe J E *Phys. Rev. A* **85** 053842 (2012)
137. Iorsh I et al. *Phys. Lett. A* **376** 185 (2012)
138. Chebykin A V et al. *Sci. Tech. J. Inform. Tech. Mech. Opt.* **94** (6) 9 (2014); *Nauchno-tekh. Vestn. Inform. Tekhnol. Mekh. Opt.* **94** (6) 9 (2014)
139. Morozov K M et al. *Opt. Spectrosc.* **122** 235 (2017); *Opt. Spektrosk.* **122** 258 (2017)
140. Ginzburg P et al., in *The Sixth Intern. Congress on Advanced Electromagnetic Materials in Microwaves and Optics, Metamorphose VI, 2012* (2012) p. 399
141. Guo Y, Jacob Z *Opt. Express* **21** 15014 (2013)
142. Liu B, Shen S *Phys. Rev. B* **87** 115403 (2013)
143. Jacob Z, Smolyaninov I I, Narimanov E E *Appl. Phys. Lett.* **100** 181105 (2012)
144. Poddubny A N et al. *Phys. Rev. B* **86** 035148 (2012)
145. Yan W, Wubs M, Mortensen N A *Phys. Rev. B* **86** 205429 (2012)
146. Bogdanov S et al. *Phys. Rev. B* **96** 035146 (2017)
147. Zalogina A S et al. *AIP Conf. Proc.* **1874** 040058 (2017)
148. Krasnok A et al. *Appl. Phys. Lett.* **108** 211105 (2016)
149. Chebykin A V et al. *Phys. Rev. A* **93** 033855 (2016)
150. Krasnok A E et al., in *Proc. of the Intern. Conf. Days on Diffraction 2015* (2015) p. 170
151. Krasnok A E et al. *Sci. Rep.* **5** 12956 (2015)
152. Chebykin A V et al. *Phys. Rev. B* **91** 205126 (2015)
153. Babicheva V E et al., in *Conf. on Lasers and Electro-Optics Europe-Technical Digest* (2014)
154. Krasnok A E et al., in *Proc. of the Intern. Conf. Days on Diffraction 2014* (2014) p. 156
155. Babicheva V E et al., Optics InfoBase Conf. Papers, CLEO_QELS FTu2C.3 (2014)
156. Slobozhanyuk A P et al. *Appl. Phys. Lett.* **104** 161105 (2014)
157. Poddubny A N, Belov P A, Kivshar Y S *Proc. SPIE* **8806** 88060T (2013)
158. Orlov A A et al., Optics InfoBase Conference Papers QELS, QTh1A.5 (2012)
159. Orlov A A et al., in *Conf. on Lasers and Electro-Optics, CLEO 2012* (2012)
160. Bogdanov S et al., Optics InfoBase Conf. Papers Part F42 2 (2017)
161. Hoffman A J et al. *Nature Mater.* **6** 946 (2007)
162. Shchelokova A V, Kapitanova P V, Belov P A *Nauchno-tekh. Vestn. Inform. Tekhnol. Mekh. Opt.* **2** (90) 23 (2014)
163. Liu Z et al. *Science* **315** 1686 (2007)
164. Rho J et al. *Nature Commun.* **1** 143 (2010)
165. Tumkur T U et al. *Appl. Phys. Lett.* **99** 151115 (2011)
166. Krishnamoorthy H N S et al. *Science* **336** 205 (2012)
167. Kim J et al. *Opt. Express* **20** 8100 (2012)
168. Yang X et al. *Nature Photon.* **6** 450 (2012)
169. Shen L, Yang T-J, Chau Y-F *Phys. Rev. B* **77** 205124 (2008)
170. Orlov AA et al. *Phys. Rev. B* **84** 045424 (2011)

171. Korobkin D et al. *Opt. Express* **18** 22734 (2010)
172. Antonova I V et al. *Semiconductors* **48** 804 (2014); *Fiz. Tekh. Poluprovodn.* **48** 827 (2014)
173. Silveirinha M G *Phys. Rev. E* **73** 046612 (2006)
174. Akimov A V et al. *Nature* **450** 402 (2007)
175. Kanungo J, Schilling J *Appl. Phys. Lett.* **97** 021903 (2010)
176. Kabashin A V et al. *Nature Mater.* **8** 867 (2009)
177. Wurtz G A et al. *Nature Nanotechnol.* **6** 107 (2011)
178. Custodio L M et al. *Phys. Rev. B* **85** 165408 (2012)
179. Ikonen P et al. *Appl. Phys. Lett.* **91** 104102 (2007)
180. Bhushan B (Ed.) *Springer Handbook of Nanotechnology* (Berlin: Springer-Verlag, 2017)
181. Ozin G A *Adv. Mater.* **4** 612 (1992)
182. Tonucci R J et al. *Science* **258** 783 (1992)
183. Ying J Y *Sci. Spectra* **18** 56 (1999)
184. Kaidashev E M “Sozdanie i issledovanie elementov novykh radiofizicheskikh ustroystv na osnove tonkikh plenok i odnomernykh nanostruktur” (“Development and research of elements of new radiophysical devices based on thin films and one-dimensional nanostructures”), Thesis for Doctoral for Physico-Mathematical Sciences (Rostov-na-Donu: Southern Federal Univ., 2018)
185. Eletsii A V *Phys. Usp.* **40** 899 (1997); *Usp. Fiz. Nauk* **167** 945 (1997)
186. Eletsii A V *Phys. Usp.* **45** 369 (2002); *Usp. Fiz. Nauk* **172** 401 (2002)
187. Othman M A K, Guclu C, Capolino F *Opt. Express* **21** 7614 (2013)
188. Cai J et al. *Nature Nanotechnol.* **9** 896 (2014)
189. Kim Y et al. *Nature Commun.* **4** 2114 (2013)
190. Lee M H et al. *Phil. Mag.* **94** 2812 (2014)
191. Chen Y-C et al. *Nature Nanotechnol.* **10** 156 (2015)
192. Felsen L, Marcuvitz N *Radiation and Scattering of Waves* (New York: Wiley, 2003); Translated into Russian: *Izluhenie i Rasseyaniye Voln* Vol. 2 (Moscow: Mir, 1978)
193. Narimanov E E, Smolyaninov I I, in *Quantum Electronics and Laser Science Conf. 2012, San Jose, Calif., United States, 6–11 May 2012*, <https://doi.org/10.1364/QELS.2012.QM2E.1>
194. Jacob Z et al. *Appl. Phys. B* **100** 215 (2010)
195. Jacob Z “Classical and quantum optics of hyperbolic metamaterials”, Ph.D. Thesis (West Lafayette, Ind.: Purdue Univ, 2010)
196. Biehs S-A et al. *Opt. Express* **19** A1088 (2011)
197. Korobkin D et al. *Opt. Express* **18** 22734 (2010)
198. Krishnamoorthy H N S et al. *Science* **336** 205 (2012)
199. Ishii S et al. *Laser Photon. Rev.* **7** 265 (2013)
200. Belov P A, Hao Y *Phys. Rev. B* **73** 11310 (2006)
201. Ikonen P et al. *Phys. Rev. B* **73** 073102 (2006)
202. Belov P A, Hao Y, Sudhakaran S *Phys. Rev. B* **73** 033108 (2006)
203. Ishii S et al., in *Conf. on Lasers and Electro-Optics-Pacific Rim, Kyoto, Japan* (2013) W13_3
204. Khalil M I et al. *Appl. Opt.* **53** 6096 (2014)
205. Ageyskiy A E et al. *Phys. Rev. B* **85** 033105 (2012)
206. Voroshilov P M et al. *J. Nanophoton.* **5** 053516 (2011)
207. Rahman A F et al. *J. Nanophoton.* **5** 051601 (2011)
208. Belov P A *Phys. Rev. B* **82** 113408 (2010)
209. Belov P A, Rahman A, Kosulnikov S Y *Proc. SPIE* **7754** 77541E (2010)
210. Kosulnikov S et al. *IEEE Trans. Antennas Propag.* **63** 4848 (2015)
211. Song M, Belov P A, Kapitanova P V *Appl. Phys. Rev.* **4** 021102 (2017)
212. Ageyskiy A et al., in *8th Intern. Congress on Advanced Electromagnetic Materials in Microwaves and Optics, Metamaterials, 2014* (2014) p. 52
213. Tyshetskiy Y et al. *J. Opt. Soc. Am. B* **31** 1753 (2014)
214. Slobozhanyuk A P et al. *Appl. Phys. Lett.* **103** 051118 (2013)
215. Belov P A et al. *Appl. Phys. Lett.* **103** 161103 (2013)
216. Maslovski S I et al., in *Proc. of 2013 Intern. Symp. on Electromagnetic Theory, EMTS 2013* (2013) p. 384
217. Belov P A *New J. Phys.* **12** 103045 (2010)
218. Belov P A *Appl. Phys. Lett.* **97** 191905 (2010)
219. Ishii S et al. *Active Plasmonics and Tuneable Plasmonic Metamaterials* (New York: John Wiley and Sons, 2013) p. 289
220. Remnev M A, Klimov V V *Phys. Usp.* **61** 157 (2018); *Usp. Fiz. Nauk* **188** 169 (2018)
221. Davidovich M V, Meshchanov V P *Antenny* **8** (240) 3 (2017)
222. Gangaraj S A H et al. *IEEE Trans. Antennas Propag.* **65** 1174 (2017)
223. Hagag M A, Drachev V, Kildishev A, in *CLEO: QELS, OSA* (2016) paper JW2A.31
224. Artigasand D, Torner L *Phys. Rev. Lett.* **94** 013901 (2005)
225. Jacob Z, Narimanov E E *Appl. Phys. Lett.* **93** 221109 (2008)
226. Sreekanth K V et al. *Nature Mater.* **15** 621 (2016)
227. Korryng J *Physica* **13** 392 (1947)
228. Moroz A J. *Phys. Condens. Matter* **6** 172 (1994)
229. Davidovich M V *Radiophys. Quantum Electron.* **49** 134 (2006); *Izv. Vyssh. Uchebn. Zaved. Radiofiz.* **49** 150 (2006)
230. Davidovich M V *Naukoemkie Tekhnol.* **17** (5) 8 (2016)
231. Klimov V *Nanoplasmonics* (Boca Raton, FL: CRC Press, Taylor and Francis Group, 2014); *Nanoplasmonika* (Moscow: Fizmatlit, 2009)
232. Novotny L, Hecht B *Principles of Nano-Optics* (Cambridge: Cambridge Univ. Press, 2006); Translated into Russian: *Osnovy Nanooptiki* (Moscow: Fizmatlit, 2009)
233. Markov G T, Chaplin A F *Vozbuzhdenie Elektromagnitnykh Voln* (Moscow: Radio i Svyaz', 1983)
234. Krokhin A A et al. *Phys. Rev. B* **93** 75418 (2016)
235. Noginov M A et al. *Appl. Phys. Lett.* **94** 151105 (2009)
236. Belov P A, Simovski C R, Ikonen P *Phys. Rev. B* **71** 193105 (2005)
237. Dickson W et al. *Phys. Rev. B* **76** 115411 (2007)
238. Kamenetskii E O *Phys. Rev. E* **57** 3563 (1998)
239. Kamenetskii E O *Microwave Opt. Technol. Lett.* **19** 412 (1998)
240. Kamenetskii E O *IEEE Trans. Antennas Propag.* **49** 361 (2001)
241. Chipouline A, Küppers F J. *Opt. Soc. Am. B* **34** 1597 (2017)
242. Davidovich M V *JETP* **127** 1 (2018); *Zh. Eksp. Teor. Fiz.* **153** 5 (2018)
243. Vendik I B, Vendik O G, Gashinova M S *Tech. Phys. Lett.* **32** 429 (2006); *Pis'ma Zh. Tekh. Fiz.* **32** (10) 30 (2006)
244. Vendik I et al. *Opto-Electron. Rev.* **14** (3) 179 (2006)
245. Davidovich M V, Stefyuk Yu V *Radiophys. Quantum Electron.* **53** 268 (2010); *Izv. Vyssh. Uchebn. Zaved. Radiofiz.* **53** 296 (2010)
246. Davidovich M V *Iteratsionnye Metody Resheniya Zadach Elektrodinamiki* (Saratov: Izd. Sarat. Univ., 2014)
247. Gradshteyn I S, Ryzhik I M *Tables of Integrals, Series and Products* (New York and London: Academic Press, 1965); Translated from Russian: *Tablitsy Integralov, Summ, Ryadov i Proizvedenii* (Moscow: GIFML, 1962)
248. Smith D R, Kolinko P, Schurig D J. *Opt. Soc. Am. B* **21** 1032 (2004)
249. Kubo R J. *Phys. Soc. Jpn.* **12** 570 (1957)
250. Greenwood D A *Proc. Phys. Soc. London* **71** 585 (1958)
251. Kadanoff L P, Baym G *Quantum Statistical Mechanics. Green's Function Methods in Equilibrium and Nonequilibrium Problems* (New York: W.A. Benjamin, 1962); Translated into Russian: *Kvantovaya Statisticheskaya Mekhanika. Funktsii Grina, Ravnovesnye i Neravnovesnye Protsessy* (Moscow: Mir, 1964)
252. Slepian G Y et al. *Phys. Rev. B* **60** 17136 (1999)
253. Gusynin V P, Sharapov S G *Phys. Rev. B* **73** 245411 (2006)
254. Gusynin V P, Sharapov S G, Carbotte J P *Phys. Rev. Lett.* **96** 256802 (2006)
255. Peres N M R, Guinea F, Castro Neto A H *Phys. Rev. B* **73** 125411 (2006)
256. Ziegler K *Phys. Rev. Lett.* **97** 266802 (2006)
257. Ziegler K *Phys. Rev. B* **75** 233407 (2007)
258. Mikhailov S A, Ziegler K *Phys. Rev. Lett.* **99** 016803 (2007)
259. Falkovsky L A, Pershoguba S S *Phys. Rev. B* **76** 153410 (2007)
260. Falkovsky L A, Varlamov A A *Eur. Phys. J. B* **56** 281 (2007)
261. Gusynin V P, Sharapov S G, Carbotte J P *Phys. Rev. B* **75** 165407 (2007)
262. Gusynin V P, Sharapov S G, Carbotte J P *J. Phys. Condens. Matter* **19** 026222 (2007)
263. Falkovsky L A *Phys. Lett. A* **372** 31 (2008)
264. Falkovsky L A *Phys. Usp.* **51** 887 (2008); *Usp. Fiz. Nauk* **178** 923 (2008)
265. Falkovsky L A *Phys. Usp.* **55** 1140 (2012); *Usp. Fiz. Nauk* **182** 1223 (2012)
266. Hanson G W J. *Appl. Phys.* **103** 064302 (2008)
267. Lovat G et al. *Phys. Rev. B* **87** 115429 (2013)
268. Alisultanov Z Z, Meilanov R P *Semiconductors* **48** 924 (2014); *Fiz. Tekh. Poluprovodn.* **48** 951 (2014)
269. Alisultanov Z Z, Kamilov I K *Phys. Solid State* **56** 854 (2014); *Fiz. Tverd. Tela* **56** 821 (2014)

270. Fisher R K, Gould R W *Phys. Rev. Lett.* **22** 1093 (1969)
271. Alekseyev L V, Narimanov E *Opt. Express* **14** 11184 (2006)
272. Kim M, Rho J *Nano Convergence* **2** 22 (2015)
273. Smith D R et al. *Appl. Phys. Lett.* **84** 2244 (2004)
274. Balmain K G, Lüttgen A A E, Kremer P C *IEEE Antennas Wireless Propag. Lett.* **1** 146 (2002)
275. Lemoult F et al. *Phys. Rev. Lett.* **104** 203901 (2010)
276. Yang K Y et al. *Phys. Rev. B* **86** 075309 (2012)
277. Jacob Z, Alekseyev L V, Narimanov E *Opt. Express* **14** 8247 (2006)
278. Wang W et al. *Opt. Express* **16** 21142 (2008)
279. Xiong Y, Liu Z, Zhang X *Appl. Phys. Lett.* **94** 203108 (2009)
280. Smith E J et al. *Appl. Phys. Lett.* **95** 083104 (2009)
281. Kildishev A V et al. *Appl. Phys. Lett.* **94** 071102 (2009)
282. Liu Z et al. *Appl. Phys. Lett.* **96** 113507 (2010)
283. Kildishev A V, Narimanov E *Opt. Lett.* **32** 3432 (2007)
284. Lu D, Liu Z *Nature Commun.* **3** 1205 (2012)
285. Andryieuski A, Lavrinenko A V, Chigrin D N *Phys. Rev. B* **86** 121108 (2012)
286. Salandrino A, Engheta N *Phys. Rev. B* **74** 075103 (2006)
287. Smolyaninov I I, Hung Y-J, Davis C C *Science* **315** 1699 (2007)
288. Ishi S, Drachev V P, Kildishev A V *Opt. Commun.* **285** 3368 (2012)
289. Ma C, Liu Z *Appl. Phys. Lett.* **96** 183103 (2010)
290. Ma C, Liu Z *J. Nanophoton.* **5** 051604 (2011)
291. Taubner T et al. *Science* **313** 1595 (2006)
292. Sun J, Shalaev M I, Litchinitser N M *Nature Commun.* **6** 7201 (2015)
293. Ming W, Blair S, Liu F *J. Phys. Condens. Matter* **26** 505302 (2014)
294. Alford T L, Feldman L C, Mayer J W *Fundamentals of Nanoscale Film Analysis* (New York: Springer, 2007); Translated into Russian: *Fundamental'nye Osnovy Analiza Nanoplenok* (Moscow: Nauchnyi Mir, 2012)
295. Evans P et al. *Nanotechnology* **17** 5746 (2006)
296. Bivas S et al. *J. Appl. Phys.* **114** 63519 (2013)
297. Wang B et al. *Phys. Rev. Lett.* **109** 073901 (2012)
298. Gilbertson Y, Francescato T, Roschuk R F *Nano Lett.* **15** 3458 (2015)
299. Li X, Zhua J, Wei B *Chem. Soc. Rev.* **45** 3145 (2016)
300. Balykin V I, Melentiev P N *Phys. Usp.* **61** 133 (2018); *Usp. Fiz. Nauk* **188** 143 (2018)
301. Smirnov B M *Phys. Usp.* **60** 1236 (2017); *Usp. Fiz. Nauk* **187** 1329 (2017)
302. Lee M H et al. *Phil. Mag.* **95** 2717 (2015)
303. Kim W K et al. *Appl. Phys. Lett.* **97** 193103 (2010)
304. Davidovich M V, Stephuk J V, Shilin I V *Proc. SPIE* **6537** 65370F (2007)
305. Vincenti M A et al. *Phys. Rev. A* **80** 053807 (2009)
306. Al'tshuler E Yu, Davidovich M V, Stefyuk Yu V *J. Commun. Technol. Electron.* **55** 98 (2010); *Radiofiz. Elektron.* **55** 105 (2010)
307. Ni X et al. *Opt. Express* **19** 25242 (2011)
308. Dubinov V Ya et al. *J. Phys. Condens. Matter* **23** 145302 (2011)
309. Dorofeenko A V et al. *Phys. Usp.* **55** 1080 (2012); *Usp. Fiz. Nauk* **182** 1157 (2012)
310. Ryzhii V, Ryzhii M, Otsuji T *J. Appl. Phys.* **101** 083114 (2007)
311. Abdollahipour B, Moomivand E *Physica E* **86** 204 (2016)
312. Popov V V, Polischuk O V, Davoyan A R *Phys. Rev. B* **86** 195437 (2012)
313. Popov V V et al. *J. Opt.* **15** 114009 (2013)
314. Popov V V et al. *J. Appl. Phys.* **94** 3556 (2003)
315. Popov V V et al. *Phys. Rev. B* **81** 073404 (2010)
316. Polischuk O V, Fateev D V, Popov V V *Semiconductors* **51** 1460 (2017); *Fiz. Tekh. Poluprovodn.* **51** 1514 (2017)
317. Gonzalez-Diaz J B et al. *Small* **4** 2202 (2008)
318. Belotelov V I et al. *Nature Nanotechnol.* **6** 370 (2011)
319. Li W et al. *Appl. Phys. Lett.* **100** 161108 (2012)
320. Krutyanskiy V L et al. *Phys. Rev. B* **87** 035116 (2013)
321. Chekhov A L et al. *Opt. Express* **22** 17762 (2014)
322. Kruk S S et al. *Nature Commun.* **7** 11329 (2016)
323. Mirmoosa M S, Kosulnikov S Yu, Simovski C R *Phys. Rev. B* **94** 075138 (2016)
324. Leviyev A et al. *APL Photon.* **2** 076103 (2017)
325. Pomozov A R et al. *Phys. Solid State* **60** 2264 (2018); *Fiz. Tverd. Tela* **60** 2224 (2018)
326. Babicheva V E et al. *Opt. Express* **23** 31109 (2015)
327. Lyashko E I, Mamistov A I *J. Opt. Soc. Am. B* **33** 2320 (2016)
328. Wilson C M et al. *Nature* **479** 376 (2011)
329. Alù A et al. *Phys. Rev. B* **75** 155410 (2007)
330. Zhukovsky S V, Andryieuski A, Lavrinenko A V, SPIE Newsroom (2014) 29 October
331. Artigasand D, Torner L *Phys. Rev. Lett.* **94** 013901 (2005)
332. Jacob Z, Narimanov E *Appl. Phys. Lett.* **93** 221109 (2008)
333. Sedova E S et al. *JETP Lett.* **104** 62 (2016); *Pis'ma Zh. Eksp. Teor. Fiz.* **104** 58 (2016)
334. Sensale-Rodriguez B *Appl. Phys. Lett.* **103** 123109 (2013)
335. Azara O A, Abdia M, Baghbana H, in *5th Int. Biennial Conf. on Ultrafine Grained and Nanostructured Materials, UFGNSM15; Proced. Mater. Sci.* **11** 270 (2015)
336. Jian-rong H, Jiu-sheng L, Guo-hua Q *J. Infrared Millimeter Terahertz Waves* **37** 7668 (2016)
337. Davidovich M V *Proc. SPIE* **11066** 1106611 (2019)
338. Thongrattanasiri S, Podolskiy V A *Opt. Lett.* **34** 890 (2009)
339. Yao J et al. *Proc. Natl. Acad. Sci. USA* **108** 11327 (2011)
340. Kim S et al. *Opt. Express* **21** 15081 (2013)
341. Atakaramians S et al. *J. Opt. Soc. Am. B* **29** 2462 (2012)
342. He Y, He S, Yang X *Opt. Lett.* **37** 2907 (2012)
343. Al'tshuler E Yu, Nefedov I S *J. Commun. Technol. Electron.* **53** 60 (2008); *Radiofiz. Elektron.* **53** 67 (2008)
344. Podolskiy V A, Narimanov E *Phys. Rev. B* **71** 201101 (2005)
345. Elser J, Podolskiy V A *Phys. Rev. Lett.* **100** 066402 (2008)
346. Xu G-D et al. *Opt. Commun.* **281** 2819 (2008)
347. Zhang Z, Fan Y *J. Opt. Soc. Am. B* **29** 2995 (2012)
348. Narimanov E E et al. *Opt. Express* **21** 14956 (2013)
349. Cortes C L, Jacob Z *Phys. Rev. B* **88** 045407 (2013)
350. Smolyaninov I I, Narimanov E E *Phys. Rev. Lett.* **105** 067402 (2010)
351. Smolyaninov I I *Phys. Rev. Lett.* **107** 253903 (2011)
352. Smolyaninov I I, Hung Y-J, Hwang E *Phys. Lett. A* **376** 2575 (2012)
353. Smolyaninov I I, Kildishev A V *Opt. Lett.* **38** 6971 (2013)
354. Sun J et al. *Appl. Phys. Lett.* **98** 101901 (2011)
355. Tristán-López F et al. *ACS Nano* **7** 10788 (2013)
356. Dimitrakakis G K, Tylianakis E, Froudakis G E *Nano Lett.* **8** 3166 (2008)
357. Glukhova O E et al. *Phys. Solid State* **57** 1009 (2015); *Fiz. Tverd. Tela* **57** 994 (2015)
358. Znatil S et al. *J. Surf. Eng. Mater. Adv. Tech.* **5** 207 (2015)
359. Vinogradov A P, Merzlikin A M *Dokl. Phys.* **46** 832 (2001); *Dokl. Ross. Akad. Nauk* **381** 472 (2001)
360. Vinogradov A P, Merzlikin A M, in *Advances in Electromagnetics of Complex Media and Metamaterials* Vol. 2 (Eds S Zouhdi, A Sihvola, M Arsalane) (New York: Springer, 2002) p. 341
361. Vinogradov A P, Aivazyan A V *Phys. Rev. E* **60** 987 (1999)
362. Wellander N *Appl. Math.* **45** 29 (2001)
363. Belov P A, Simovski C R *Phys. Rev. B* **73** 045102 (2006)
364. Ferrari L et al. *Prog. Quantum Electron.* **40** 1 (2015)